

1 0983 1917 (51 (14) (15)

> LIBRARY Michigan State University

This is to certify that the thesis entitled

A NUMERICAL MODEL OF DIFFUSION LIMITED DISSOLUTION FROM DEEP ATLANTIC CARBONATE SEDIMENT

presented by

KIRSTEN V. WRIGHT

has been accepted towards fulfillment of the requirements for the

Master of Science degree in

Geological Sciences

Major Professor's Signature

Date

MSU is an Affirmative Action/Equal Opportunity Institution

PLACE IN RETURN BOX to remove this checkout from your record. TO AVOID FINES return on or before date due. MAY BE RECALLED with earlier due date if requested.

DATE DUE	DATE DUE	DATE DUE

6/01 c:/CIRC/DateDue.p65-p.15

A NUMERICAL MODEL OF DIFFUSION LIMITED DISSOLUTION FROM DEEP ATLANTIC CARBONATE SEDIMENT

By

Kirsten V Wright

A THESIS

Submitted to
Michigan State University
In partial fulfillment of the requirements
For the degree of

MASTER OF SCIENCE

Geological Sciences

2003

ABSTRACT

A NUMERICAL MODEL OF DIFFUSION LIMITED DISSOLUTION FROM DEEP ATLANTIC CARBONATE SEDIMENT

By

Kirsten V Wright

Though hiatuses occur across the Atlantic throughout its history, mechanisms explaining time periods of missing sediment record are not clear. Atlantic seafloor below the CCD is overlain by water undersaturated with respect to CaCO₃, and dissolution of carbonate from the sediment would be limited by diffusion of ions toward the sediment water interface. The flux of Ca2+ depends on the concentration gradient and diffusion coefficient. The concentration gradient can be estimated from DSDP measurements, but the diffusion coefficient is approximated by an empirical relationship, which depends on porosity. Porosity data allow fitting of a function dependent on depth. Based on these relationships, a one dimensional finite difference model was developed. It seems robust with respect to nearly all of the parameters, but appears to be most sensitive to porosity. Investigation of reaction limited dissolution at the sediment water interface was also performed. The removal of carbonate from the sediment column was minimal. For the 10,000year time step, the reduction in thickness was on the order of microns, and was around 1% for the entire 100Ma. This is not enough to create a noticeable hiatus.

TABLE OF CONTENTS

LIST OF TABLES	iv
LIST OF FIGURES	vi
INTRODUCTION	1
THE MODEL RELATIONSHIPS	8
THE NUMERICAL MODEL	14
ASSUMPTIONS	20
PARAMETER ESTIMATION	26
RESULTS	30
SENSITIVITY ANALYSIS	41 43 47
SEDIMENT-WATER INTERFACE MODEL	50
CONCLUSIONS	54
DISCUSSION	56
APPENDICES	58
REFERENCES	72

LIST OF TABLES

TABLE 4.1
Sample calculation of effect of advection due to reduction in porosity.
TABLE 6.1
TABLE 6.2
TABLE 6.3
Calculated change in thickness for 50 layers initially 10m thick. Values are μm for a 10,000 yr time step. Total reduction in thickness over 100Ma is given in the rightmost column in mm.
TABLE 6.43
Calculated depths of bounding surfaces for 50 layers initially 1m thick.
TABLE 6.5
TABLE 6.6
TABLE 6.73
Calculated change in thickness for 50 layers initially 0.01m thick. Values are nm for a 10,000 yr time step. Total reduction in thickness over 100M is given in the rightmost column in mm.
TABLE 7.14. Statistics for analysis of sensitivity of bounding surface depth to variation in D _s .
TABLE 7.2
TABLE 7.3
Variation in model output from extreme values of porosity. Values are for a single cell initially bounded by 24m and 29m.
TABLE 9.15-
Dissolution from the top layer of the three simulated sediment columns.

TAB	BLE i.1	58
	DSDP sites used for accumulation rates.	
TAB	BLE ii.1	6
	Interstitial pore water measurements from DSDP for site 6 Ca ²⁺ concentration from equation 4.2 in which the constar from minimizing the sum of the residual squared values.	03. Predicted
TABI	BLE iii.1	68-69
	Porosity Measurements of Deep Atlantic Carbonate Sedin	nent from DSDF

LIST OF FIGURES

FIGURE 1.1	
Accumulation Rates for 35 DSDP site on Atlantic oceanic crust under least 4000m of water. Rates are calculated from SYNATLAN database (Wolf-Welling et al 1997), which has depths for 0.5Ma increments.	
FIGURE 1.2	2
Frequency of accumulation rates for 35 DSDP site in the Atlantic on oceanic crust in under at least 4000m of water. Mode is 0 m per 0.5M with 888 out of 3622 values.	
FIGURE 1.3	3
Sediment accumulation for all SYNATLAN sites with dating between 1 and 20Ma. Thickness is the total sediment between 18 and 20Ma. Indicated hiatuses are locations with zero thickness for the entire periods.	
FIGURE 1.4	4
Sediment accumulation for site 513. Temporal resolution is 0.5Ma and accumulation is shown as meters per 0.5Ma increment.	d
	_
FIGURE 1.5	
SYNATLAN sites selected as carbonate sediment on oceanic crust un at least 4000m of water. Solid circles indicate that at least on hiatus w found at the site, and open circles are locations where no hiatus was measured.	der
SYNATLAN sites selected as carbonate sediment on oceanic crust un at least 4000m of water. Solid circles indicate that at least on hiatus was found at the site, and open circles are locations where no hiatus was measured.	der <i>v</i> as
SYNATLAN sites selected as carbonate sediment on oceanic crust un at least 4000m of water. Solid circles indicate that at least on hiatus w found at the site, and open circles are locations where no hiatus was	der <i>v</i> as
SYNATLAN sites selected as carbonate sediment on oceanic crust un at least 4000m of water. Solid circles indicate that at least on hiatus was found at the site, and open circles are locations where no hiatus was measured. FIGURE 2.1	der vas 8
SYNATLAN sites selected as carbonate sediment on oceanic crust un at least 4000m of water. Solid circles indicate that at least on hiatus was found at the site, and open circles are locations where no hiatus was measured. FIGURE 2.1	der vas 8
SYNATLAN sites selected as carbonate sediment on oceanic crust un at least 4000m of water. Solid circles indicate that at least on hiatus was found at the site, and open circles are locations where no hiatus was measured. FIGURE 2.1 Setup of one dimensional diffusion model. $x=$ depth, $q=$ flux. FIGURE 2.2 Form of concentration with depth: $C(x) = C_{max} - (C_{range} \cdot e^{-k_c \cdot x})$	der vas 8
SYNATLAN sites selected as carbonate sediment on oceanic crust un at least 4000m of water. Solid circles indicate that at least on hiatus was found at the site, and open circles are locations where no hiatus was measured. FIGURE 2.1	der vas 8
SYNATLAN sites selected as carbonate sediment on oceanic crust un at least 4000m of water. Solid circles indicate that at least on hiatus w found at the site, and open circles are locations where no hiatus was measured. FIGURE 2.1	der vas 8 9
SYNATLAN sites selected as carbonate sediment on oceanic crust un at least 4000m of water. Solid circles indicate that at least on hiatus was found at the site, and open circles are locations where no hiatus was measured. FIGURE 2.1	der vas 8 9
SYNATLAN sites selected as carbonate sediment on oceanic crust un at least 4000m of water. Solid circles indicate that at least on hiatus w found at the site, and open circles are locations where no hiatus was measured. FIGURE 2.1	der vas 8 9

FIGURE 2.512	2
Form of porosity with depth: $p(x) = p_{min} + p_{range} \cdot e^{\frac{x}{k_r}}$	
FIGURE 3.114 The setup of matrix final	4
FIGURE 3.21	5
The MATLAB code.	
FIGURE 3.316 The model variables	6
FIGURE 3.417 Location of the bounding surfaces and cells in the model.	7
FIGURE 4.1	0
FIGURE 4.224 Measurements of salinity for DSDP sites in the deep Atlantic basin.	4
FIGURE 5.1	
FIGURE 5.228 Measurements of porosity for DSDP sites in the deep Atlantic basin. The	_
solid line represents the fitted function: $p(x) = 58.5 + 16.5 \cdot e^{\frac{-x}{36.4m}}$	
FIGURE 6.1	1
FIGURE 6.2	1
FIGURE 6.3	2

FIGUF	RE 6.43	
	Change in thickness of layers initially 1m thick to 50m depth through 100 million years. Each calculated value is the change in thickness in micron for a 100,000 year period.	
FIGUI	RE 6.5	3
FIGUF	RE 6.6	3
FIGUF	RE 7.14 Example distribution of D _s introduced into the model for sensitivity analysis.	1
FIGUI	RE 7.24 Distribution of depth of bounding surface 3 resulting from variation in D_{s} i the model.	2 n
FIGUI	RE 7.34 Standard deviation of depth of bounding surfaces for 500 realizations incorporating variation in D _s .	3
FIGUF	RE 7.4	5
FIGUI	RE 7.5	5
FIGUI	RE 7.6	6
FIGUI	RE 7.7	Ī
FIGUI	RE 7.84 Distribution of measured porosity values used to estimate the constants i the function of porosity with depth.	_

FIGURE 7.949
Depth of bounding surfaces for layers initially 10 m thick to 500m depth through 100 million years with pelagic clay accumulation rate of 0.03mm/1000yr.
Change in thickness of layers initially 10 m thick to 500m depth through 100 million years with pelagic clay accumulation rate of 0.03mm/1000yr. Each calculated value is the change in thickness in microns for a 100,000 year period.
FIGURE 8.150
Modifications to the model code for kinetic dissolution from the sediment- water interface. Additions are shown in bold.
FIGURE 8.2
FIGURE 8.3
FIGURE 8.4
FIGURE i.159 Map of Atlantic DSDP sites.
FIGURE i.2
FIGURE iii.1

Introduction

Investigation of deposits under the deep Atlantic shows hiatuses, time periods of missing sediment. Either erosion or lack of deposition must occur to generate one of these gaps, but mechanisms that cause them are unclear. Though erosion and nondeposition can rarely be differentiated in the stratigraphic record, potential hiatus producing processes can be suggested. One such mechanism for creating a hiatus is dissolution of calcium carbonate from beneath the sediment water interface, which would be controlled by pore water diffusion.

Studies conducted for the Deep Sea Drilling Project (DSDP) allow high resolution dating of sediment cores from many locations in the Atlantic. The SYNATLAN database contains Atlantic sites that have been dated for 0.5Ma intervals and was developed by Wolf-Welling et al (1997), appendix 1. Sites

chosen from this database focus on deposits on oceanic crust in water at least 4000m deep to ensure that they are well below the CCD. Also, the physiographic feature of each location was considered for eliminating those not in the pelagic basin. Age-depth relationships from the selected sites were used to

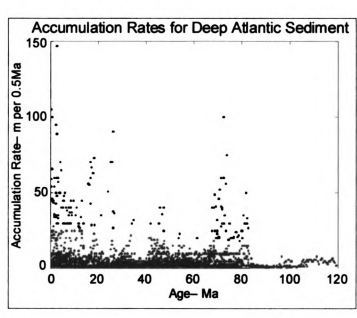


Figure 1.1. Accumulation Rates for 35 DSDP site on Atlantic oceanic crust under at least 4000m of water. Rates are calculated from SYNATLAN database (Wolf-Welling et al 1997), which has depths for 0.5Ma increments.

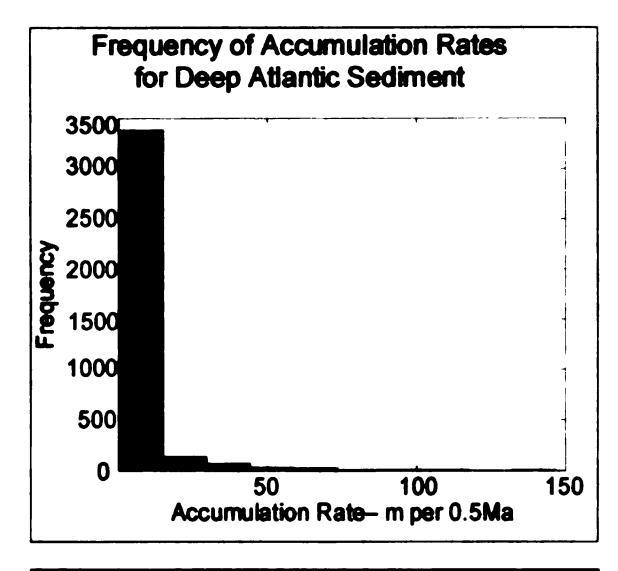


Figure 1.2. Frequency of accumulation rates for 35 DSDP site in the Atlantic on oceanic crust in under at least 4000m of water. Mode is 0 m per 0.5Ma with 888 out of 3622 values.

calculate accumulation rates
(thickness per unit time) (figure 1.1).
Hiatuses are indicated by values of
zero. Figure 1.2 shows the frequency
of these rates; 888 of the 3622, nearly
1/4, of the values are zero. The
average accumulation rate is 4.5m,
and the mean without the hiatuses is
6.0m. Hiatus duration in the Atlantic
ranges from 0.5Ma to greater than

100Ma (Wolf-Welling 1999, Ehrmann and Thiede 1985).

Physical processes and conditions in the oceans indicate that sediment should be continuously raining down to the sea floor (Thurmann 1994).

Carbonate particles settle through the water to the carbonate compensation depth, though they do not deposit on seafloor that is deeper than the CCD.

Windblown clay particles are laterally continuous across the oceans and typically deposit at a rate of 1mm/1000yr (Thurmann 1994) to 3mm/1000yr (Ehrmann and Thiede 1985), though much smaller rates will also be evaluated. These rates result in 1 to 3 meters per Ma producing recognizable thickness of sediment.

Despite theoretically continuous deposition, erosion mechanisms are limited. A major change in ocean water composition to chemically erode sediment should result in a hiatus that is spatially continuous. There is no time period in the Atlantic record that shows basin-wide hiatus. The thickness of

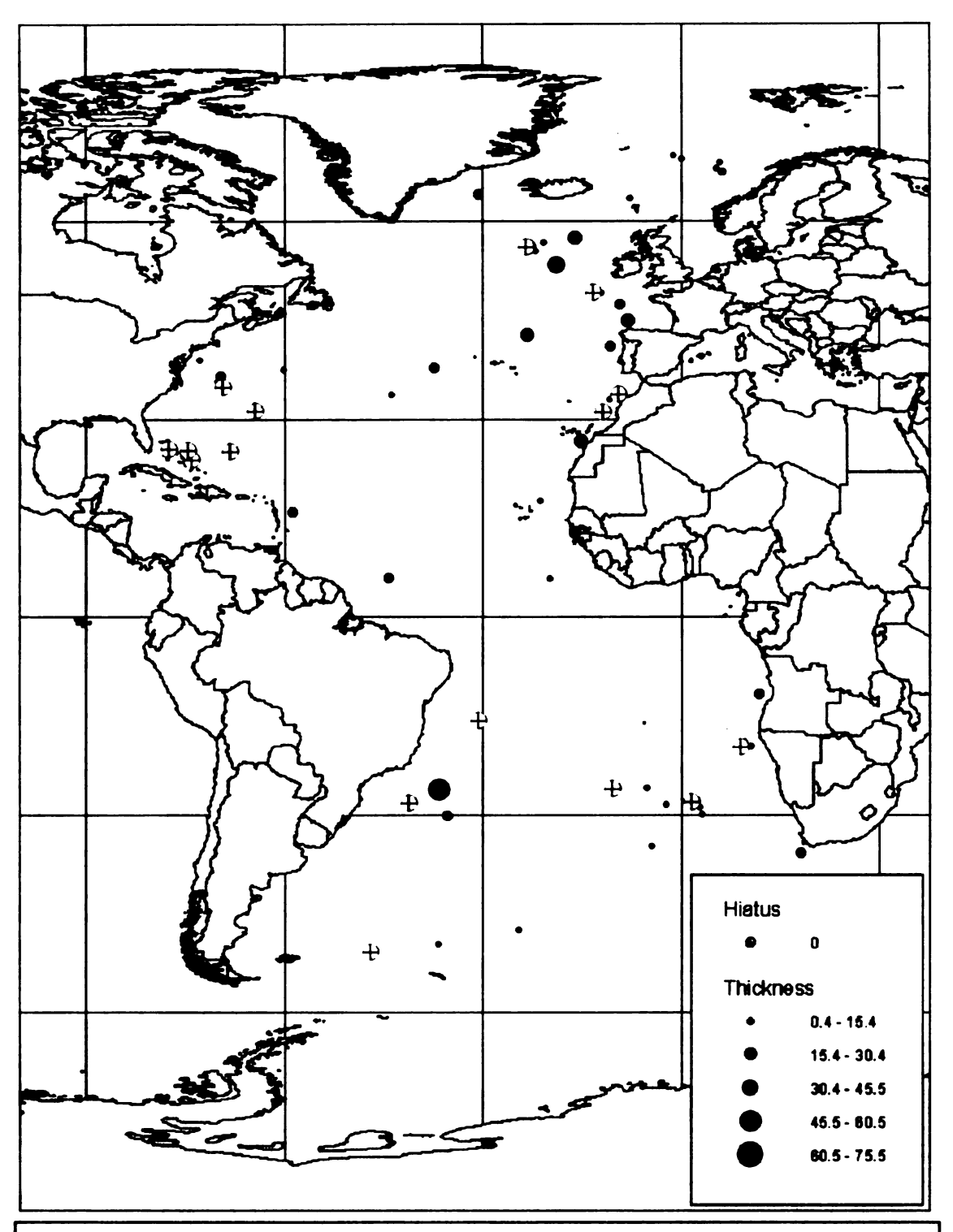


Figure 1.3. Sediment accumulation for all SYNATLAN sites with dating between 18 and 20Ma. Thickness is the total sediment between 18 and 20Ma. Indicated hiatuses are locations with zero thickness for the entire period.

sediment for 18 to 20Ma is shown in figure 1.3, and the accumulation rates compiled for all sites (figure 1.1) show no time period without accumulated sediment. Also, each site shows variation in accumulation rate through time.

Sediment for site 513 is shown in figure 1.4. The resolution of dating is 0.5Ma.

so accumulation is meters per 0.5Ma increment, which varies from zero to greater than 35. This pattern is apparent throughout the Atlantic (figure i.2, appendix I), and the periods of hiatus and sediment presence do not coincide across the sites (figure 1.1).

Deep ocean currents could cause mechanical erosion, but flow is slow with regard to physically moving sediment

(Ehrmann and Thiede 1985). Also, currents could not explain why hiatuses happen throughout the Atlantic. Even

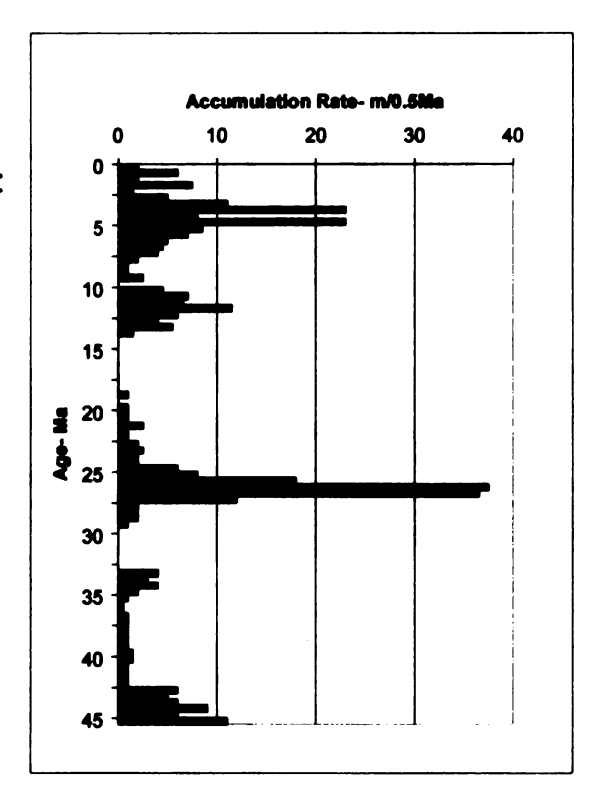


Figure 1.4. Sediment accumulation for site 513. Temporal resolution is 0.5Ma and accumulation is shown as meters per 0.5Ma increment.

though flow patterns may vary, hiatuses from currents should be confined to portions of the seafloor. The DSDP and SYNATLAN sites span the Atlantic (figure i.1, appendix 1) and values of zero accumulation occur at nearly all of the SYNATLAN sites (Wolf-Welling et al 1997). The selected deep ocean sites which have at least one hiatus (figure 1.5) are spread throughout the Atlantic (except for areas without data).

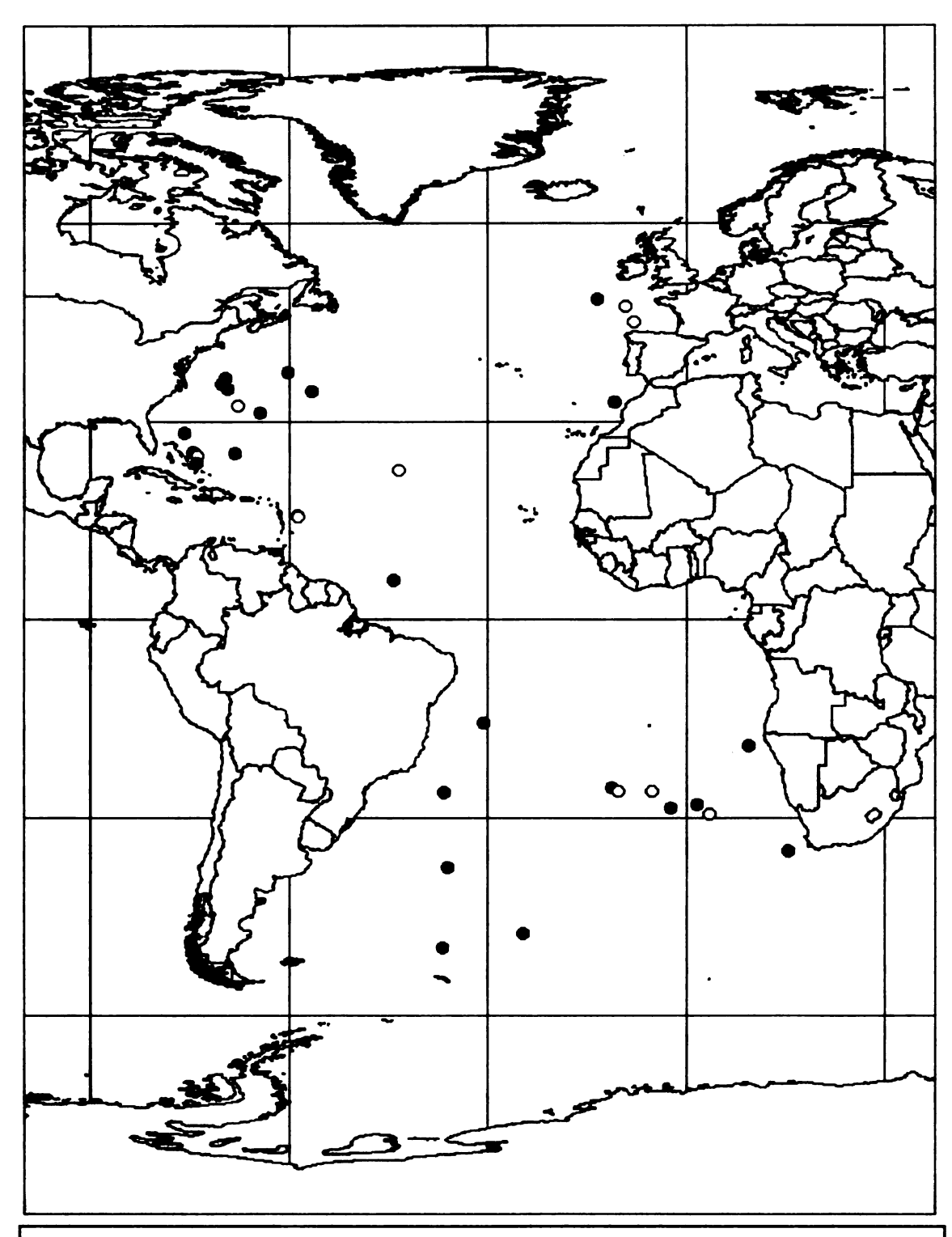


Figure 1.5. SYNATLAN sites selected as carbonate sediment on oceanic crust under at least 4000m of water. Solid circles indicate that at least one hiatus was found at the site, and open circles are locations where no hiatus was measured.

The incompleteness of the sediment record has been studied by many researchers. Garrels and Mackenzie (1971) looked at the mass-age distribution of global sediment and attributed the decrease in sediment with age to higher probability of erosion with increasing time. This is more appropriate for the terrestrial sediment which dominated their study. Veizer and Jansen (1985) studied oceanic sediment and attributed the reduction in sediment with age to subduction of oceanic crust, but this does not explain lack of sediment on existing ocean floor. Sadler and Strauss (1990) observe that accumulation rate decreases with longer time period of measurement. They attribute this to unsteady deposition, but do not address zero accumulation. Moore et al (1978) investigated the frequency of hiatuses through time in the ocean basins, and assert that variation is due to changes in boundary conditions of the basins. Proposing that rate of supply relative to the rate of removal determines accumulation, they refer to the "corrosiveness" of the bottom water. This is the potential of the water to chemically erode carbonate and depends on advection and the chemical nature of the solution. They do acknowledge the presence of clay residue, but assume active dissolution of the sediment takes place.

The potential mechanism of sediment removal by dissolution can be evaluated by considering the system dynamics. Below the CCD, bottom water is undersaturated with respect to calcium carbonate, but the sediment surface should be covered by pelagic clay, preventing dissolution directly from the sediment-water interface. Below this interface, ions from breakdown of CaCO₃ have to travel through the pore water away from grain surfaces. Saturation

would be reached before significant removal of sediment, then further dissolution would be limited by diffusion toward the undersaturated overlying water. To explore this, a numerical model was created to calculate how much sediment could be dissolved in a reasonable time scale.

The Model Relationships

To simulate dissolution from carbonate sediment of the deep Atlantic, a one-dimensional model was developed. Conceptually, the carbonate particles at depth should equilibrate with the pore water creating a saturated solution.

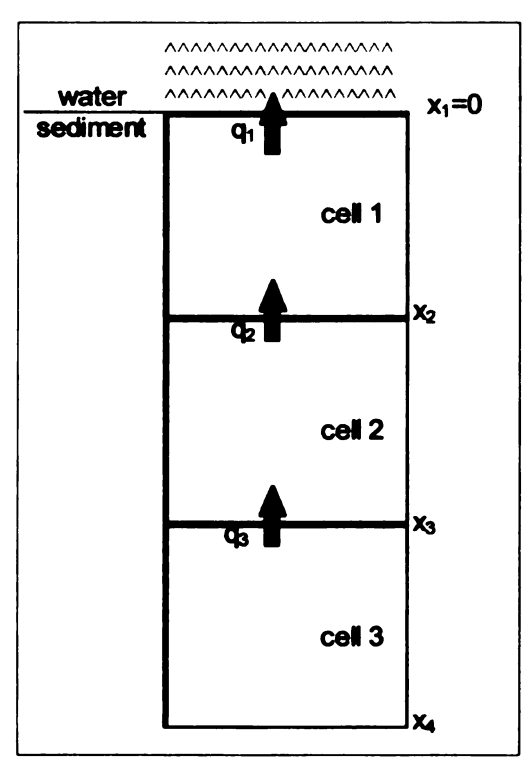


Figure 2.1. Setup of one dimensional diffusion model. x= depth, q= flux.

Because deep Atlantic bottom water is undersaturated with respect to CaCO₃, Ca²⁺ will diffuse from the sediment toward the sediment-water interface. Shown later, the rate that carbonate could dissolve in open water is much faster than Ca²⁺ can diffuse out of the sediment, so diffusion should be the limiting mechanism. Though other processes such as mineralization of organic matter may influence this system, the simple diffusion of ions from CaCO₃ will be examined. Adding other features would

confuse the importance of this particular process.

One consequence of conceptual model is that dissolution is greatest near the sediment-water interface. The result is that this mechanism could only create a hiatus at the sediment surface. To generate a hiatus within the column, deposition would have to resume and bury the eroded sediment.

Depth is represented as x, with zero as the sediment-water interface and positive values below that. Each cell is delineated as the space between arbitrarily defined depths (figure 2.1). Using Fick's first law:

$$q = D \cdot \frac{\partial C}{\partial x}$$

q =flux- mass/area*time
D =diffusion coefficient- area/time
C =concentration- mass/volume
x =depth- length

the flux at each depth is calculated.

Then, the change in mass for each cell can be calculated according to mass balance:

2.2
$$\triangle moles(cell_n) = q_{n+1} - q_n$$

Assuming that no other solid phase contributes to the calculated flux, the change in mass represents the change in amount of calcium carbonate in the sediment of that cell.

The concentration with depth is estimated using the form (Adler et al 2000):

2.3
$$C(x) = C_{\text{max}} - (C_{\text{range}} \cdot e^{-k_c \cdot x})$$

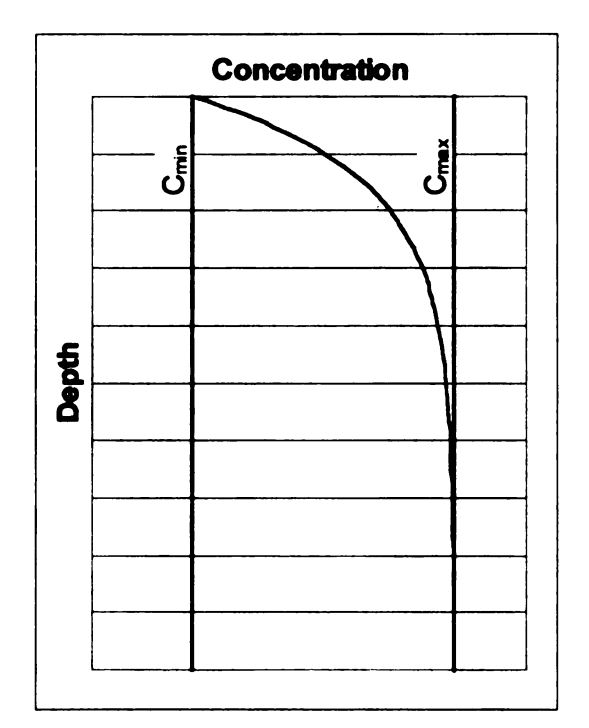


Figure 2.2. Form of concentration with depth:

$$C(x) = C_{\text{max}} - (C_{\text{range}} \cdot e^{-k_c \cdot x})$$

C_{min} =maximum concentration- mass/volume
C_{min} =minimum concentration- mass/volume
C_{range} =C_{max}-C_{min} -mass/volume
k_c =concentration constant- 1/length

Using C_{max} and C_{min} allows the calculated concentration to be constrained within a measured range (figure 2.2). Here, C_{min} represents the concentration in the water at the sediment-water interface, and C_{max} represents the steady state concentration approached at depth. The concentration constant,

 k_c , controls how quickly the concentration reaches C_{max} with increasing depth. The derivative of this form of C(x) is :

2.4
$$\frac{\partial C}{\partial x} = k_c \cdot C_{range} \cdot e^{-k_c \cdot x}$$

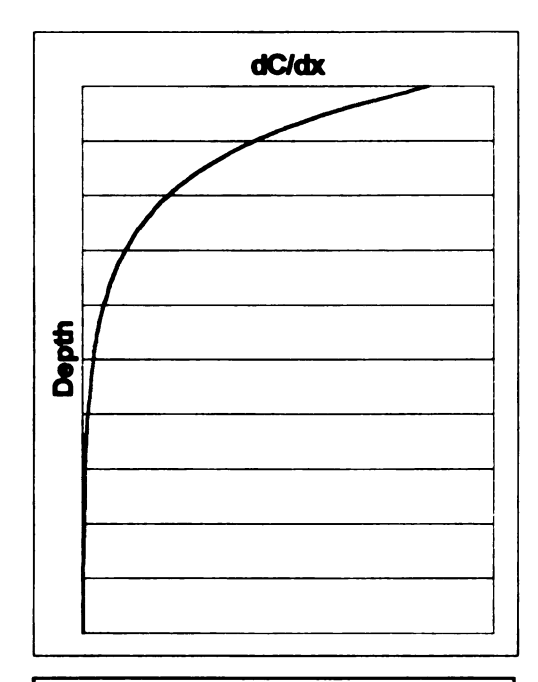


Figure 2.3. Form of concentration gradient with depth:

$$\frac{\partial C}{\partial \mathbf{x}} = \mathbf{k}_c \cdot C_{range} \cdot e^{-\mathbf{k}_c \cdot \mathbf{x}}$$

and yields reasonable values. For instance, as $x \to \infty$, $\frac{\partial C}{\partial x} \to zero$; this simulates diffusion reaching equilibrium at depth. Also, as $x \to zero$, $\frac{\partial C}{\partial x}$ does not go to ∞ , as some functions do.

The second term in Fick's first law is the diffusion coefficient. The diffusion coefficients for particular ions in infinitely dilute solutions, D°, have been well documented. Temperature has a significant

effect on diffusion because it determines how quickly ions move; colder temperatures result in slower movement, reflected in a smaller coefficient (Boudreau 1997):

D°=infinite dilution diffusion coefficient

2.5
$$D^{\circ} = (m_o + m_1 \cdot T) \cdot 10^{-6} \, cm^2 \, sec^{-1}$$

The diffusion coefficient in sediment pore

D°=infinite dilution diffusion coefficient mass/time m₀=linear regression constant 1 m₁=linear regression constant 2 T =temperature in °C

water, D_s, needs to account for the volume of water and the tortuosity. Since the ions travel within the solution and the volume is no longer 100% solution, porosity can be used to adjust D°. Highly tortuous sediment leads to difficulty for ions to

diffuse due to the longer paths of travel; tortuosity being the actual length of the sinuous diffusion path divided by the straight line distance between its ends. This also reduces diffusion and the coefficient. A diffusion coefficient modified for sediment is (Drever 1982):

$$D_s = \frac{D^o \cdot p}{\tau^2}$$

The problem is that obtaining an independent value for tortuosity is unfeasible. Measuring it is impractical, and its expected variation is large even at short distances. Fortunately, Adler et al (2000) formulated an empirical relationship for D_s sediment as a function of porosity in oceanic carbonate sediment:

$$D_s = \frac{D^o}{1 - \ln(p^2)}$$

This makes porosity necessary to calculate the sediment diffusion coefficient.

The form of the porosity function (Adler et al 2001):

$$p(x) = p_{\min} + p_{range} \cdot e^{\frac{-x}{k_r}}$$

D_s=diffusion coefficient in sediment mass/time τ =tortuosity p =porosity

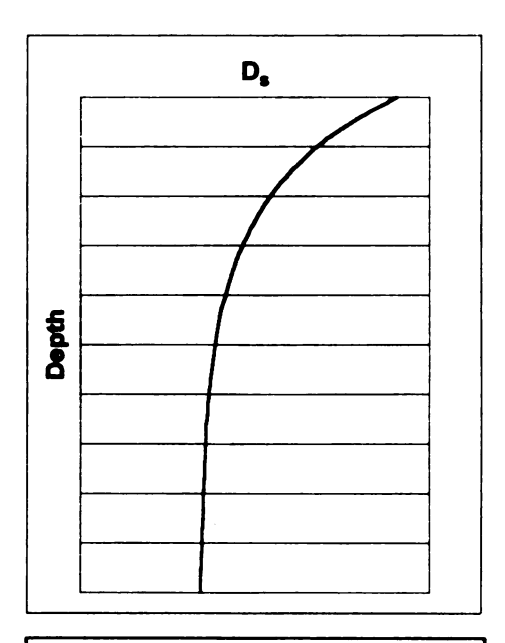


Figure 2.4. Form of the diffusion coefficient in sediment pore water with depth:

$$D_s = \frac{D^o}{1 - \ln(p^2)}$$

Prance = Presc Print

k_o =porosity constant- length

is similar to the concentration function, but is altered because porosity becomes less with depth. Therefore, p_{mex} represents the porosity nearest the sediment-water interface, and p_{min} represents the final porosity approached at depth.

Returning to Fick's First Law, and applying it to sediment gives:

$$q_s = D_s \cdot \frac{\partial C}{\partial x}$$

q_e =flux through solution in sediment mass/area*time

Substituting equation 2.7 yields:

2.10
$$q_s(x) = \frac{D^o}{1 - \ln(p(x)^2)} \cdot \frac{\partial C(x)}{\partial x}$$

Expanding the function using equations 2.4 and 2.8 provides:

2.11
$$q_s(x) = \frac{D^o}{1 - \ln\left[\left(p_{\min} + p_{range} \cdot e^{\frac{-x}{k_r}}\right)^2\right]} \cdot k_c \cdot C_{range} \cdot e^{-k_c \cdot x}$$

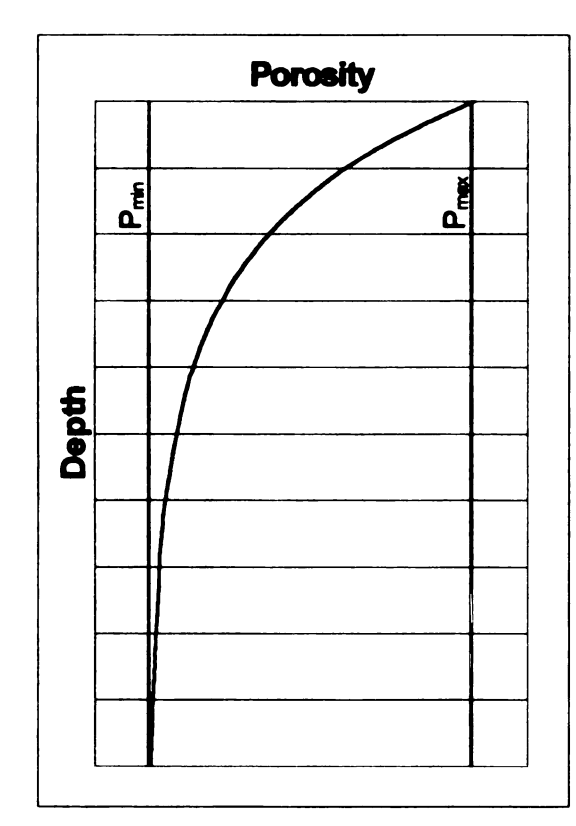


Figure 2.5. Form of porosity with depth: $p(x) = p_{\min} + p_{range} \cdot e^{\frac{-x}{k_p}}$

Using this equation, the flux from calcium carbonate at each depth can be determined allowing calculation of the change in thickness of sediment layers.

Bounding surfaces, arbitrary layer boundaries, are set at the beginning of the model. The top surface is initially zero, the sediment-water interface, but it deepens due to pelagic clay deposition. For the layers, the flux through each surface is used to find the change in mass. The change in mass is translated into change in thickness and the new

depth of each surface is calculated. Since only the carbonate is dissolving, the minimum thickness of each layer is controlled by the initial percent carbonate of the sediment. The depth of the surfaces tracked through time shows the reduction of the layers. These relationships and equations were then translated into numerical code used in MATLAB.

The Numerical Model

The initial, time=0, depths of the bounding surfaces are defined in vector b which is entered in line 3 of the model code. Line 4 defines this vector as lastdep. At each time step, lastdep is used as the depths of the bounding surfaces from the previous time step. Lines 1 and 2, are comments that do not affect the calculations; this is shown by the % which precedes the text. Line 5 initiates the calculation of the minimum thickness for each layer using an average percent carbonate for the sediment column, see appendix IV for details.

Before the flux can be found, several constants need to be defined. In line 7 the p_{mex} , p_{min} , and k_p , are defined for the porosity function, equation 2.8; the numerical values will be discussed later. The numbers for the concentration gradient function, equation 2.4, are defined in line 11. D^o is set forth in line 15.

The model constructs a matrix called **final**, which records the depth of every surface at all time steps (figure 3.1). Each column of the matrix represents the depths of the bounding surfaces at a particular time step. From left to right across the matrix, indexed by *y*, proceeds from time=0 to time=final. Each row of

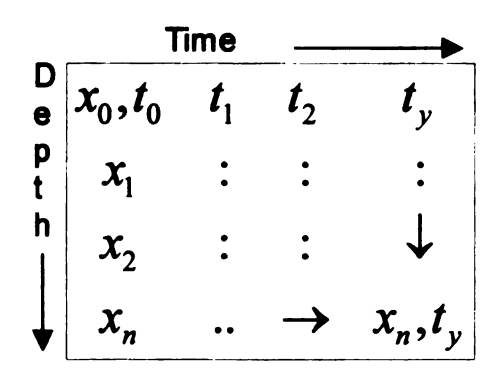


Figure 3.1. The setup of matrix final

the matrix represents a single bounding surface through time. Down the rows of the matrix, indexed by n, moves down the sediment column. For example, the location of n=3 and y=8 represents the depth of the third bounding surface from the sediment-water interface after seven time steps. The first

```
%core has b. a vector of original depths
   %b is a vector of depths in oceanic carbonate sediment
   load core50cm
 4 lastdep=b:
   cpercent%this performs the minimum thickness calculation for b
   %porosity parameters, p(x)=Pmin+(Pmax-Pmin)e^(-d/kp)
   Pmax=0.750; Pmin=0.585; Prange=Pmax-Pmin; kp=36.4;
 8
   %units: none, none, m
10 %Concentration parameters, dC/dx=k*(Cmax-Cmin)e^(kd)
11 Cmax=24.2;Cmin=1.78;Crange=Cmax-Cmin;kc=2.75*10^-3;
12 %units: mol/m^3, mol/m^3, mol/m^3, 1/m
13
14 %Diffusion coefficient in dilute solution
15 Do=1.701*10^2;%units: m^2/10000yr
16
17 Wifinal will be a matrix of depths of the layers, each column represents a time step
18 final(:,1)=b;
19 n=length (b);
20
21 %iy counts time steps, each time step is 10000 yr
22 for iy = 1:10000
23
     %initial first depth, then add 3mm/1000yr (0.0003m/100yr) for burial by clay
24
     final(1,iy+1)=b(1)+0.03*(iy);
25
        for ia =1:n
26
          x=lastdep(ia):
27
                %flux calculates the amount of flux upward as mol/m2*100yr
28
          flux(ia)=(Do*kc*Crange*exp(-kc*x))/(1-log((Pmin+Prange*exp(-x/kp))^2));
29
30
31
   %the dissolution can then be calculated: flux out-flux in=dissolution
32
        %first term calculates the dissolution for that laver
33
        %the second term converts mol/m2*10^5vr to m/10^5vr w/ density, gfw & porosity
34
        for ib =1:n-1
35
          P=Pmin+Prange*exp(-lastdep(ib+1)/kp);
36
          dissolve(ib)=(flux(ib+1)-flux(ib))/((2.7*10^4)*(1-P));
37
        end
38
        %change in thickness is shorter than depth vector
39
        for ic =1:n-1
          newthick=lastdep(ic+1)-lastdep(ic)+dissolve(ic);
          if newthick<minthick(ic)
             final(ic+1,iy+1)=final(ic,iy+1)+minthick(ic);
          final(ic+1,iy+1)=final(ic,iy+1)+newthick;
45
          end
46
        end
        lastdep=final(:,iy+1);
47
48 end
```

Figure 3.2. The MATLAB code

b	= vector of initial depths of bounding surfaces defined by modeler
lastdep	= vector of depths of bounding surfaces from the previous time step reset with each time step
final	= yxn matrix of depths of bounding surfaces at every time step model output
y	= number of time steps defined by modeler
iy	= matrix index of time step proceeds from time 1 to y during the model
n	= number of bounding surfaces defined by vector b
ia	= vector index of bounding surfaces for calculating flux proceeds from depth 1 to n during each time step
flux	= vector of flux values at bounding surfaces for current time step recalculated in each time step
ib	= vector index of cells for calculating amount dissolved proceeds from cell 1 to n-1 during each time step
dissolve	= vector of thickness removed from each cell for current time step recalculated in each time step
ic	= vector index of cells for calculating thickness proceeds from cell 1 to n-1 during each time step
newthic	k = thickness of current cell for current time step recalculated for each cell within every time step

Figure 3.3. The model variables

column of matrix final contains the initial depths, making the second column the results after the first time step.

In line 18, the first column of matrix **final** is formed from vector **b**, which consists of the initial depths of the bounding surfaces. The variable n, line 19, is defined as the number of bounding surfaces, or the number of values in **b**. The size of each time step is controlled by the units from the constants. D^o is calculated in $m^2/10^4$ yr; therefore, the time step is ten thousand years. The number of time steps is set in line 22; this model goes to 10^8 years.

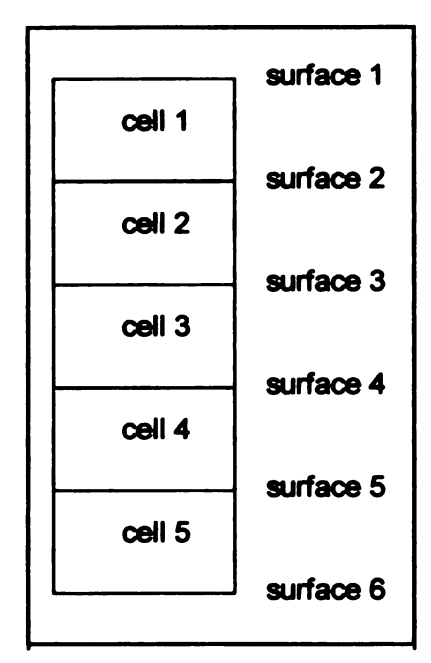


Figure 3.4. Location of the bounding surfaces and cells in the model.

The first row of matrix **final** is defined in line 24. It starts with the initial value of the top depth from vector **b**. A deposition rate of 3mm/1000yr is added to this (Ehrmann 1985). Since the time step is 10^4 years and length is meters, $3 \cdot 10^{-2} \frac{m}{10,000 \, yr}$ is used. Every time step uses the initial value, **b**(1), then adds the deposition rate multiplied by the number of the time step.

Lines 25 through 29 create a vector of flux values at the bounding surfaces within each time

step. First, line 25 establishes the steps down the sediment column; for each value of ia, from 1 to n, the calculation in lines 26 through 28 will be performed. To compute the flux for each surface, the depth of that surface from the previous time step is used, line 26. Depth, x, is taken from vector **lastdep** which contains the depths of all the bounding surfaces from the preceding time step. Then in line 28, x is used to calculate the flux for that surface by applying equation 2.11. The end statement in line 29 forces the model back to line 25 and through the flux calculation until all surfaces are finished for that time step.

Beginning with line 34, the computations transition to using cells instead of bounding surfaces. Index *ib* counts from cell 1, bounded by surface 1 and 2, (figure 3.4) until cell *n*-1, which is bounded by surface *n* at the bottom. In line 36, the flux out of the cell is subtracted from the flux into the cell, giving the change in

moles, equation 2.2. The change in moles of CaCO₃ is then converted to change in thickness utilizing gram formula weight and density:

3.1
$$\left(\Delta CaCO_3 \frac{mole}{m^2 \cdot 10^4 \, yr} \right) \cdot \frac{100g}{mole} \cdot \frac{m^3}{2.7 \cdot 10^6 \, g} = \frac{\left(\Delta CaCO_3 m / 10^4 \, yr \right)}{2.7 \cdot 10^4}$$

This change in thickness would be appropriate if the sediment was solid carbonate, but porosity needs to be accounted for. This is done by dividing by the percent sediment. For example, if 1mm of solid is removed, but the sediment has 75% porosity, then:

$$3.2 1mm \cdot \frac{1}{0.25} = 4mm$$

4 mm of sediment was actually eliminated. This is the reason for the final term, (1-p), in line 36.

Now that the thickness removed is known, the new depths of the bounding surfaces can be determined. Each cell's new thickness is calculated by using its previous thickness and adding the change in thickness:

3.3 NewThickness =
$$Pr$$
 eviousThickness + Δ Thickness

3.4 NewThickness =
$$(Pr\ eviousBottom - Pr\ eviousTop) + \Delta Thickness$$

This is accomplished in line 40. Note that *∆thickness* will be negative, resulting in reduction of the cell. Lines 41 and 42 ensure that a cell cannot dissolve more carbonate than it contains. If the computed thickness is less than the non-carbonate thickness, the model assigns the depth as the surface above plus the minimum thickness calculated from the percent carbonate. Otherwise, the model assigns the new depth by adding the cell's thickness to the surface at the top of the cell. For example, in cell 3 at time 1, *ic*=3 and *iy*=1. The bottom of the cell,

lastdep(4), and the top of the cell, lastdep(3), from the previous time step are used as the previous thickness. The previous thickness plus the change in thickness for cell 3, dissolve(3), equals the cell thickness after the first time step. Looking at line 44, the bounding surface at the top of cell 3 for the current time step is found in matrix final, row 3, column 2, or final(ic, iy+1). By adding the thickness of the cell, the depth of the bottom bounding surface is found and placed in matrix final, row 4, column 2. The end statement in line 46 sends the model back to line 39 to calculate the next deeper cell. Note that the depth of surface 1 is defined earlier by using pelagic accumulation rate in line 24, allowing the first row value, final(1,2), to be known.

Once all of the bounding surfaces for the current time step are calculated, the vector **lastdep** is redefined before the next time step. The current time step filled column *iy*+1 of matrix **final**; line 47 traces that column to reset the values of **lastdep**. The final end statement sends the model to line 22 to compute the next time step.

Assumptions

To create a model that focuses on simple diffusion, certain assumptions must be made. The system must be in a state that makes diffusion the primary transport mechanism. Limitations on the transport of the sediment and pore water are necessary. Plus, the influence of other ions in the system needs to be negligible. Particular characteristics are also necessary to generalize from the Ca²⁺ ion and its measurements. Finally, the mineralogy and lateral variation of the sediment needs to be consistent.

Equilibrium of the calcium carbonate with the pore water must occur if dissolution is not limited by the rate of surface reaction. Then, the overlying water needs to have a lower concentration of Ca²⁺ for it to diffuse toward the sediment-water interface. The gradient of lower Ca²⁺ toward the overlying water is shown by DSDP measurements (figure 5.1) which will be discussed with the

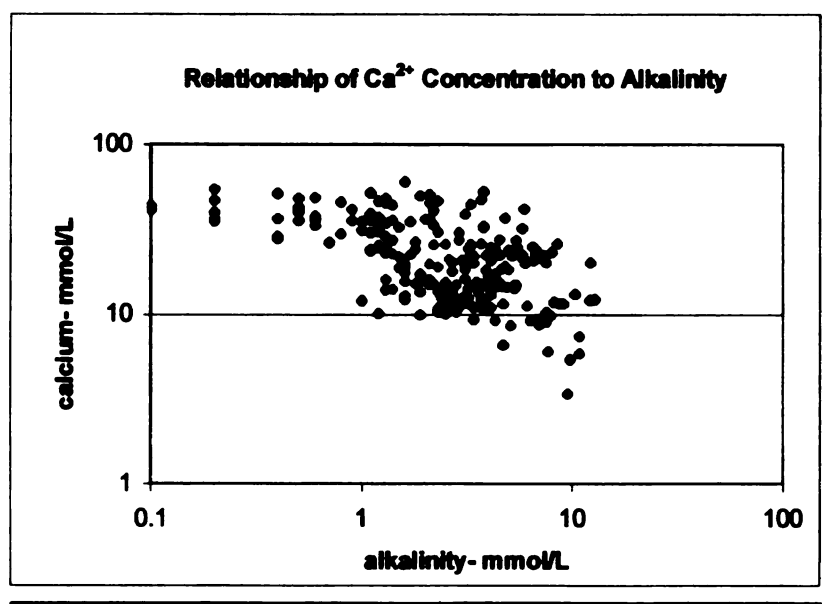


Figure 4.1. Comparison of alkalinity to calcium concentration in pore water of carbonate sediments from DSDP.

The lower

concentration of Ca²⁺

in the sediment pore

solution seems to be

balanced by alkalinity

to account for

equilibrium with respect

to calcium carbonate.

Comparison of

parameter estimation.

alkalinity to Ca²⁺ concentration (figure 4.1) suggests an inverse relationship; as one of these ions increases, the other ion decreases. The correlation does not appear strong, but the measurements come from several locations and various depths. Plus, the dynamics of inorganic carbon are complex, and may interfere with the Ca²⁺-alkalinity relationship.

For molecular diffusion to be the primary means of transport, advection must be negligible. This is justifiable for deep Atlantic sediment because the lateral variation in hydraulic head is minute relative to its value. The lack of advection results in a lack of mechanical dispersion, leaving diffusion as the main transport mechanism. Since molecular diffusion is the primary transport process, the assumption in Fick's law of Gaussian distribution is probably not critically violated. Brownian motion of diffusing molecules in solution will result in a normal distribution. If advection was present, it would increase dissolution and introduce mechanical dispersion. Also, the rate of transport due to advection is much greater than diffusion, and the CaCO₃ would probably not reach equilibrium with the pore water.

As the sediment is buried by pelagic clay, the porosity is reduced. The change in pore space results in expulsion of water, leading to slight advection of pore solution toward the sediment-water interface. A sample calculation of the amount of Ca²⁺ carried by this mechanism examines the importance of it relative to molecular diffusion. A cell at the sediment-water interface initially 0.01m thick was chosen because it is located where the porosity gradient us high. Plus, clay deposition in one time step (10,000yr) will deepen the cell 0.03m, more than its

original thickness. This setting should show the greatest influence of pore water movement. Calculations (table

removed by advection is four	4.1) show that the Calcium				
•	removed by advection is four				

	Initial	Final
Porosity	0.75	0.7499600
Thickness- m	0.01	0.0099999
Pore Volume- m ³	0.0075	0.0074995
Change in water volum	e- m³	4.77E-07
Calcium concentration-	mol/m ³	0.125
Ca ²⁺ removed by advec	ction- mol	5.96E-08
Ca ²⁺ removed by diffus		6.94E-04

Table 4.1. Sample calculation of effect of advection due to reduction in porosity.

orders of magnitude less than Ca²⁺ removed by molecular diffusion.

Dispersion of sediment and water due to bioturbation is ignored in the model, too. In a study of deep-sea carbonate sediment, Kier (1984) investigated anomalous isotope dates, showing that bioturbation could explain the problem by mixing older sediment with more recent deposits. She used a bioturbation coefficient of $200\frac{cm^2}{ka}$; this converts to $0.2\frac{m^2}{10^4y}$. This is three orders of magnitude smaller than the diffusion coefficient for Ca²⁺ in sediment, which is greater than $100\frac{m^2}{10^4y}$ near the sediment-water interface. Like advection, bioturbation would increase dissolution by exposing sediment particles to the overlying undersaturated water.

To estimate the Ca²⁺ concentration gradient, a function of concentration with depth was formulated. This presumes that the concentration is at steady state and is not a function of time. Steady state condition is shown by the shape of concentration with depth (figure 5.1). If non-steady state conditions were present, the shape of the curve would be altered from uniform decrease in Ca²⁺

toward the sediment-water interface. For example, if microbes were altering the pore water chemistry to enhance dissolution or cause precipitation of Ca²⁺, the concentration would suddenly change at the range of depths where the microbes existed. Also, a spike in concentration at depth could indicate a non-uniform source of Ca²⁺ or lack of transport through the pore water.

The numerical values in the concentration function and its derivative were estimated using measurements of deep Atlantic sediment pore water from DSDP sites. For the gradient to be accurate, the measured Ca²⁺ needs to be proportional to the Ca²⁺ free in solution and any measurement error should be regular across samples. The actual value of concentration could be inaccurate by a consistent amount, and still produce an acceptable derivative. Graphically, this is equivalent to shifting the location of a curve, but not altering its shape; the change in concentration with depth will remain unaltered. The likeliest causes of measurement error are the change in pressure as the sediment is brought to the surface and the extraction of pore water from the core (World Data Center for Marine Geology & Geophysics 2000). The same conditions are experienced by all of the samples, so measurements should be consistent relative to each other. For the effective concentration to be relatively consistent, speciation of Ca²⁺ needs to be uniform with depth. The activity coefficient should not vary greatly with depth because the pore water at various depths is fairly similar, see sensitivity analysis.

Focusing on the concentration of Ca²⁺ also presumes that the electrical potential gradient caused by other ions does not significantly contribute to the

diffusion of Ca²⁺. "Diffusion in most pore waters in sufficiently like diffusion in dilute solution that we can normally ignore the complications arising from the multicomponent interactions" (Boudreau 1997). Boudreau supports this proclamation by deriving equations for the correction factor to the diffusion coefficient and showing that it is insignificant. The exception is when the main electrolytes (Cl⁻ and Na⁺) are involved, they need to be considered. Salinity measurements

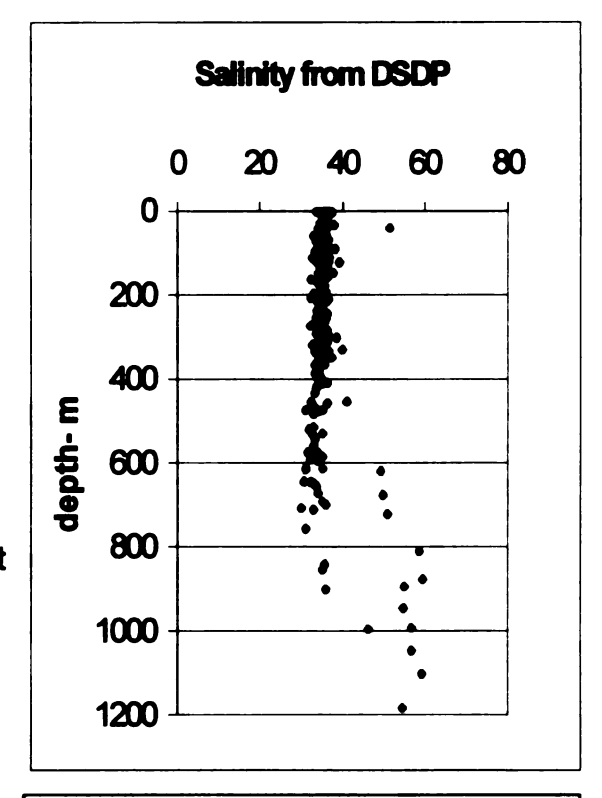


Figure 4.2. Measurements of salinity for DSDP sites in the deep Atlantic basin.

from deep Atlantic sediment pore water show the trend of the main electrolytes (figure 4.2). The values are rather consistent with depth and do not show an obvious trend (The data that deviate from the trend are almost exclusively from one site).

Moles of Ca²⁺ removed are equated to the moles of CaCO₃ dissolved from a cell. This assumes that there is no other contributor of Ca²⁺ to the pore water. Though clay minerals may interact with Ca²⁺, they are not included. Sorption, which incorporates absorption into the clay structure and adsorption to the surface, should be at equilibrium. The time step of the model, 10⁴yr, is much longer than the rate of cation exchange. Measurement of this rate in terrestrial clay sediment shows a half life of 2 to 3 seconds (Langmuir 1997). This disparity

is eleven orders of magnitude, so even though the mineral assemblage could be different for pelagic clay, cation exchange should be in equilibrium in 10,000yr.

This leaves carbonate as the supplier of Ca²⁺.

Finally, using a one dimensional model assumes that the sediment is laterally uniform. The processes influencing sediment deposition across the pelagic realm within an ocean are comparatively uniform relative to coastal or terrestrial depositional environments. Acknowledging that the sediment on the Atlantic crust should be fairly consistent allows conclusions to be drawn from the model. Recognizing the potential variation in sediment limits the generalizations made to other locations.

Parameter Estimation

The foundation of calculating transport by diffusion is Fick's first law, equation 2.1, which requires estimation of a diffusion coefficient and the concentration gradient. The concentration gradient can be determined by using the derivative of a concentration function if an analytical solution is possible. However, determining the diffusion coefficient for an ion in pore water solution is more complex. Departure from standard temperature conditions needs to be considered as well as the complications resulting from the surrounding sediment. Tortuosity affects the rate of diffusion and is nearly impossible to characterize. This makes an analytical solution impossible, demanding a more empirical

approach.

Measurements of pore water

chemistry in deep Atlantic sediment are
available from the Deep Sea Drilling

Project (World Data Center for Marine
Geology & Geophysics 2000). The Ca²⁺
ion is used instead of alkalinity because of
the complex relationships involved in the
thermodynamics of inorganic carbon.

Unlike alkalinity, moles of Ca²⁺ can be
equated to moles of CaCO₃ dissolved,
see assumptions. Of the sites that are on

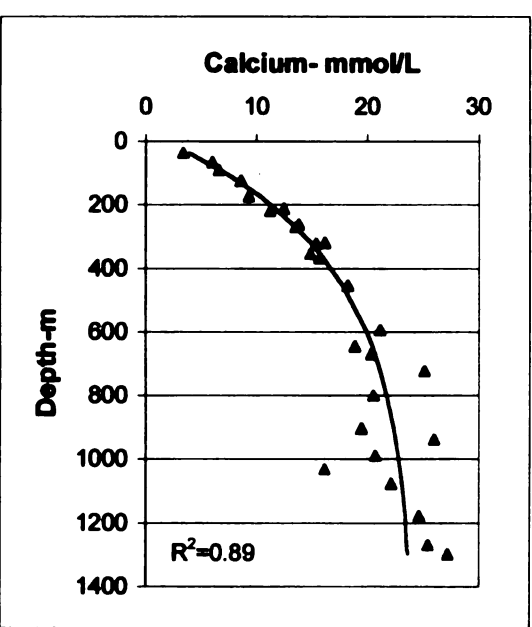


Figure 5.1. Measurements of pore water Ca^{2+} concentrations in mmol/L for site 603. The solid line represents the fitted function: $Ca^{2+}(x) = 24.2 - \left(22.42 \cdot e^{-0.00275 \cdot x}\right)$

oceanic crust, pore water Ca²⁺ is available for 29 locations, appendix II. Site 603

lies under 4633 meters of water and has the most measurements available, so its values were used for calibrating the concentration function, equation 2.3. Shown in figure 5.1, the resulting equation is:

$$C(x) = C_{\text{mex}} - (C_{\text{range}} \cdot e^{-k_c \cdot x})$$

$$C_{\text{mex}} = 24.2 \text{ mol/m}^3$$

$$C_{\text{min}} = 1.78 \text{ mol/m}^3$$

$$C_{\text{range}} = 22.4 \text{ mol/m}^3$$

$$C_{\text{range}} = 22.4 \text{ mol/m}^3$$

$$k_c = 2.75 \cdot 10^{-3} \text{ m}^{-1}$$

$$E_{\text{range}} = 27.5 \cdot 10^{-3} \text{ m}^{-1}$$

The constants were found simultaneously by minimizing the squared residual values. The R² is 0.89, and the larger departures from the estimated values occur below 500m, which is the deepest modeled depth. The derivative, equation 2.4, is then:

$$\frac{\partial C}{\partial x} = 0.00275 m^{-1} \cdot 22.4 \frac{mol}{m^3} \cdot e^{-0.00275 m^{-1} \cdot x}$$

Determination of the diffusion coefficient for Ca²⁺ in the sediment pore water, D_s, begins with the coefficient in pure water, D^o. Here, all diffusion coefficients refer to Ca²⁺ since no other ions are used. The values of m_o and m₁, equation 2.6, are from linear regression for infinite dilution (Boudreau 1997, p. 115):

$$D^{o} = (m_{o} + m_{1} \cdot T) \cdot 10^{-6} cm^{2} \sec^{-1}$$

$$D^{o} = (3.60 + 0.179 \cdot 10) \cdot 10^{-6} cm^{2} \sec^{-1}$$

$$D^{o} = 5.39 \cdot 10^{-6} \frac{cm^{2}}{\sec}$$

$$D^{o} = 170 \frac{m^{2}}{10,000 yr}$$

Though temperature may vary down the sediment column, a single temperature is used. Variation by several degrees leads to less change in D_s than will be introduced for sensitivity analysis of D_s. This D^o is appropriate for open water and needs to be adjusted for sediment effects. The only additional information necessary for the empirical relation of equation 2.7 is porosity.

Adler et al (2001) used a function, equation 2.8, for porosity with depth in Pacific carbonate sediment, which was formulated by Rabouille and Gaillard (1991). The form of this relationship retains many of the physical characteristics of porosity. The exponential component controls the overall shape of the curve, which shows a regular reduction with depth. The magnitude of the porosity

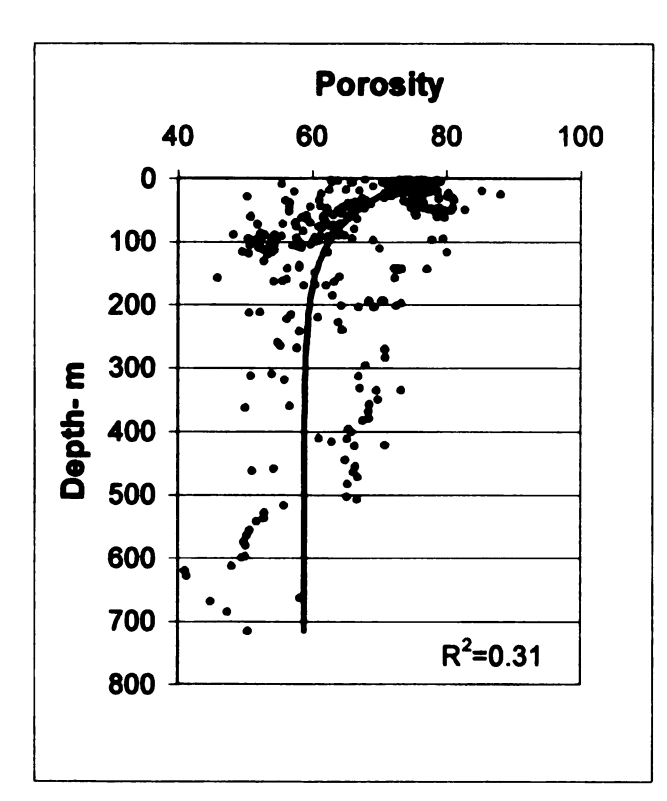


Figure 5.2. Measurements of porosity for DSDP sites in the deep Atlantic basin. The solid line represents the fitted function:

$$p(x) = 58.5 + 16.5 \cdot e^{36.4m}$$

constant, k_p , determines how quickly porosity reaches its minimum value. P_{max} and P_{min} constrain the curve between particular porosity values. Physically, P_{max} represents the initial porosity at deposition, and P_{min} is the porosity after compaction has reached its greatest influence. The magnitude of k_p shows how much burial is required to compact the sediment. The numerical values of the

constants were found using porosity measurements from deep Atlantic sediment, (figure 5.2 and appendix III):

$$p(x) = p_{\min} + p_{range} \cdot e^{\frac{-x}{k_p}}$$

$$p_{\min} = 0.750$$

$$p_{\min} = 0.585$$

$$p_{range} = 0.165$$

$$p_{range} = 0.165$$

$$p_{range} = 36.4$$

$$p(x) = 0.585 + 0.165 \cdot e^{\frac{-x}{36.4m}}$$

The DSDP measurements are based on density and water content, and they include nine sites and 197 values for carbonate sediment in the deep Atlantic basin. All of these were used to find the constants for equation 5.4 by simultaneously minimizing the squared residual values. The R² value is 0.31, which is much less than the R² for concentration. Some of the scatter can be attributed to using several sites, and the variation is evaluated in the sensitivity analysis.

Results

Calculations were performed on three hypothetical sediment packages.

Each started with layers of uniform thickness beginning at zero depth (table 6.1).

This allowed investigation of sediment removal at depth, while providing detail for the upper portion of the sediment column. Uniform thickness within each simulation allowed comparison of the amount dissolved from shallow and deep sediment.

# of Layers		
50	10	500
50	1	50
50	0.01	0.5

Table 6.1. Hypothetical sediment columns developed for model simulations.

Due to the pelagic clay deposition, the top surface was 300 meters deep at the end of all three simulations. The final depth of the deep column (table 6.2) was 797.52, showing a reduction of 2.48m from 500m of sediment over the 100Ma period. As seen in figure 6.1, the depth of the surfaces becomes greater through the simulation, but reduction in thickness is imperceptible on the graph. The change in thickness for several time steps is given in table 6.3, note that units are microns. The carbonate removal is greatest near the sediment-water interface and deteriorates with depth (figure 6.2 and table 6.3); this is controlled by the concentration gradient. The total reduction in thickness of each layer is shown in millimeters and follows the same trend. Over the 100Ma period 2476mm of sediment was dissolved from the 500m column. This matches the 2.48m from table 6.2.

The calculations for the intermediate column are shown in tables 6.4 and 6.5, and figures 6.3 and 6.4. The elimination of sediment is still greatest near the sediment-water interface, with the top layer reduced by 15mm over 100Ma. The

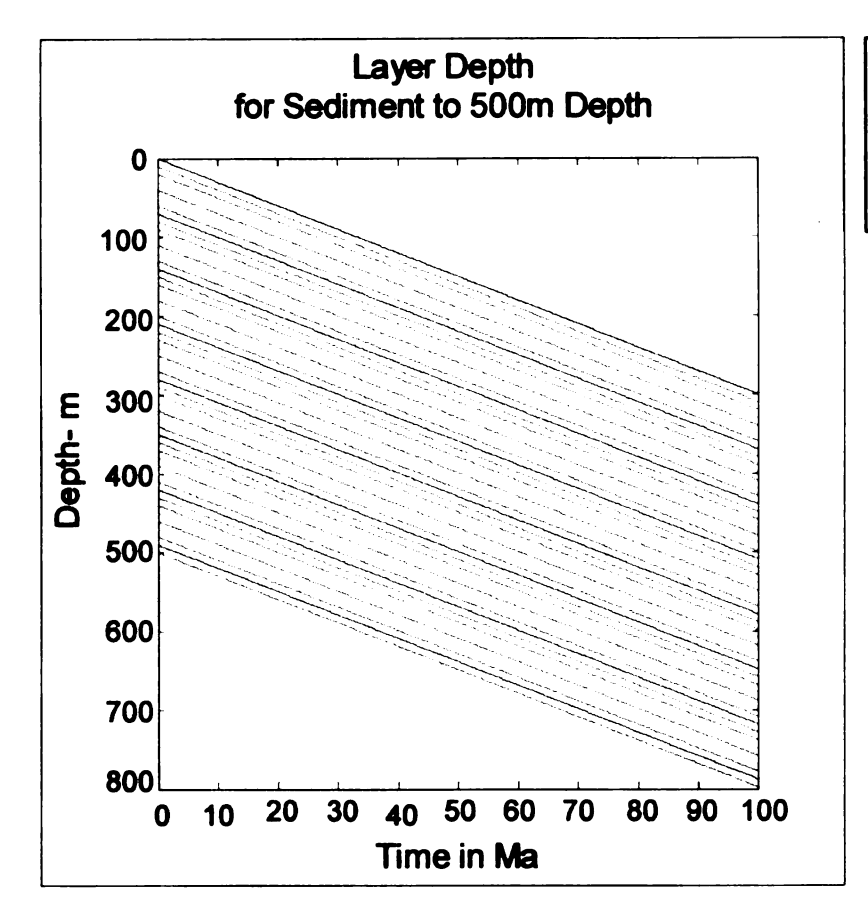


Figure 6.1. Depth of bounding surfaces for layers initially 10m thick to 500m depth through 100 million years.

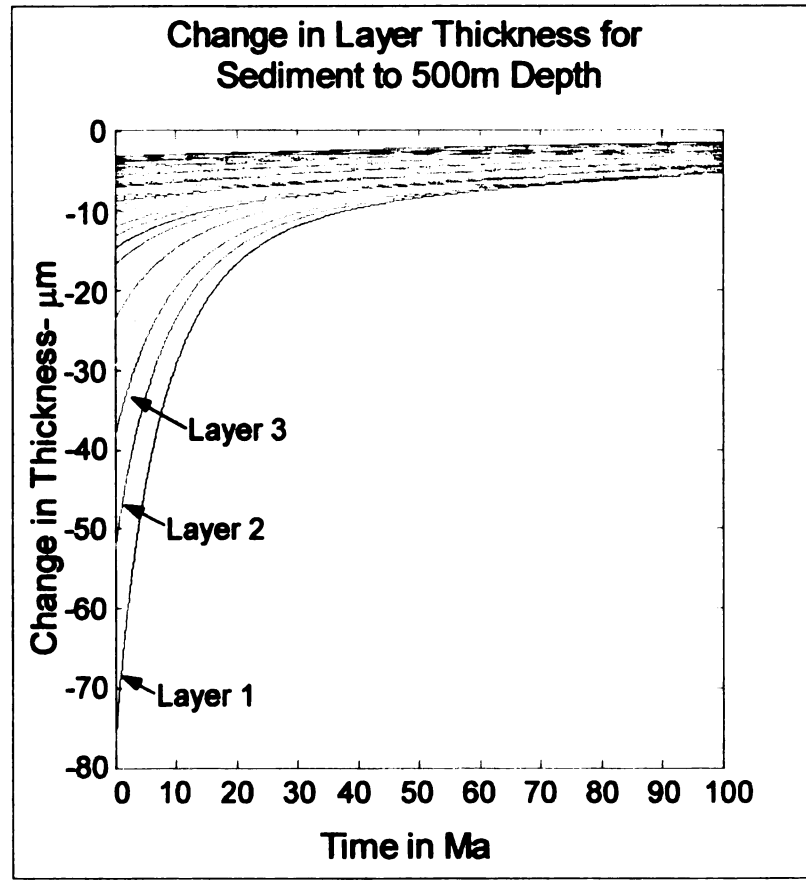


Figure 6.2. Change in thickness of layers initially 10 m thick to 500m depth through 100 million years. Each calculated value is the change in thickness in microns for a 100,000 year period.

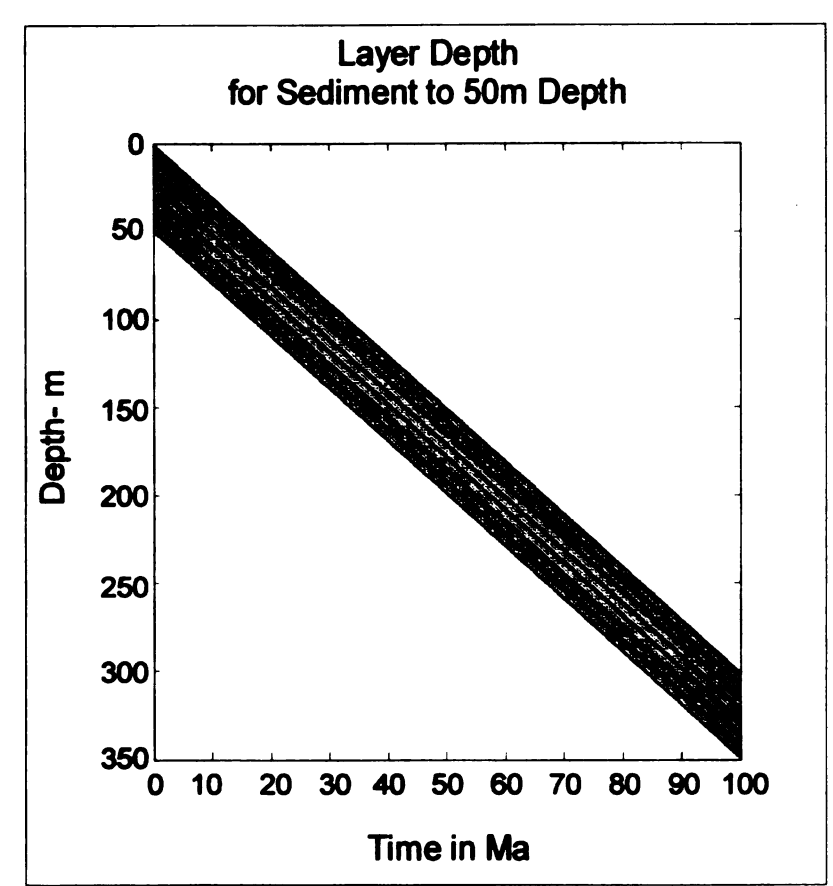


Figure 6.3. Depth of bounding surfaces for layers initially 1m thick to 50m depth through 100 million years.

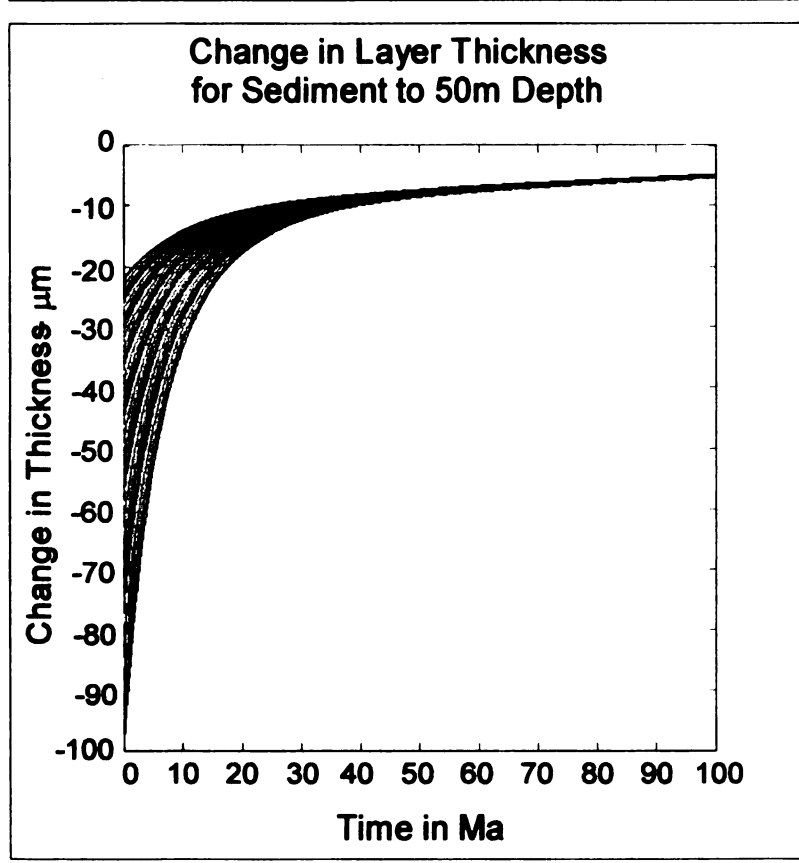


Figure 6.4. Change in thickness of layers initially 1m thick to 50m depth through 100 million years. Each calculated value is the change in thickness in microns for a 100,000 year period.

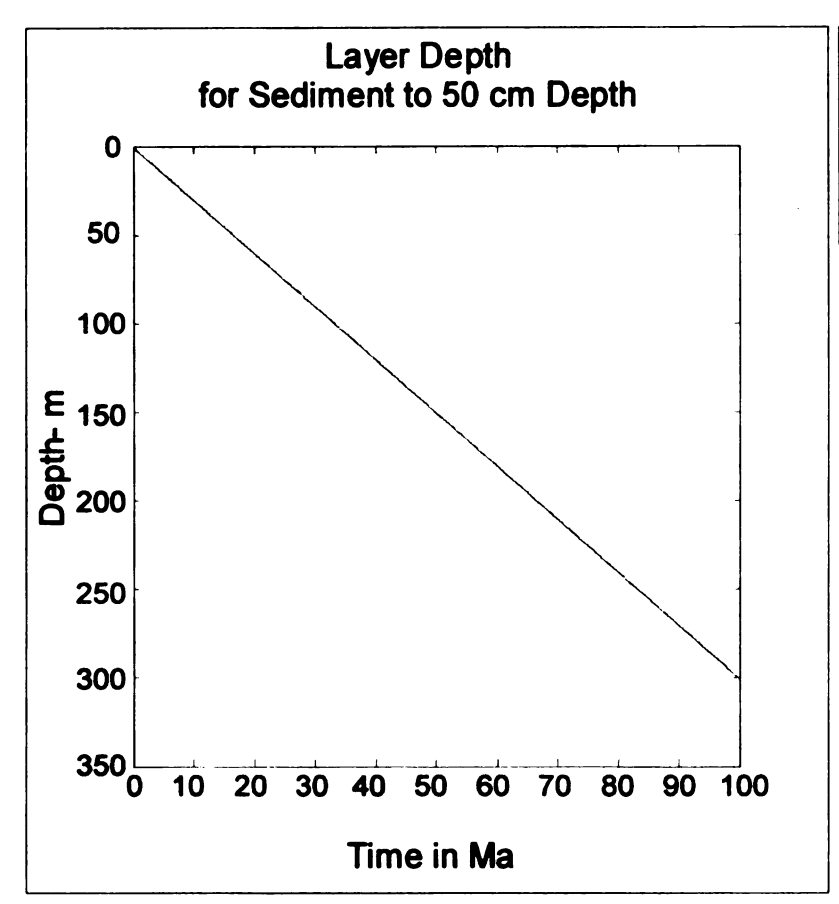


Figure 6.5. Depth of bounding surfaces for layers initially 0.01m thick to 0.5m depth through 100 million years.

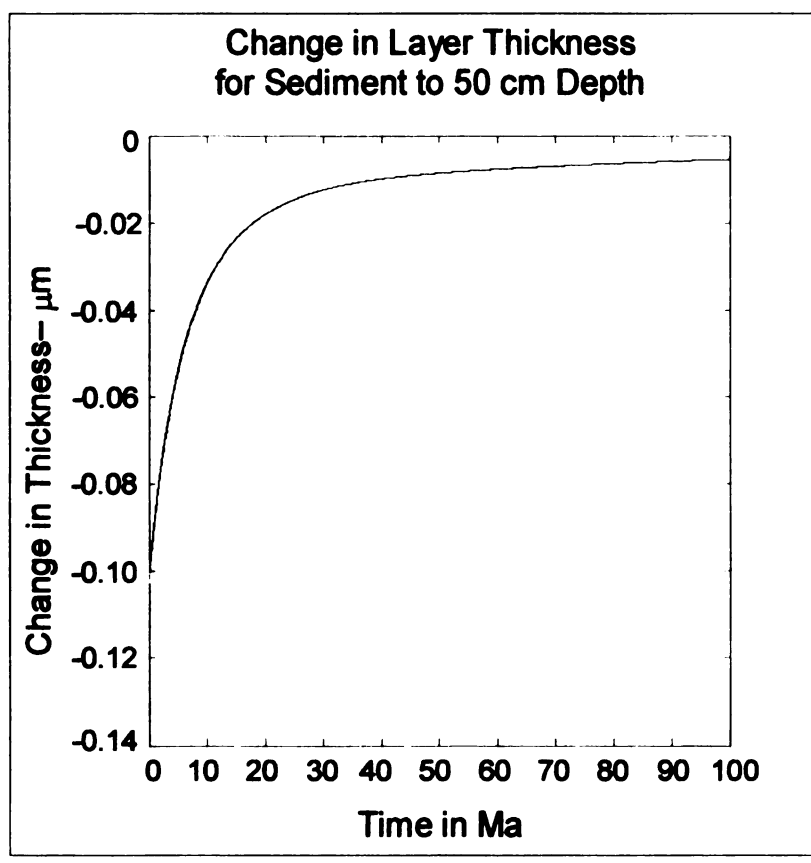


Figure 6.6. Change in thickness of layers initially 0.01m thick to 0.5m depth through 100 million years. Each calculated value is the change in thickness in microns for a 100,000 year period.

10.00 10.30 12.99 39.95 30 20.00 20.30 22.99 49.92 3 30.00 30.30 32.98 59.89 3 40.00 40.30 42.98 69.87 3 50.00 50.30 52.98 79.85 3 60.00 60.30 62.98 89.83 3 70.00 70.30 72.98 89.82 3 80.00 80.30 82.97 109.81 3 90.00 90.30 92.97 119.80 3 110.00 100.30 102.97 129.78 3 110.00 110.30 112.97 139.77 4 120.00 120.30 122.97 149.77 4 130.00 130.30 132.97 159.76 4 140.00 140.30 142.97 169.75 4 150.00 150.30 152.97 179.74 4 160.00 160.30 <t< th=""><th>00.00 09.86 19.75 29.64 39.55 49.46 59.38 69.30 79.23 89.16 99.09 09.03 18.96 28.90</th></t<>	00.00 09.86 19.75 29.64 39.55 49.46 59.38 69.30 79.23 89.16 99.09 09.03 18.96 28.90
10.00 10.30 12.99 39.95 30 20.00 20.30 22.99 49.92 3 30.00 30.30 32.98 59.89 3 40.00 40.30 42.98 69.87 3 50.00 50.30 52.98 79.85 3 60.00 60.30 62.98 89.83 3 70.00 70.30 72.98 99.82 3 80.00 80.30 82.97 109.81 3 90.00 90.30 92.97 119.80 3 110.00 100.30 102.97 129.78 3 110.00 110.30 112.97 139.77 4 120.00 120.30 122.97 149.77 4 130.00 130.30 132.97 159.76 4 140.00 140.30 142.97 169.75 4 150.00 150.30 152.97 179.74 4 160.00 160.30 <t< th=""><th>09.86 19.75 29.64 39.55 49.46 59.38 69.30 79.23 89.16 99.09 09.03 18.96</th></t<>	09.86 19.75 29.64 39.55 49.46 59.38 69.30 79.23 89.16 99.09 09.03 18.96
20.00 20.30 22.99 49.92 3 30.00 30.30 32.98 59.89 3 40.00 40.30 42.98 69.87 3 50.00 50.30 52.98 79.85 3 60.00 60.30 62.98 89.83 3 70.00 70.30 72.98 99.82 3 80.00 80.30 82.97 109.81 3 90.00 90.30 92.97 119.80 3 100.00 100.30 102.97 129.78 3 110.00 110.30 112.97 139.77 44 120.00 120.30 122.97 149.77 4 130.00 130.30 132.97 159.76 4 140.00 140.30 142.97 169.75 4 150.00 150.30 152.97 179.74 4 160.00 160.30 162.97 189.73 4 170.00 170.30	19.75 29.64 39.55 49.46 59.38 59.30 79.23 89.16 99.09 09.03 18.96
30.00 30.30 32.98 59.89 33 40.00 40.30 42.98 69.87 33 50.00 50.30 52.98 79.85 3 60.00 60.30 62.98 89.83 33 70.00 70.30 72.98 99.82 3 80.00 80.30 82.97 109.81 33 90.00 90.30 92.97 119.80 33 100.00 100.30 112.97 139.77 44 120.00 120.30 122.97 149.77 4 130.00 130.30 132.97 159.76 44 140.00 140.30 142.97 169.75 44 160.00 150.30 152.97 179.74 4 160.00 150.30 152.97 179.74 4 160.00 150.30 152.97 179.74 4 160.00 150.30 152.97 179.74 4 160.00 150.30 152.97 179.74 4 160.00 150.30 152.97 179.74 4 160.00 150.30 162.97 189.73 44 170.00 170.30 172.96 199.72 44 180.00 180.30 182.96 209.72 4 180.00 190.30 192.96 219.71 44 200.00 200.30 202.96 229.70 44 210.00 210.30 212.96 239.69 5 220.00 220.30 222.96 249.69 5 230.00 230.30 232.96 259.68 55 240.00 240.30 242.96 269.68 55 240.00 240.30 242.96 269.68 55 250.00 250.30 252.96 279.67 5 260.00 260.30 262.96 289.66 56 280.00 280.30 262.96 399.66 56 280.00 280.30 262.96 399.66 56 280.00 280.30 302.96 329.66 56 280.00 280.30 302.96 329.66 56 330.00 330.30 332.96 339.64 56 330.00 310.30 312.96 339.64 56 330.00 320.30 322.96 339.64 56 330.00 320.30 322.96 339.64 56 330.00 320.30 322.96 339.64 56 330.00 340.30 342.95 369.62 66	29.64 39.55 49.46 59.38 69.30 79.23 89.16 99.09 09.03 18.96
40.00 40.30 42.98 69.87 33 50.00 50.30 52.98 79.85 36 60.00 60.30 62.98 89.83 33 70.00 70.30 72.98 99.82 36 80.00 80.30 82.97 109.81 33 90.00 90.30 92.97 119.80 33 100.00 100.30 102.97 129.78 31 110.00 110.30 112.97 139.77 44 120.00 120.30 122.97 149.77 4 130.00 130.30 132.97 159.76 4 140.00 140.30 142.97 169.75 4 150.00 150.30 152.97 179.74 4 160.00 160.30 162.97 189.73 4 170.00 170.30 172.96 199.72 4 180.00 180.30 182.96 209.72 4 190.00 190	39.55 49.46 59.38 69.30 79.23 89.16 99.09 09.03 18.96
50.00 50.30 52.98 79.85 3 60.00 60.30 62.98 89.83 3 70.00 70.30 72.98 99.82 3 80.00 80.30 82.97 109.81 3 90.00 90.30 92.97 119.80 3 100.00 100.30 102.97 129.78 3 110.00 110.30 112.97 139.77 44 120.00 120.30 122.97 149.77 44 120.00 120.30 132.97 159.76 4 140.00 140.30 142.97 169.75 4 150.00 150.30 152.97 179.74 4 160.00 160.30 162.97 189.73 4 170.00 170.30 172.96 199.72 4 180.00 180.30 182.98 209.72 4 190.00 190.30 192.96 219.71 4 200.00 20.30	49.46 59.38 69.30 79.23 89.16 99.09 09.03 18.96
60.00 60.30 62.98 89.83 33 70.00 70.30 72.98 99.82 36 80.00 80.30 82.97 109.81 37 90.00 90.30 92.97 119.80 36 100.00 100.30 102.97 129.78 35 110.00 110.30 112.97 139.77 44 120.00 120.30 122.97 149.77 4 130.00 130.30 132.97 159.76 45 140.00 140.30 142.97 169.75 45 150.00 150.30 152.97 179.74 44 160.00 160.30 162.97 189.73 45 170.00 170.30 172.96 199.72 44 180.00 180.30 182.96 209.72 4 190.00 190.30 192.96 219.71 44 200.00 20.30 202.96 229.70 44 210.00	59.38 69.30 79.23 89.16 99.09 09.03 18.96
70.00 70.30 72.98 99.82 30 80.00 80.30 82.97 109.81 3 90.00 90.30 92.97 119.80 3 100.00 100.30 102.97 129.78 33 110.00 110.30 112.97 139.77 44 120.00 120.30 122.97 149.77 4 130.00 130.30 132.97 159.76 45 140.00 140.30 142.97 169.75 45 150.00 150.30 152.97 179.74 44 160.00 160.30 162.97 189.73 45 170.00 170.30 172.96 199.72 44 180.00 180.30 182.96 209.72 4 190.00 190.30 192.96 219.71 44 200.00 200.30 202.96 229.70 44 210.00 210.30 212.96 239.69 5 220.00	69.30 79.23 89.16 99.09 09.03 18.96
80.00 80.30 82.97 109.81 3 90.00 90.30 92.97 119.80 3 100.00 100.30 102.97 129.78 3 110.00 110.30 112.97 139.77 44 120.00 120.30 122.97 149.77 4 130.00 130.30 132.97 159.76 4 140.00 140.30 142.97 169.75 4 150.00 150.30 152.97 179.74 4 160.00 160.30 162.97 189.73 4 170.00 170.30 172.96 199.72 4 180.00 180.30 182.96 209.72 4 190.00 190.30 192.96 219.71 4 200.00 200.30 202.96 229.70 4 210.00 210.30 212.96 239.69 5 220.00 220.30 222.96 249.69 5 230.00 230.30 232.96 259.68 5 240.00 240.30	79.23 89.16 99.09 09.03 18.96
90.00 90.30 92.97 119.80 33 100.00 100.30 102.97 129.78 33 110.00 110.30 112.97 139.77 44 120.00 120.30 122.97 149.77 4 130.00 130.30 132.97 159.76 43 140.00 140.30 142.97 169.75 43 150.00 150.30 152.97 179.74 44 160.00 160.30 162.97 189.73 44 170.00 170.30 172.96 199.72 44 180.00 180.30 182.96 209.72 4 190.00 190.30 192.96 219.71 44 200.00 200.30 202.96 229.70 44 210.00 210.30 212.96 239.69 50 220.00 220.30 222.96 249.69 50 230.00 230.30 232.96 259.68 50 240	39.16 99.09 09.03 18.96
100.00 100.30 102.97 129.78 33 110.00 110.30 112.97 139.77 44 120.00 120.30 122.97 149.77 4 130.00 130.30 132.97 159.76 43 140.00 140.30 142.97 169.75 43 150.00 150.30 152.97 179.74 44 160.00 160.30 162.97 189.73 43 170.00 170.30 172.96 199.72 44 180.00 180.30 182.96 209.72 43 190.00 190.30 192.96 219.71 44 200.00 200.30 202.96 229.70 44 210.00 210.30 212.96 239.69 56 220.00 220.30 222.96 249.69 56 230.00 230.30 232.96 259.68 56 240.00 240.30 242.96 269.68 56 <td< td=""><td>99.09 09.03 18.96</td></td<>	99.09 09.03 18.96
110.00 110.30 112.97 139.77 44 120.00 120.30 122.97 149.77 4 130.00 130.30 132.97 159.76 4 140.00 140.30 142.97 169.75 4 150.00 150.30 152.97 179.74 4 160.00 160.30 162.97 189.73 4 170.00 170.30 172.96 199.72 4 180.00 180.30 182.96 209.72 4 190.00 190.30 192.96 219.71 4 200.00 200.30 202.96 229.70 4 210.00 210.30 212.96 239.69 5 220.00 220.30 222.96 249.69 5 230.00 230.30 232.96 259.68 5 240.00 240.30 242.96 269.68 5 250.00 250.30 252.96 279.67 5 260.00 260.30 262.96 289.66 5 290.00 290.30 </td <td>09.03 18.96</td>	09.03 18.96
120.00 120.30 122.97 149.77 44 130.00 130.30 132.97 159.76 45 140.00 140.30 142.97 169.75 45 150.00 150.30 152.97 179.74 44 160.00 160.30 162.97 189.73 45 170.00 170.30 172.96 199.72 46 180.00 180.30 182.98 209.72 47 190.00 190.30 192.96 219.71 46 200.00 200.30 202.96 229.70 47 210.00 210.30 212.96 239.69 56 220.00 220.30 222.96 249.69 5 230.00 230.30 232.96 259.68 5 240.00 240.30 242.96 269.68 5 250.00 250.30 252.96 279.67 5 260.00 260.30 262.98 289.66 5 270.00 270.30 272.96 299.66 5 290.00 <td< td=""><td>18.96</td></td<>	18.96
130.00 130.30 132.97 159.76 44 140.00 140.30 142.97 169.75 44 150.00 150.30 152.97 179.74 44 160.00 160.30 162.97 189.73 44 170.00 170.30 172.96 199.72 44 180.00 180.30 182.96 209.72 4 190.00 190.30 192.96 219.71 44 200.00 200.30 202.96 229.70 44 210.00 210.30 212.96 239.69 56 220.00 220.30 222.96 249.69 5 230.00 230.30 232.96 259.68 5 240.00 240.30 242.96 269.68 5 250.00 250.30 252.96 279.67 5 260.00 260.30 262.96 289.66 5 270.00 270.30 272.96 299.66 5 280.00 280.30 282.96 309.65 5 300.00 3	
140.00 140.30 142.97 169.75 44 150.00 150.30 152.97 179.74 44 160.00 160.30 162.97 189.73 44 170.00 170.30 172.96 199.72 44 180.00 180.30 182.96 209.72 4 190.00 190.30 192.96 219.71 44 200.00 200.30 202.96 229.70 44 210.00 210.30 212.96 239.69 56 220.00 220.30 222.96 249.69 5 230.00 230.30 232.96 259.68 5 240.00 240.30 242.96 269.68 5 250.00 250.30 252.96 279.67 5 260.00 260.30 262.96 289.66 5 270.00 270.30 272.96 299.66 5 280.00 280.30 282.96 319.65 5 300.00 300.30 302.96 329.64 5 310.00 31	
150.00 150.30 152.97 179.74 44 160.00 160.30 162.97 189.73 44 170.00 170.30 172.96 199.72 44 180.00 180.30 182.96 209.72 4 190.00 190.30 192.96 219.71 44 200.00 200.30 202.96 229.70 44 210.00 210.30 212.96 239.69 50 220.00 220.30 222.96 249.69 50 230.00 230.30 232.96 259.68 50 240.00 240.30 242.96 269.68 50 250.00 250.30 252.96 279.67 50 260.00 260.30 262.96 289.66 50 270.00 270.30 272.96 299.66 50 280.00 280.30 282.96 309.65 50 290.00 290.30 292.96 319.65 50 310.00 310.30 312.96 339.64 60 320.00	38.84
160.00 160.30 162.97 189.73 44 170.00 170.30 172.96 199.72 44 180.00 180.30 182.96 209.72 47 190.00 190.30 192.96 219.71 44 200.00 200.30 202.96 229.70 46 210.00 210.30 212.96 239.69 56 220.00 220.30 222.96 249.69 57 230.00 230.30 232.96 259.68 56 240.00 240.30 242.96 269.68 56 250.00 250.30 252.96 279.67 56 260.00 260.30 262.96 289.66 56 270.00 270.30 272.96 299.66 56 280.00 280.30 282.96 309.65 57 290.00 290.30 292.96 319.65 56 310.00 310.30 312.96 339.64 56 320.00 320.30 322.96 349.63 67 340.00	48.78
170.00 170.30 172.96 199.72 44 180.00 180.30 182.96 209.72 47 190.00 190.30 192.96 219.71 44 200.00 200.30 202.96 229.70 49 210.00 210.30 212.96 239.69 56 220.00 220.30 222.96 249.69 57 230.00 230.30 232.96 259.68 56 240.00 240.30 242.96 269.68 56 250.00 250.30 252.96 279.67 56 260.00 260.30 262.96 289.66 56 270.00 270.30 272.96 299.66 56 280.00 280.30 282.96 309.65 57 290.00 290.30 292.96 319.65 56 310.00 310.30 312.96 339.64 56 320.00 320.30 322.96 349.63 66 330.00 320.30 322.96 349.63 67 340.00	58.73
180.00 180.30 182.96 209.72 4 190.00 190.30 192.96 219.71 44 200.00 200.30 202.96 229.70 44 210.00 210.30 212.96 239.69 5 220.00 220.30 222.96 249.69 5 230.00 230.30 232.96 259.68 5 240.00 240.30 242.96 269.68 5 250.00 250.30 252.96 279.67 5 260.00 260.30 262.96 289.66 5 270.00 270.30 272.96 299.66 5 280.00 280.30 282.96 309.65 5 290.00 290.30 292.96 319.65 5 300.00 300.30 302.96 329.64 5 310.00 310.30 312.96 349.63 6 320.00 320.30 322.96 349.63 6 320.00 340.30 342.95 369.62 6	68.88
190.00 190.30 192.96 219.71 44 200.00 200.30 202.96 229.70 44 210.00 210.30 212.96 239.69 56 220.00 220.30 222.96 249.69 57 230.00 230.30 232.96 259.68 57 240.00 240.30 242.96 269.68 57 250.00 250.30 252.96 279.67 56 260.00 260.30 262.96 289.66 56 270.00 270.30 272.96 299.66 56 280.00 280.30 282.96 309.65 57 290.00 290.30 292.96 319.65 56 300.00 300.30 302.96 329.64 59 310.00 310.30 312.96 339.64 66 320.00 320.30 322.96 349.63 67 340.00 340.30 342.95 369.62 63	78.62
200.00 200.30 202.96 229.70 44 210.00 210.30 212.96 239.69 56 220.00 220.30 222.96 249.69 57 230.00 230.30 232.96 259.68 57 240.00 240.30 242.96 269.68 57 250.00 250.30 252.96 279.67 56 260.00 260.30 262.96 289.66 56 270.00 270.30 272.96 299.66 56 280.00 280.30 282.96 309.65 57 290.00 290.30 292.96 319.65 56 300.00 300.30 302.96 329.64 56 310.00 310.30 312.96 339.64 66 320.00 320.30 322.96 349.63 67 340.00 340.30 342.95 369.62 63	38.57
210.00 210.30 212.96 239.69 56 220.00 220.30 222.96 249.69 57 230.00 230.30 232.96 259.68 57 240.00 240.30 242.96 269.68 57 250.00 250.30 252.96 279.67 54 260.00 260.30 262.96 289.66 56 270.00 270.30 272.96 299.66 56 280.00 280.30 282.96 309.65 57 290.00 290.30 292.96 319.65 56 300.00 300.30 302.96 329.64 56 310.00 310.30 312.96 339.64 66 320.00 320.30 322.96 349.63 67 340.00 340.30 342.95 369.62 63	98.52
220.00 220.30 222.96 249.69 5 230.00 230.30 232.96 259.68 5 240.00 240.30 242.96 269.68 5 250.00 250.30 252.96 279.67 5 260.00 260.30 262.96 289.66 5 270.00 270.30 272.96 299.66 5 280.00 280.30 282.96 309.65 5 290.00 290.30 292.96 319.65 5 300.00 300.30 302.96 329.64 5 310.00 310.30 312.96 339.64 6 320.00 320.30 322.96 349.63 6 340.00 340.30 342.95 369.62 6	08.47
230.00 230.30 232.96 259.68 52 240.00 240.30 242.96 269.68 53 250.00 250.30 252.96 279.67 54 260.00 260.30 262.96 289.66 56 270.00 270.30 272.96 299.66 56 280.00 280.30 282.96 309.65 57 290.00 290.30 292.96 319.65 56 300.00 300.30 302.96 329.64 56 310.00 310.30 312.96 339.64 66 320.00 320.30 322.96 349.63 67 340.00 340.30 342.95 369.62 63	18.43
240.00 240.30 242.96 269.68 53 250.00 250.30 252.96 279.67 54 260.00 260.30 262.96 289.66 55 270.00 270.30 272.96 299.66 56 280.00 280.30 282.96 309.65 57 290.00 290.30 292.96 319.65 56 300.00 300.30 302.96 329.64 59 310.00 310.30 312.96 339.64 66 320.00 320.30 322.96 349.63 67 340.00 340.30 342.95 369.62 63	28.38
250.00 250.30 252.96 279.67 54 260.00 260.30 262.96 289.66 55 270.00 270.30 272.96 299.66 56 280.00 280.30 282.96 309.65 57 290.00 290.30 292.96 319.65 56 300.00 300.30 302.96 329.64 59 310.00 310.30 312.96 339.64 66 320.00 320.30 322.96 349.63 67 330.00 330.30 332.95 359.63 62 340.00 340.30 342.95 369.62 63	38.34
260.00 260.30 262.96 289.66 56 270.00 270.30 272.96 299.66 56 280.00 280.30 282.96 309.65 57 290.00 290.30 292.96 319.65 56 300.00 300.30 302.96 329.64 56 310.00 310.30 312.96 339.64 66 320.00 320.30 322.96 349.63 67 330.00 330.30 332.95 359.63 67 340.00 340.30 342.95 369.62 67	48.29
270.00 270.30 272.96 299.66 56 280.00 280.30 282.96 309.65 57 290.00 290.30 292.96 319.65 56 300.00 300.30 302.96 329.64 56 310.00 310.30 312.96 339.64 66 320.00 320.30 322.96 349.63 67 330.00 330.30 332.95 359.63 67 340.00 340.30 342.95 369.62 67	58.25
280.00 280.30 282.96 309.65 5 290.00 290.30 292.96 319.65 5 300.00 300.30 302.96 329.64 5 310.00 310.30 312.96 339.64 6 320.00 320.30 322.96 349.63 6 330.00 330.30 332.95 359.63 6 340.00 340.30 342.95 369.62 6	68.21
290.00 290.30 292.96 319.65 56 300.00 300.30 302.96 329.64 59 310.00 310.30 312.96 339.64 66 320.00 320.30 322.96 349.63 66 330.00 330.30 332.95 359.63 66 340.00 340.30 342.95 369.62 66	78.17
300.00 300.30 302.96 329.64 59 310.00 310.30 312.96 339.64 60 320.00 320.30 322.96 349.63 60 330.00 330.30 332.95 359.63 60 340.00 340.30 342.95 369.62 60	38.13
310.00 310.30 312.96 339.64 66 320.00 320.30 322.96 349.63 66 330.00 330.30 332.95 359.63 66 340.00 340.30 342.95 369.62 66	98.09
320.00 320.30 322.96 349.63 6 330.00 330.30 332.95 359.63 6 340.00 340.30 342.95 369.62 6	08.06
330.00 330.30 332.95 359.63 67 340.00 340.30 342.95 369.62 67	18.02
340.00 340.30 342.95 369.62 63	27.99
	37.95
350.00 350.30 352.95 379.62 64	47.92
	57.89
	37.86
	77.83
	37.80
	97.77
	07.74
	17.72
	27.69
	37.66
	47.64
	57.61
	37.59
	<i>) 1</i> . ਹਰ
	77.57
500.00 500.29 502.95 529.56 79	

Table 6.2.
Calculated
depths of
bounding
surfaces for
50 layers
initially 10m
thick.

	Change	in Thickne	ess in µm	for an Inte	erval of	Reduction
				ayers of S		for 100Ma
	Initial	0.1Ma	1Ma	10Ma	100Ma	in mm
Layer 1	-76.50	-75.64	-67.80	-29.44	-5.30	136.08
2	-52.45	-51.96	-47.50	-23.66	-5.17	117.02
3	-38.38	-38.08	-35.34	-19.67	-5.04	103.94
4	-29.54	-29.35	-27.56	-16.83	-4.90	94.50
5	-23.70	-23.57	-22.35	-14.76	-4 .78	87.37
6	-19.68	-19.59	-18.73	-13.21	-4 .65	81.81
7	-16.83	-16.76	-16.15	-12.03	-4 .53	77.33
8	-14.75	-14.71	-14.25	-11.11	-4.41	73.60
9	-13.20	-13.17	-12.82	-10.38	-4.29	70.43
10	-12.02	-12.00	-11.73	-9.78	-4 .17	67.67
11	-11.10	-11.08	-10.87	-9.28	-4.06	65.21
12	-10.37	-10.36	-10.18	-8.86	-3.95	63.00
13	-9.78	-9.76	-9.62	-8.50	-3.85	60.96
14	-9.28	-9.27	-9.15	-8.18	-3.75	59.06
15	-8.86	-8.85	-8.75	-7.89	-3.64	57.29
16	-8.50	-8.49	-8.40	-7.63	-3.55	55.60
17	-8.18	-8.17	-8.09	-7.38	-3.45	54.01
18	-7.89	-7.88	-7.81	-7.15	-3.36	52.47
19	-7.62	-7.62	-7.55	-6.94	-3.27	51.01
20	-7.38	-7.37	-7.31	-6.74	-3.18	49.59
21	-7.15	-7.15	-7.09	-6.54	-3.10	48.22
22	-6.94	-6.93	-6.88	-6.36	-3.01	46.89
23	-6.74	-6.73	-6.68	-6.18	-2.93	45.61
24	-6.54	-6.54	-6.49	-6.01	-2.85	44.37
25	-6.36	-6.35	-6.30	-5.84	-2.78	
26	-6.18	-6.17	-6.13	-5.68	-2.70	41.99
27	-6.01	-6.00	-5.96	-5.53	-2.63	40.85
28	-5.84	-5.84	-5.79	-5.38	-2.56	39.75
29	-5.68	-5.68	-5.63	-5.23	-2.49	38.66
30	-5.52	-5.52	-5.48	-5.09	-2.42	37.62
31	-5.37	-5.37	-5.33	-4 .95	-2.36	36.61
32	-5.23	-5.22	-5.18	-4.81	-2.29	35.61
33	-5.08	-5.08	-5.04	-4.68	-2.23	34.64
34	-4 .95	-4.94	-4.91	-4.56	-2.17	33.71
35	-4.81	-4.81	-4.77	-4.43	-2.11	32.80
36	-4.68	-4.68	-4.64	-4.31	-2.06	31.91
37	-4 .55	-4 .55	-4.52	-4 .20	-2.00	31.05
38	-4.43	-4.43	-4.39	-4 .08	-1.95	30.21
39	-4.31	-4 .31	-4.27	-3.97	-1.89	29.39
40	-4.19	-4 .19	-4 .16	-3.86	-1.84	28.60
41	-4.08	-4.08	-4.05	-3.76	-1.79	27.82
42	-3.97	-3.96	-3.94	-3.66	-1.75	27.07
43	-3.86	-3.86	-3.83	-3.56	-1.70	26.34
44	-3.76	-3.75	-3.73	-3.46	-1.65	25.62
45	-3.65	-3.65	-3.62	-3.37	-1.61	24.94
46	-3.55	-3.55	-3.53	-3.28	-1.56	24.25
47	-3.46	-3.46	-3.43	-3.19	-1.52	23.60
48	-3.36	-3.36	-3.34	-3.10	-1.48	
49	-3.27	-3.27	-3.25	-3.02	-1.44	
50	-3.18	-3.18	-3.16	-2.93	-1.40	21.74

Table 6.3. Calculated change in thickness for 50 layers initially 10m thick. Values are μm for a 10,000 yr time step. Total reduction in thickness over 100Ma is given in the rightmost column in mm.

Reduction for Entire Column 2476 mm

Initial Doub (m)	Dooth of 0 414c	Dorth et 114e	Donth at 10Ma	Denth at 100Ma
Initial Depth (m)	0.30	3.00	30.00	300.00
0.00		4.00	30.99	300.98
1.00	1.30	5.00	31.99	301.97
2.00	2.30		32.98	302.96
3.00	3.30	6.00		
4.00	4.30	7.00	33.98	
5.00	5.30	8.00	34.97 35.97	304.93 305.91
6.00	6.30	9.00	36.96	306.90
7.00	7.30 8.30	9.99	37.96	307.89
8.00 9.00	9.30	10.99 11.99	38.95	308.87
10.00	10.30	12.99	39.95	309.86
11.00		13.99	40.95	310.85
12.00	11.30 12.30	14.99	41.94	311.84
13.00	13.30	15.99	42.94	312.82
14.00	14.30	16.99	43.94	313.81
	15.30		44.93	
15.00		17.99	45.93	
16.00	16.30	18.99		315.79 316.78
17.00	17.30	19.99	46.92 47.92	317.77
18.00	18.30	20.99	48.92	318.75
19.00	19.30	21.99	49.91	319.74
20.00	20.30	22.99	50.91	320.73
21.00	21.30	23.99		321.72
22.00	22.30	24.99	51.91 52.91	322.71
23.00	23.30	25.99 26.99	53.90	323.70
24.00	24.30 25.30	27.99	54.90	324.69
25.00				325.68
26.00 27.00	26.30 27.30	28.98 29.98	55.90 56.89	326.67
28.00	28.30	30.98	57.89	327.66
29.00	29.30	31.98	58.89	328.65
	30.30	32.98	59.89	329.64
30.00	31.30			330.63
31.00		33.98	60.88	
32.00		34.98 35.98	61.88 62.88	331.62 332.61
33.00	33.30 34.30	36.98	63.88	333.60
34.00 35.00	35.30	37.98	64.88	334.59
36.00 37.00		38.98	65.87 66.87	
37.00		39.98	66.87 67.87	
38.00		40.98	67.87 69.87	338.55
39.00		41.98	68.87	
40.00 41.00		42.98 43.98	69.86 70.86	
42.00		44.98	70.86	
43.00		45.98	71.86	
44.00		45.98 46.98	73.86	
45.00		47.98	74.85	
46.00		48.98	74.65 75.85	
47.00		49.98	76.85	
48.00		50.98	77.85	
49.00			78.85	
50.00		52.98	79.85	
50.00	50.30	52.90	18.00	348.40

Table 6.4.
Calculated depths of bounding surfaces for 50 layers initially 1m thick.

		in Thickne				Reduction for
	10,000yr	for 50, 1m	Thick La	ayers of So	ediment	100Ma
[Initial	0.1Ma	1Ma	10Ma	100Ma	in mm
Layer 1	-9.94	-9.81	-8.63	-3.36	-0.54	15.05
2	-9.47	-9.35	-8.25	-3.27	-0.53	14.74
3	-9.04	-8.92	-7.90	-3.19	-0.53	14.47
4	-8.63	-8.52	-7.57	-3.11	-0.53	14.19
5	-8.25	-8.15	-7.26	-3.03	-0.53	13.93
6	-7.89	-7.80	-6.96	-2.96	-0.53	13.68
7	-7.56	-7.48	-6.69	-2.89	-0.53	13.45
8	-7.25	-7.17	-6.43	-2.82	-0.53	13.22
9	-6.96	-6.88	-6.19	-2.76	-0.53	13.01
10	-6.68	-6.61	-5.96	-2.70	-0.52	
11	-6.43	-6.36	-5.74	-2.64	-0.52	12.60
12	-6.18	-6.12	-5.54	-2.58	-0.52	
13	-5.95	-5.89	-5.34	-2.52	-0.52	12.23
14	-5.74	-5.68	-5.16	-2.47	-0.52	12.05
15	-5.53 5.24	-5.48	-4.99	-2.42	-0.52	11.89
16	-5.34	-5.29	-4.82	-2.37	-0.52	11.73
17	-5.16	<u>-5.11</u>	-4.67	-2.32	-0.51	11.57
18	-4.98	-4.94 4.79	-4.52	-2.28	-0.51	11.42
19	-4.82 4.66	-4.78	-4.38	-2.23 -2.19	-0.51	11.28
20 21	<u>-4.66</u> -4.52	-4.62	-4.24 -4.12		-0.51 -0.51	11.13
22	-4.32 -4.38	<u>-4.48</u> <u>-4.34</u>	-4.12 -4.00	-2.15 -2.11	-0.51 -0.51	11.01 10.87
23	-4 .36	-4.34 -4.21	-3.88	-2.11	-0.51 -0.51	10.75
23 24	-4.11	-4 .21	-3. 77	-2.07	-0.51	10.75
25	-3.99	-3.96	-3.66	-2.00	-0.50	10.52
26	-3.88	-3.85	-3.56	-1.97	-0.50	10.40
27	-3.77	-3.74	-3.47	-1.93	-0.50	10.29
28	-3.66	-3.63	-3.38	-1.90	-0.50	10.18
29	-3.56	-3.53	-3.29	-1.87	-0.50	10.08
30	-3.46	-3.44	-3.20	-1.84	-0.50	9.98
31	-3.37	-3.35	-3.12	-1.81	-0.50	9.89
32	-3.29	-3.26	-3.05	-1.79	-0.50	
33	-3.20	-3.18	-2.97	-1.76	-0.49	
34	-3.12	-3.10	-2.90	-1.73	-0.49	
35	-3.04	-3.02	-2.83	-1.71	-0.49	9.53
36	-2.97	-2.95	-2.77	-1.68	-0.49	9.44
37	-2.90	-2.88	-2.71	-1.66	-0.49	9.36
38	-2.83	-2.81	-2.65	-1.64	-0.49	9.29
39	-2.77	-2.75	-2.59	-1.61	-0.49	9.21
40	-2.70	-2.69	-2.53	-1.59	-0.48	9.13
41[-2.64	-2.63	-2.48	-1.57	-0.48	9.06
42	-2.59	-2.57	-2.43	-1.55	-0.48	9.00
43	-2.53	-2.51	-2.38	-1.53	-0.48	8.92
44	-2.48	-2.46	-2.33	-1.51	-0.48	8.86
45	-2.42	-2.41	-2.28	-1.49	-0.48	8.79
46	-2.38	-2.36	-2.24	-1.47	-0.48	8.73
47	-2.33	-2.31	-2.20	-1.46	-0.48	8.66
48	-2.28	-2.27	-2.16	-1.44	-0.47	8.61
49	-2.24	-2.23	-2.12	-1.42	-0.47	8.54
50	-2.19	-2.18	-2.08	-1.41	-0.47	8.49

Table 6.5.
Calculated change in thickness for 50 layers initially 1m thick. Values are µm for a 10,000 yr time step. Total reduction in thickness over 100Ma is given in the rightmost column in mm.

Reduction for Entire Column 544.16 mm

Initial Depth (m)	Depth at 0.1Ma	Depth at 1Ma	Depth at 10Ma Depth a	t 100Ma
0.00	0.30		30.00	300.00
0.01	0.31	3.01	30.01	300.01
0.02	0.32	3.02	30.02	300.02
0.03	0.33	3.03	30.03	300.03
0.04	0.34	3.04	30.04	300.04
0.05	0.35	3.05	30.05	300.05
0.06	0.36	3.06	30.06	300.06
0.07	0.37	3.07	30.07	300.07
0.08	0.38	3.08	30.08	300.08
0.09	0.39	3.09	30.09	300.09
0.10	0.40	3.10	30.10	300.10
0.11	0.41	3.11	30.11	300.11
0.12	0.42	3.12	30.12	300.12
0.13	0.43	3.13	30.13	300.13
0.14	0.44	3.14	30.14	300.14
0.15	0.45	3.15	30.15	300.15
0.16	0.46		30.16	300.16
0.17	0.47	3.17	30.17	300.17
0.18	0.48		30.18	300.18
0.19	0.49	3.19	30.19	300.19
0.20	0.50	3.20	30.20	300.20
0.21	0.51	3.21	30.21	300.21
0.22	0.52		30.22	300.22
0.23	0.53		30.23	300.23
0.24	0.54		30.24	300.24
0.25	0.55		30.25	300.25
0.26	0.56		30.26	300.26
0.27	0.57		30.27	300.27
0.28	0.58		30.28	300.28
0.29	0.59		30.29	300.29
0.30	0.60		30.30	300.30
0.31	0.61	3.31	30.31	300.31
0.32	0.62		30.32	300.32
0.33	0.63		30.33	300.32
0.34	0.64		30.34	300.33
0.35	0.65		30.35	300.34
0.36	0.66		30.36	300.35
0.37	0.67		30.37	300.36
0.38			30.38	300.37
0.39			30.39	300.38
0.40			30.40	300.39
0.41	0.71	3.41	30.41	300.40
0.42			30.42	300.41
0.43			30.43	300.42
0.44	0.74		30.44	300.43
0.45			30.45	300.44
0.46			30.46	300.45
0.47	0.77		30.47	300.46
0.48			30.48	300.47
0.49			30.49	300.48
0.50	0.80	3.50	30.50	300.49

Table 6.6.
Calculated depths of bounding surfaces for 50 layers initially 0.01m thick.

	Change 10,000yr fo			for an Inte ayers of S		Reduction for 100Ma
	Initial	0.1Ma	1Ma	10Ma	100Ma	in mm
Layer 1	-0.1028	-0.1014		-0.0341	-0.0054	
2	-0.1027	-0.1013	-0.0889		-0.0054	
3	-0.1027	-0.1013	-0.0889	-0.0341	-0.0054	0.16
4	-0.1026	-0.1012	-0.0889	-0.0341	-0.0054	0.15
5	-0.1026	-0.1012	-0.0888	-0.0341	-0.0054	0.15
6	-0.1025	-0.1011	-0.0888	-0.0341	-0.0054	0.15
7	-0.1025	-0.1011	-0.0887	-0.0340	-0.0054	0.16
8	-0.1024	-0.1010	-0.0887	-0.0340	-0.0054	0.15
9	-0.1024	-0.1010	-0.0887	-0.0340	-0.0054	0.15
10	-0.1023	-0.1009	-0.0886		-0.0054	
11	-0.1023	-0.1009	-0.0886	-0.0340	-0.0054	0.15
12	-0.1022	-0.1008	-0.0885	-0.0340	-0.0054	0.16
13	-0.1021	-0.1008	-0.0885	-0.0340	-0.0054	0.15
14	-0.1021	-0.1007	-0.0885	-0.0340	-0.0054	0.15
15		-0.1007	-0.0884		-0.0054	
16		-0.1006	-0.0884	-0.0340	-0.0054	
17	-0.1019	-0.1006	-0.0883	-0.0340	-0.0054	
18		-0.1005	-0.0883		-0.0054	
19		-0.1005	-0.0882		-0.0054	
20	-0.1018	-0.1004	-0.0882	-0.0339	-0.0054	
21	-0.1017	-0.1004	-0.0882		-0.0054	
22		-0.1003	-0.0881	-0.0339	-0.0054	
23		-0.1003	-0.0881	-0.0339	-0.0054	
24		-0.1002	-0.0880	-0.0339	-0.0054	
25		-0.1002	-0.0880	-0.0339	-0.0054	
26		-0.1001	-0.0880	-0.0339	-0.0054	
27		-0.1001	-0.0879	-0.0339	-0.0054	
28		-0.1000	-0.0879	-0.0339	-0.0054	
29		-0.1000	-0.0878	-0.0338	-0.0054	
30		-0.0999	-0.0878	-0.0338	-0.0054	
31	-0.1012	-0.0999	-0.0878	-0.0338	-0.0054	
32		-0.0998	-0.0877	-0.0338	-0.0054	
33		-0.0998	-0.0877	-0.0338	-0.0054	
34		-0.0997	-0.0876			0.15
35		-0.0997	-0.0876		-0.0054	
36		-0.0996	-0.0876		-0.0054	
37		-0.0996	-0.0875		-0.0054	
38		-0.0995	-0.0875	-0.0338	-0.0054	
39		-0.0995			-0.0054	
40				-0.0337		
41		-0.0994		-0.0337	-0.0054	
42				-0.0337	-0.0054	
43				-0.0337	-0.0054	
44 45		-0.0993	-0.0872		-0.0054	
45 46		-0.0992	-0.0872		-0.0054	
40 47		-0.0992	-0.0872	-0.0337 -0.0337	-0.0054	
48		-0.0991 -0.0991	-0.0871 -0.0871	-0.0337	-0.0054 -0.0054	
40 49		-0.0990	-0.0870	-0.0337	-0.0054	
49 50		-0.0990	-0.0870	-0.0337	-0.0054	
50	70.1003	-0.0550	-0.0070	-0.033/	-0.0004	0.13

Table 6.7.
Calculated change in thickness for 50 layers initially 0.01m thick. Values are nm for a 10,000 yr time step. Total reduction in thickness over 100Ma is given in the rightmost column in mm.

Reduction for Entire Column 7.58 mm total reduction of the 50m column was 544mm (table 6.5) or 0.54m (table 6.4). The surfaces shown in figure 6.3 deepen through the simulation; this appears more pronounced than for the 500m column, but is identical because the pelagic accumulation rate was the same. Clay deposition dominates this sediment column; the thickness of the layers is barely perceptible on the depth scale that accommodates the final column.

A detailed examination of the top 0.5m of sediment was achieved with the shallow column. The removal of sediment is still greatest near the sediment-water interface, but the change in thickness is similar for all of the layers at each time step. The top layer was reduced by 0.15mm, and the column decreased in total thickness by 7.6mm for 100Ma. Relative to the increase in depth from clay deposition, the layers of this column are indiscernible (figure 6.5). Also, individual surfaces in figure 6.6 cannot be seen at the scale necessary for the change of thickness. The sediment removal for each time step is much less near the end of the simulation because clay deposition has moved them relatively far from the sediment-water interface.

Sensitivity Analysis

Diffusion Coefficient

Since the diffusion coefficient through sediment cannot be directly measured, it is the most difficult variable in the model to approximate. Sensitivity of depth of bounding surfaces to D_s was investigated. Arbitrary variation was introduced into the model within the calculation for flux at each surface. Within each time step and at every bounding surface, D_s was calculated then a component was added or subtracted to achieve different D_s values before the flux calculation. This created a different D_s for each layer that also changed for

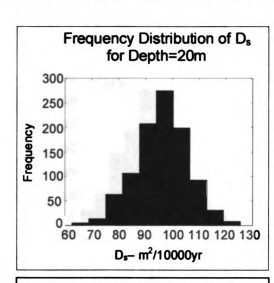


Figure 7.1. Example distribution of D_s introduced into the model for sensitivity analysis.

each time step. The values for the surfaces represent differences in the sediment likely at deposition, and the changes with time correspond to alteration expected during early diagenesis. The model was run 500 times to achieve enough results to evaluate the variation of the input relative to the variation of the output.

Since no measurements of D_s are

available, a normal distribution was arbitrarily chosen with enough standard deviation to establish a range of D_s values wide enough to compare to the model output. For example, the distribution of D_s introduced for surface 3 is shown in figure 7.1. Its mean is $96.34m^2/10,000yr$, which is very close to the calculated value of D_s at 20m, 96.07. The standard deviation is about 10% of D_s , which

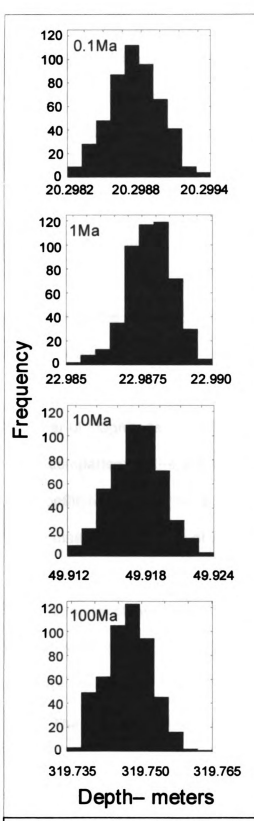


Figure 7.2. Distribution of depth of bounding surface 3 resulting from variation in D_s in the model.

gives a range of 62.7 to 125.5. The resulting variation in depth is shown in figure 7.2 and table 7.1. Note that the mean for each time matches the depth for surface 3 in table 6.2.

The standard deviation of each layer's depth is shown in figure 7.3. Each line represents the standard deviation of the bounding surfaces at a particular time step; four times are listed on the graph. The depth of surface one is based on pelagic clay deposition and does not incorporate diffusion, so its standard deviation is zero for all time steps. For the other surfaces, the standard deviation increases through time. Since the average values of depth and D_s for each layer are different,

	Mean		Coefficient of Variation		
Ds	96.3383	10.2579	1.06E-01		
Layer 3 De	epth				
0.1Ma	20.2987	2.68E-04	1.32E-05		
1Ma	22.9878	8.28E-04	3.60E-05		
10Ma	49.9178	2.50E-03	5.01E-05		
100Ma	319.7471	4.90E-03	1.53E-05		

Table 7.1. Statistics for analysis of sensitivity of bounding surface depth to variation in D_8 .

evaluation of them for all layers together is not appropriate. Bounding surface 3 will be analyzed because it is the first surface surrounded by diffusion influenced surfaces.

Since the values for

D_s and bounding surface

depth are different by nearly
an order of magnitude,

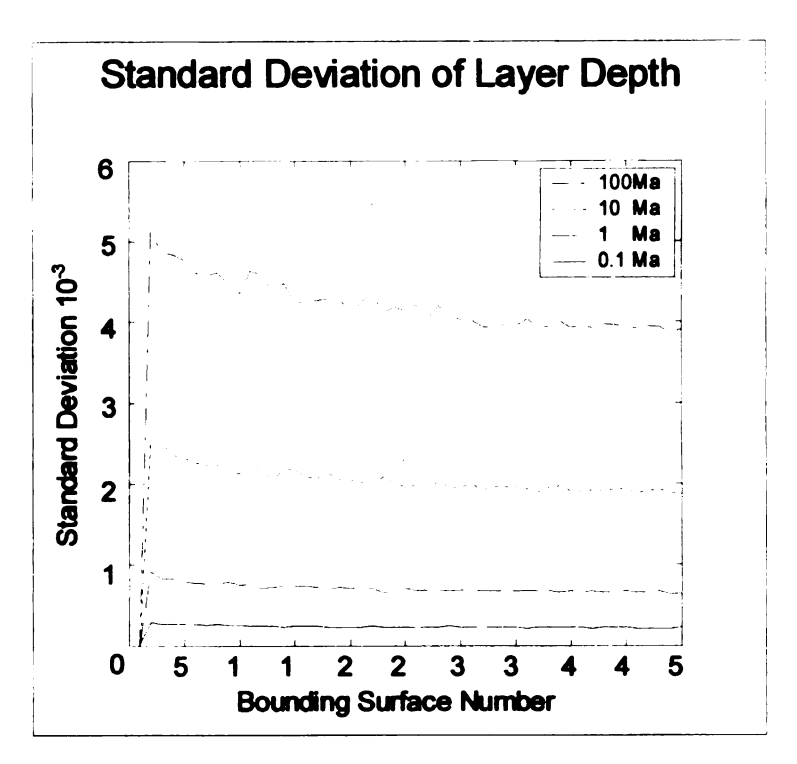


Figure 7.3. Standard deviation of depth of bounding surfaces for 500 realizations incorporating variation in D_{s} .

direct comparison of the standard deviation may not be the best assessment. The coefficient of variation is based on the standard deviation but is normalized by the mean. Regardless of which is evaluated, the variation in depth is at least four orders of magnitude less than the variation in D_s (table 7.1). This indicates that this model of dissolution is not very sensitive to the diffusion coefficient through sediment.

Activity

The difference in speciation of Ca²⁺ at shallow sediment depth versus in deep sediment can be assessed by looking at the activity coefficient for the pore water solutions. All of the available ions at site 603 were used. The shallowest depth where several ions were measured was 36.75m and the deepest was

1076.15. Using PHREEQC to evaluate the solutions gave activity coefficients for Ca^{2+} of $10^{-0.579}$ at 36m and $10^{-0.582}$ at 1076m. These were inserted into the model by multiplying the concentration, equation 2.3, by the coefficient:

7.1
$$C(x) = \gamma \cdot (C_{max} - (C_{range} \cdot e^{-k_c \cdot x}))$$
 γ =activity coefficient

The resulting gradient equation is:

7.2
$$\frac{\partial C}{\partial x} = \gamma \cdot k_c \cdot C_{range} \cdot e^{-k_c \cdot x}$$

The model was modified at line 28 where the concentration gradient is calculated within the flux equation, and results were found with 36m and 1076m coefficients.

Graphically the difference between the shallow and deep models is imperceptible, and the depth of bounding surfaces is identical except at very high resolution. The change in layer thickness (figures 7.4 and 7.5) is less than for the original model. This is expected because the activity of Ca²⁺ is less than its concentration. It was not included in the original model because measurements

Surface	Initial	Depth at 1Ma		Depth a	at 100Ma
number	Depth (m)	γ for 36m	γ for 1076m	γ for 36m	γ for 1076m
1	0	2.970	2.970	299.970	299.970
5	40	42.969	42.969	339.952	339.952
10	90	92.969	92.969	389.935	389.934
15	140	142.969	142.969	439.921	439.920
20	190	192.969	192.969	489.908	489.908
25	240	242.969	242.969	539.898	539.897
30	290	292.968	292.968	589.889	589.888
35	340	342.968	342.968	639.881	639.880
40	390	392.968	392.968	689.874	689.873
45	440	442.968	442.968	739.867	739.867
50	490	492.968	492.968	789.862	789.861

for many of the ions in the pore water were not available, and the activity coefficient would have introduced unwarranted error.

Table 7.2. Depth of selected bounding surfaces from models including activity coefficient for shallow sediment and for deep sediment, γ for 36m is $10^{-0.579}$ and γ for 1076m is $10^{-0.582}$.

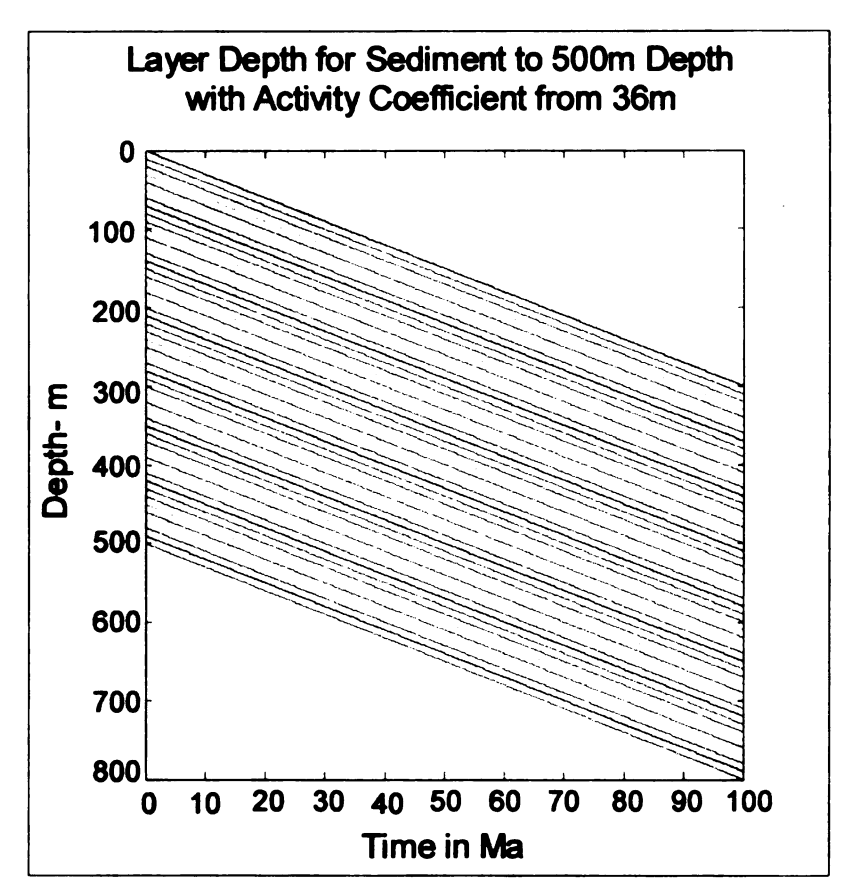


Figure 7.4. Depth of bounding surfaces for layers initially 10 m thick to 500m depth through 100 million years with activity coefficient from 36m.

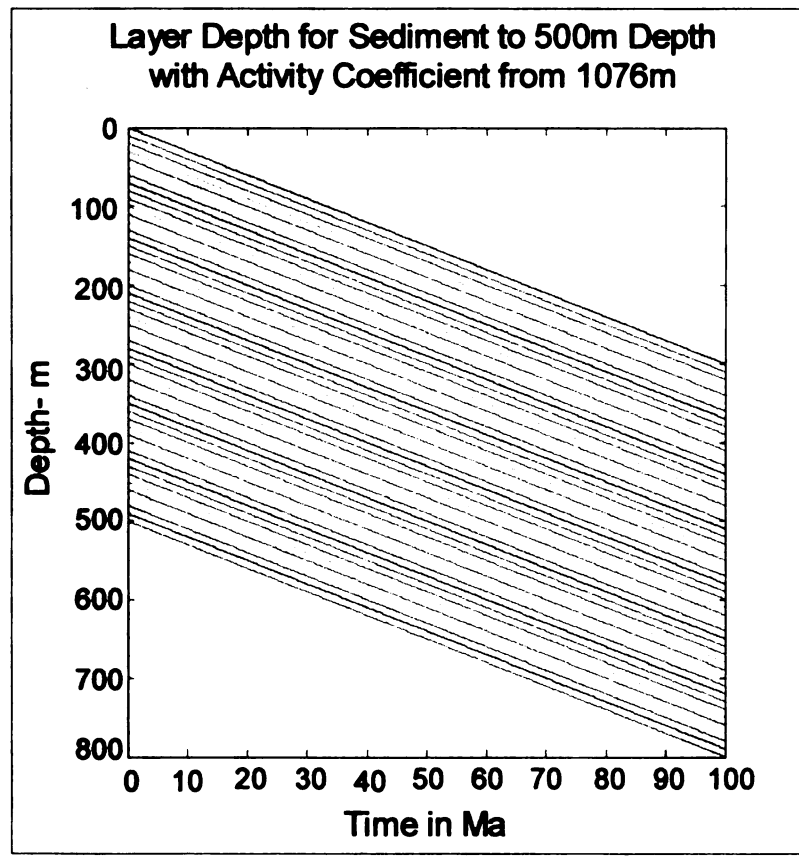


Figure 7.5. Depth of bounding surfaces for layers initially 10 m thick to 500m depth through 100 million years with activity coefficient from 1076m.

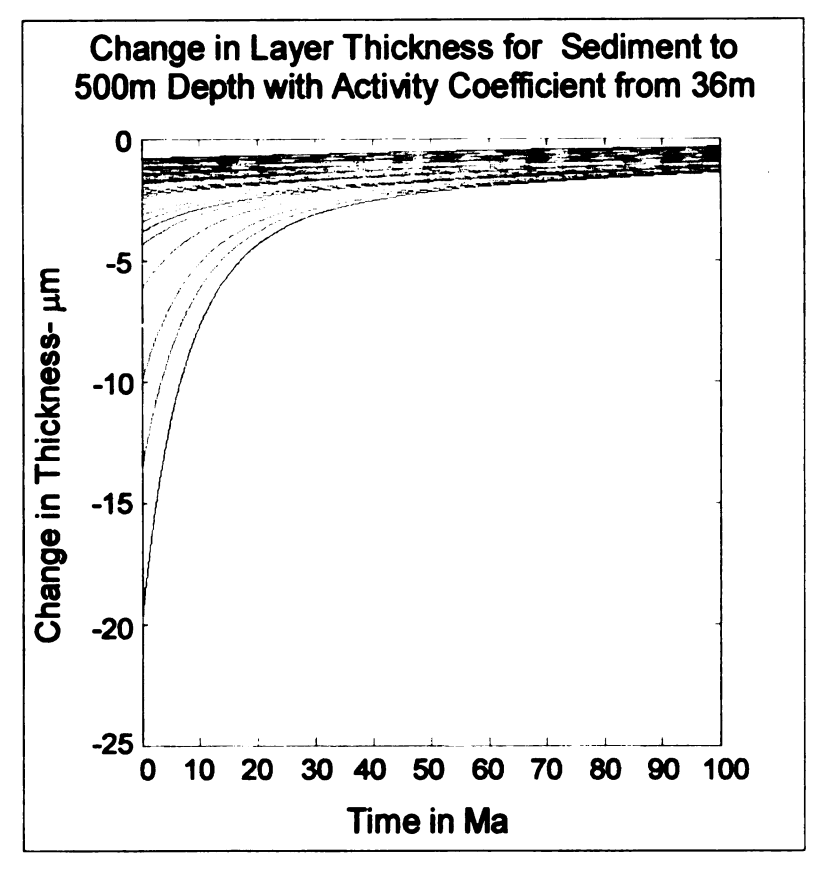


Figure 7.6. Change in thickness of layers initially 10 m thick to 500m depth through 100 million years with activity coefficient from 36m. Each calculated value is the change in thickness in microns for a 100,000 year period.

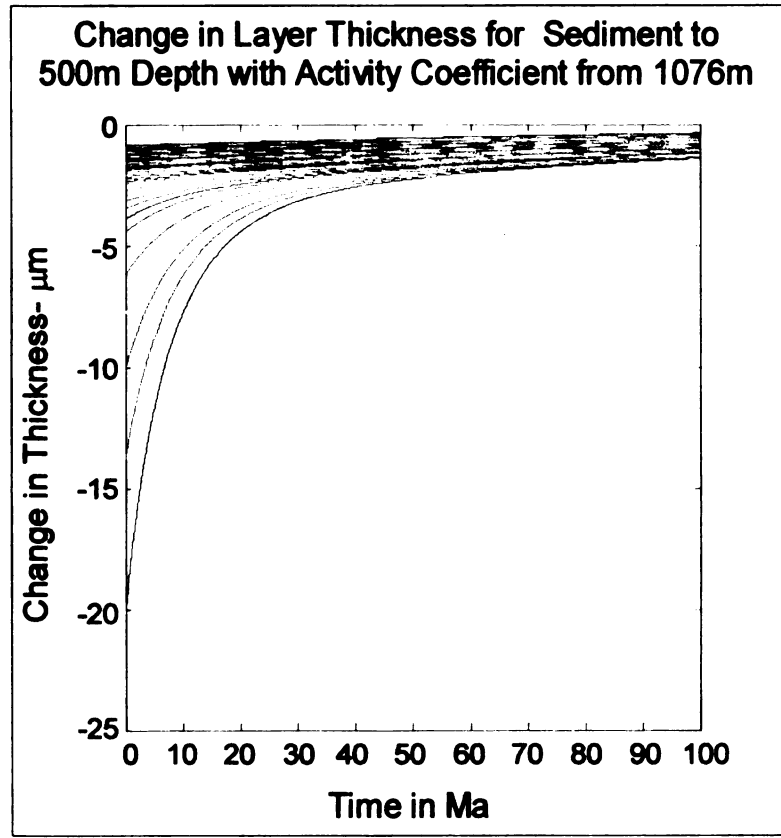


Figure 7.7. Change in thickness of layers initially 10 m thick to 500m depth through 100 million years with activity coefficient from 1076m. Each calculated value is the change in thickness in microns for a 100,000 year period.

Porosity

Physical mechanisms indicate that porosity should consistently decrease with depth, but measurements show irregularities (figure 5.2). Some of this can be attributed to variation in the sediment at deposition. The highest porosity measurement was 88.07% at a depth of 24.42m, and the lowest porosity

Porosity- %	Change in Th	ickness
	10,000уг µm	100Ma meter
50.20	-9.87	-0.098
65.94	-18.62	-0.183
88.07	-82.05	-0.765

Table 7.3. Variation in model output from extreme values of porosity. Values are for a single cell initially bounded by 24m and 29m.

measurement near the same depth (0 to 50m) was 50.20% at 28.66m. To investigate the error that could be caused by this, the reduction in thickness was calculated using a hypothetical cell with bounding surfaces at 24m and 29m.

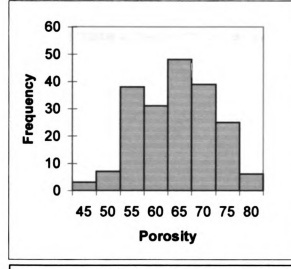


Figure 7.8. Distribution of measured porosity values used to estimate the constants in the function of porosity with depth.

Three porosity values were used in separate calculations: the minimum, the p(x) prediction, and the maximum (table 7.3). The changes in thickness for the first 10,000yr increment vary considerably relative to each other, but all of them are small relative to the 5m thickness of the cell. The total reduction of the cell during

100Ma also varies, but even for the maximum porosity, the removal is less than one meter. The differences calculated here may be more than the actual

changes caused by the error in porosity with depth because a systematic error

was introduced. The actual variation of porosity seems normally distributed and is shown in figure 7.8.

Pelagic Clay

The sensitivity of the model to pelagic clay accumulation was investigated by using a rate two orders of magnitude smaller than the original rate. In the original model, the depth of the layers after 100Ma was dominated by clay thickness, so a faster rate was not explored, but less clay may allow more sediment removal. The small rate was equivalent to 30 microns per 1000 years and resulted in a depth of 3m instead of 300m after 100Ma. Through time, the change in thickness did not become less as dramatically as in the original model because the layers were not moved as far from the sediment-water interface. The total reduction of each layer was about one millimeter from 10cm, which still does not make a measurable removal.

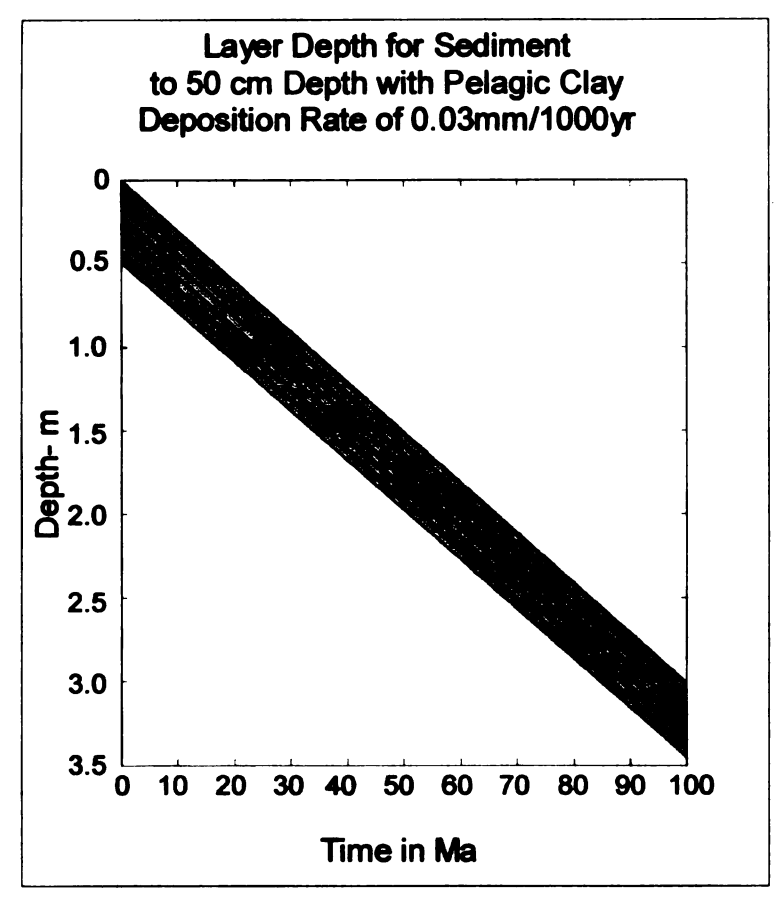


Figure 7.9. Depth of bounding surfaces for layers initially 0.01m thick to 0.5m depth through 100 million years with pelagic clay accumulation rate of 0.03mm/1000yr.

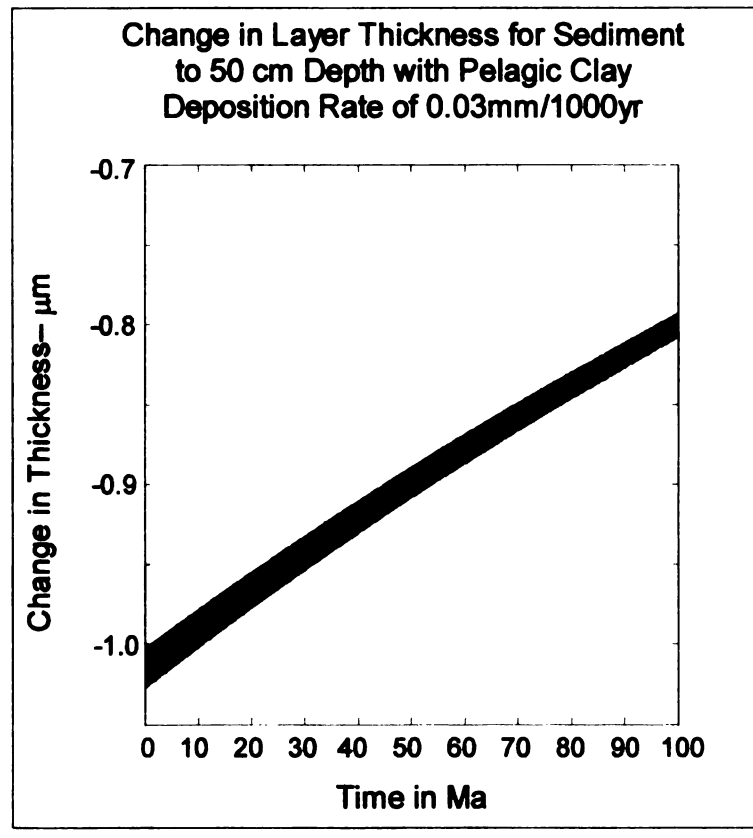


Figure 7.10. Change in thickness of layers initially 0.01m thick to 0.5m depth through 100 million years. with pelagic clay accumulation rate of 0.03mm/1000yr. Each calculated value is the change in thickness in microns for a 100,000 year period.

Sediment-water Interface Model

Since the sediment at the sediment-water interface is exposed to open water, the concentration of Ca²⁺ immediately adjacent to the grain surface will be the same as the overlying water. On ocean floor below the CCD, dissolution will be controlled by the rate of detachment (surface reaction) of species from the mineral surface (Drever 1982). This is not included in the primary model because its purpose is to investigate the potential importance of molecular diffusion, and additional features may obscure the results. Usually clay deposition would remove the carbonate sediment from exposure to the overlying water, but some areas within the pelagic Atlantic may not experience clay deposition. For instance, a temporally persistent current could keep clay from

```
5
    %cpercent %this performs the minimum thickness calculation for b
15
    Do=1.701*10^2;%units: m^2/10000yr
16
16a %kinetic dissolution parameters, rate=kk*(1-om)^nk
16b kk=100;om=0.84;nk=4.5;
16c %units: r=mmol/m^2day
16d r=kk*(1-om)^nk:
16e krate=r*10^-3*365.242*10^5:%mol/m^2*10000vr
17 %final will be a matrix of depths of the layers, each column represents a time step
28
        flux(ia)=(Do*kc*Crange*exp(-kc*x))/(1-log((Pmin+Prange*exp(-x/kp))^2));
28a
         %reassign flux for top of column
28b
         if lastdep(ia)==0
28c
         flux(ia)=krate:
28d
         end
29
      end
30
    final(1,iy+1)=b(1);%+0.03*(iy);
```

Figure 8.1. Modifications to the model code for kinetic dissolution from the sediment-water interface. Additions are shown in **bold**.

depositing, even at low velocity. To simulate this, the flux at x=0 is redefined using the rate equation for dissolution of carbonate sediment due to undersaturation (Kier 1980):

8.1
$$rate = k_{L}(1-\Omega)^{n}$$

The modified model code, figure 8.1, includes the rate equation and its constants inserted between lines 16 and 17 of the original model. If the saturation state of the overlying water does not vary with time, the flux from exposed carbonate sediment at the sediment-water interface is constant. The constants for flux at the sediment-water interface were taken from the work of Kier (1984), Berelson et al (1990) and Berelson et al (1994):

The rate of dissolution is calculated in line 16d, and is converted to the model units of $\frac{mol}{m^2 \cdot 10^4 y}$ in line 16e; this value is used for the duration of the model. Lines 28b to 28d insert the modified flux if the depth of an interface is zero. A % was added to line 30 before the addition of 0.03(iy) to remove clay deposition, and the rest of the model code is unchanged.

The results from an initial column that is 50m deep with layers 1m thick show an additional hindrance to surface reaction dissolution (figure 8.2).

According to DSDP measurements, carbonate sediment in the Atlantic contains

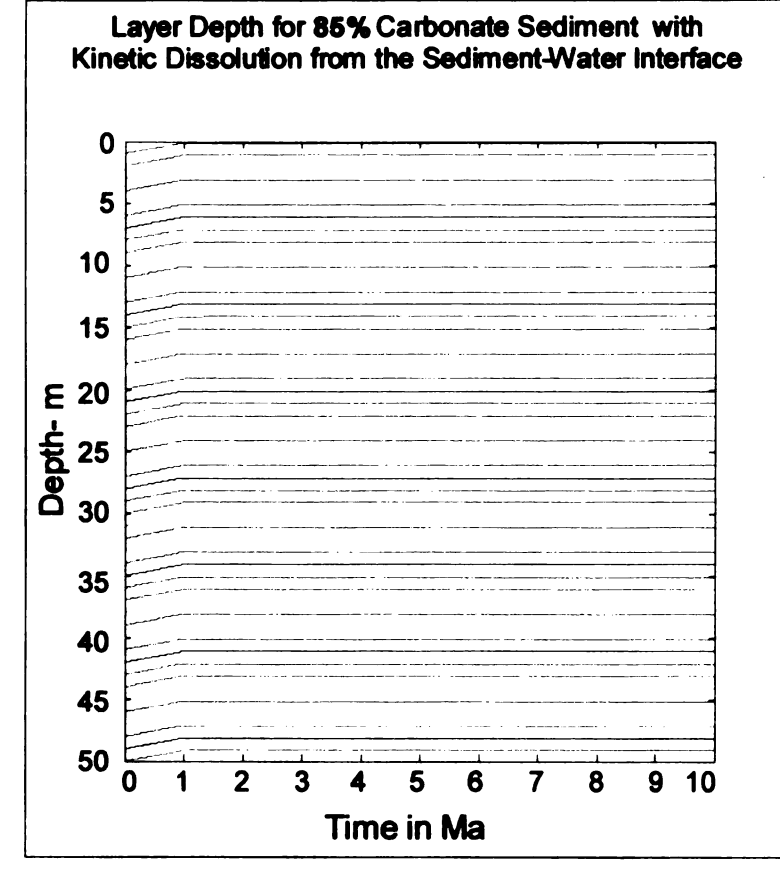


Figure 8.2 . Depth of bounding surfaces for layers initially 1m thick through 10Ma (note the change in time scale) with reaction limited dissolution from the sediment-water interface.

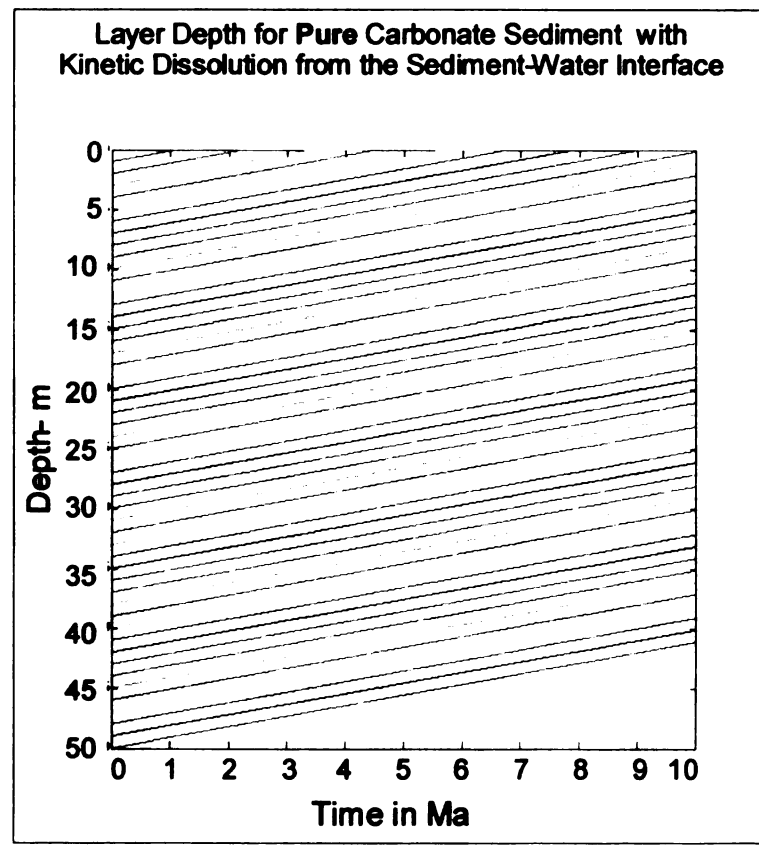


Figure 8.3. Depth of bounding surfaces for layers initially 1m thick through 10Ma with reaction limited dissolution from the sediment-water interface assuming pure carbonate sediment.

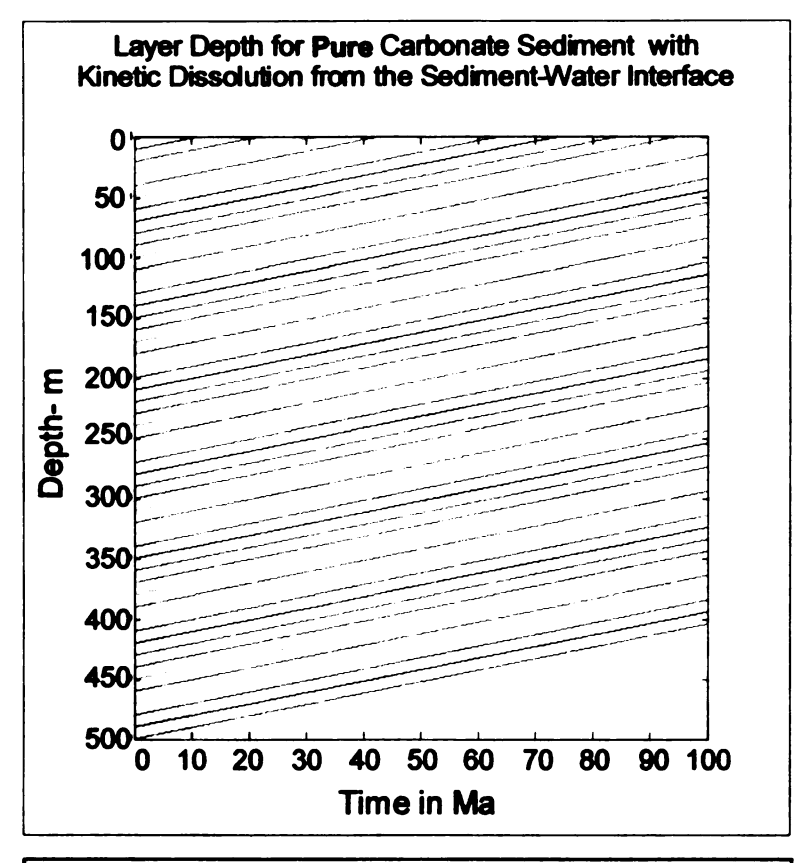


Figure 8.4. Depth of bounding surfaces for layers initially 10m thick through 100Ma with reaction limited dissolution from the sediment-water interface assuming pure carbonate sediment.

an average of 85%

CaCO₃. This means that
15% of each layer would
remain after all of the
carbonate had dissolved,
preventing the next lower
layer from being exposed
to open water. The
effect of this can be seen
at about 1Ma. The top
layer thins to its
minimum thickness, then
dissolution virtually stops
as the surface reaction

mechanism is no longer active. Note that even nearly pure carbonate sediment would still leave residual clay at the surface which would remove the carbonate from the undersaturated water. Changing the sediment to 100% carbonate allows reaction controlled dissolution to continue and complete removal of layers (figure 8.3). By designing conditions that allow dissolution due to undersaturation to persist, 9m of sediment was dissolved in 10Ma. Looking at a 500m column through 100Ma (figure 8.4), reveals the potential of this mechanism. The first 20m of sediment is removed at 21Ma, and nearly 100m of sediment is eliminated in 100Ma.

Conclusions

In the original model, the reduction in thickness of the individual layers is very small, even in the top layer. In each column the decrease in thickness of this layer over 100Ma is approximately 1.5% (table 9.1). The removal from the entire sediment column for each simulation is nominal relative to its magnitude; less than one meter was dissolved from 50m of sediment and less than 2% was removed from any column. Even accounting for percent carbonate in the

Top Layer			W	hole Colum	าก
Initial Thickness	Final Thickness	Percent Dissolved	Initial Final Thickness Thickness		Percent Dissolved
me	meters		me	ters	
10	9.86	1.40	500	497.52	0.50
1	0.985	1.50	50	49.46	1.09
0.01	0.00985	1.50	0.5	0.49	1.52

Table 9.1. Dissolution from the top layer of the three simulated sediment columns.

sediment, dissolution by diffusion would not remove a significant proportion of the carbonate from a natural layer.

Imposing persistent reaction controlled dissolution from the sediment-water interface created significant sediment removal. However, the necessary conditions that would allow this restrict the potential locations where it could happen. Pelagic clay deposition must be eliminated, which is conceivable, but the sediment also has to be practically pure carbonate. Dissolution controlled by surface reaction would proceed until the clay residue was continuous across the sediment surface. The required thickness of clay would depend on the zone of mixing through the clay of the pore solution and the overlying water (which is difficult to determine, but usually on the order of a few millimeters (Chapra 1997)). But, if all of the sediment at the top of the sediment column was nearly

100% carbonate, notable thickness might be removed before enough clay accumulated. Most deep Atlantic carbonate sediment is between 85% and 95% CaCO³ (appendix III). Using the average accumulation rate of 4.5m per 0.5Ma, the sediment would have to be 99.78% pure carbonate to leave only 1cm of clay, which is thicker than the likely mixing length. Even though many measurements show thinner layers, only a small percentage of clay is required to stop this process.

Combining diffusion through the sediment with reaction controlled dissolution from the sediment-water interface might removed enough carbonate to create a hiatus. Nonetheless, particular conditions would have to be aligned, so a hiatus by this mechanism would be limited in extent and duration. Perhaps this is why carbonate persists for millions of years despite undersaturated water.

Discussion

Dissolution of deposited carbonate by diffusion through the sediment does not allow enough removal to create a perceptible hiatus. Other physical processes need to be invoked to explain their existence. One such mechanism that could enhance carbonate removal is mineralization of organic carbon. The rates of decomposition found by researchers (Honjo et al 1982, Berelson et al 1990 and Wenzhofer et al 2001) are similar to the rate surface reaction limited dissolution (equation 8.3), and carbonate dissolution attributable to breakdown of organic matter is about half that (Wenzhofer et al 2001). Also, degradation is restricted to the upper few centimeters of sediment and limited in duration. The amount of organic carbon which is deposited is very minor relative to CaCO₃, and it would be eliminated before significant carbonate was removed. Plus, deposition of organic carbon on the ocean floor is primarily restricted to within 30° of the equator and near the continental margins (Jahnke 1996), which limits the geographical extent of this process.

Bioturbation could expose carbonate to the overlying water, allowing surface reaction limited dissolution to continue. Removal of carbonate is directly related its exposed area at the sediment surface and that area is proportional to the percent carbonate in the sediment (Kier 1984). The clay content is enriched by dissolution of CaCO₃, but fresh carbonate could be introduced by bioturbation. The mixing zone from bioturbation is approximately 8cm (Kier 1984), and average deep Atlantic carbonate sediment is 85% pure carbonate. It would take

only 53.3cm (8cm/15%) of sediment to fill the mixing zone with non-carbonate sediment.

Another possibility is that the dynamics of alkalinity in the pore solution allows additional dissolution of CaCO₃. To explore the complexity of this system, extensive characterization of the fluid would be required. Also, change in ocean chemistry in the past could have created greater dissolution. This could not explain hiatuses at regional and local scales, nor the variation in duration. Finally, oceanic conditions could have caused lack of deposition, but different conditions to effect hiatuses of both local and global extent are difficult to contrive.

Appendix I

Sediment Accumulation Data

DSDP sites that have age-depth relationships in SYNATLAN database at http://www.geomar.de/~twolf/ListADModels.html by Wolf-Welling et al (1997). Each of these sites is on oceanic crust under at least 4000m of water.

Leg	Site	Latitude	Longitude	Water Depth
11	99	23°41.1420'N	73°50.9880W	4914
11	100	24°41.2680'N	73°47.9820′W	5325
11	101	25°11.9280'N	74°26.3100'W	4868
11	105	34°53.7180'N	69°10.3980′W	5251
11	106	36°26.0100'N	69°27.6900′W	4500
12	119	45° 1.9020'N	7°58.4880'W	4447
36	328	49°48.6720'S	36°39.5280'W	5095
39	354	5°53.9520'N	44°11.7780'W	4045
39	355	15°42.5880'S	30°36.0300W	4901
39	358	37°39.3120'S	35°57.8220′W	4962
40	361	35° 3.9720'S	15°26.9100'E	4549
41	370	32°50.2500'N	10°46.5600'W	4214
43	382	34°25.0380'N	56°32.2500′W	5526
43	385	37°22.1700'N	60° 9.4500'W	4936
43	386	31°11.2080'N	64°14.9400'W	4782
43	387	32°19.2000'N	67°40.0020W	5117
44	391	28°13.7280'N	75°36.7620'W	4974
45/46	396	22°28.8780'N	43°30.9480'W	4450
48	400	47°22.9020'N	9°11.8980'W	4399
50	416	32°50.1780'N	10°48.0600'W	4191
51-53	417	25° 6.6300'N	68° 2.4780'W	5468
51-53	418	25° 2.1000'N	68° 3.4380'W	5514
71	513	47°34.9920'S	24°38.4000′W	4373
72	515	26°14.3280'S	36°30.1680'W	4250
73	520	25°31.3980'S	11°11.1420W	4207
73	521	26° 4.4280'S	10°15.8700′W	4125
73	522	26° 6.8400'S	5° 7.7820W	4441
73	523	28°33.1320'S	2°15.0780′W	4562
73	524	29°29.0520'S	3°30.7380'E	4796
74	527	28° 2.4900'S	1°45.7980'E	4428
75	530	19°11.2620'S	9°23.1480'E	4629
78	542	15°31.0200'N	58°42.7980'W	5016
78	543	15°42.7380'N	58°39.2220'W	5633
80	550	48°30.9120'N	13°26.3700'W	4420
93	603	35°29.6580'N	70° 1.6980′W	4633

Table i.1. DSDP sites used for accumulation rates.

Selected Atlantic DSDP Site Locations

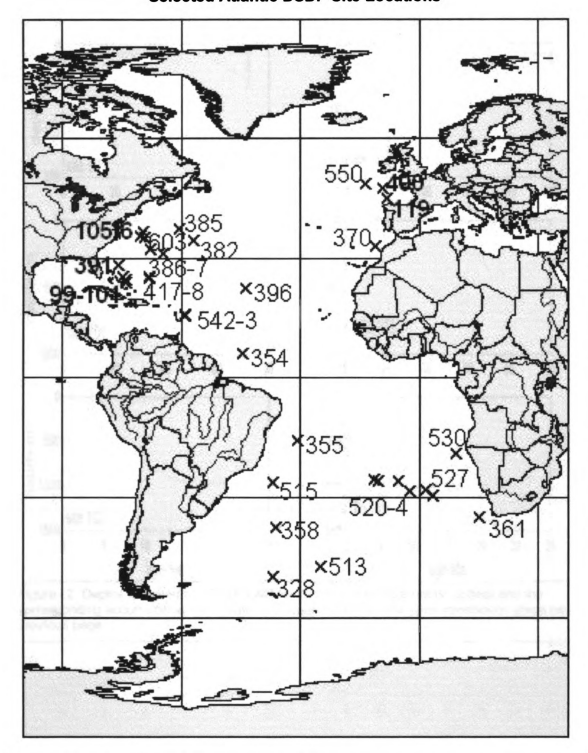


Figure i.1 Locations of DSDP sites with carbonate sediment on oceanic crust under at least 4000m of water. Site information given on previous page.

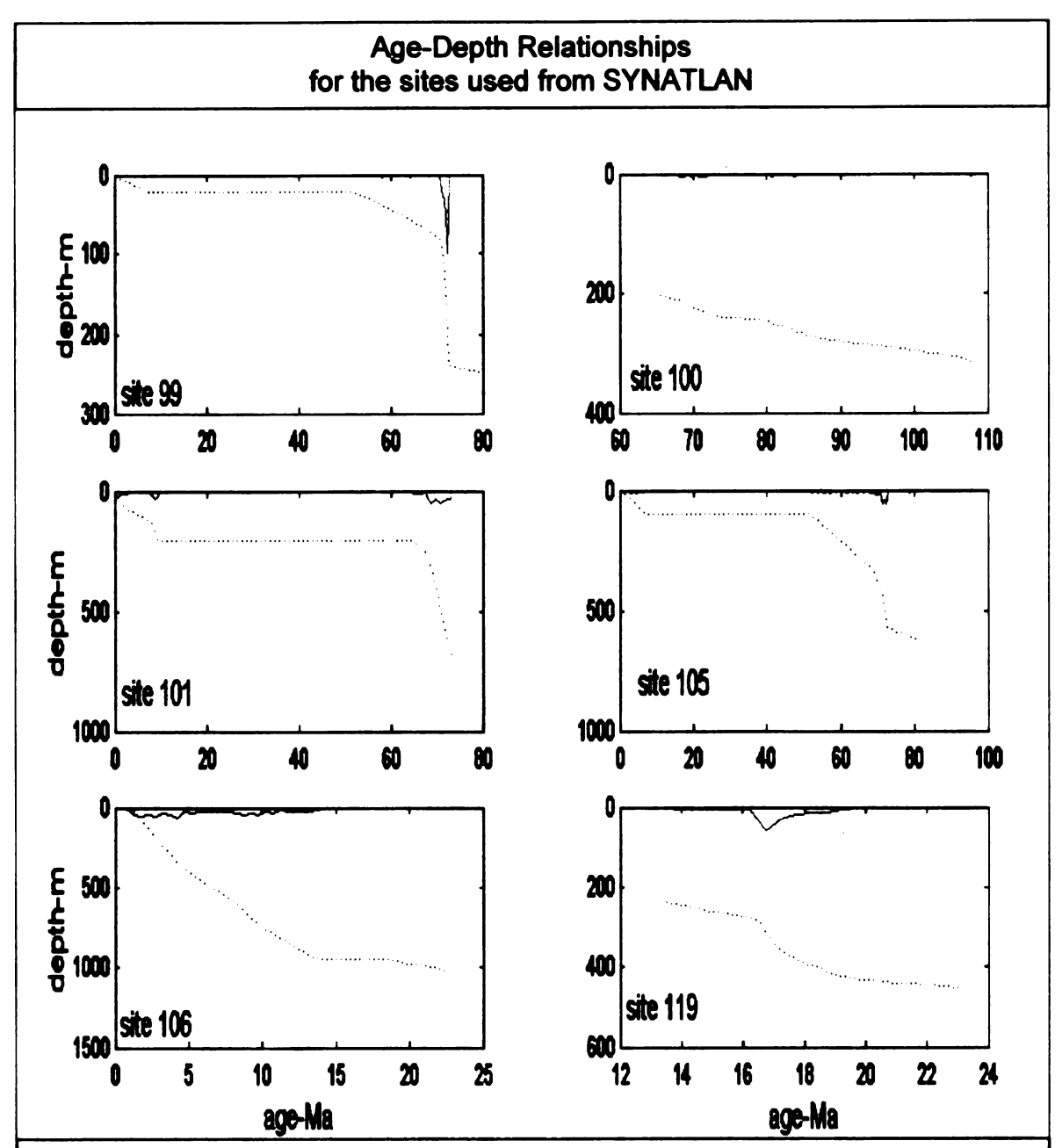
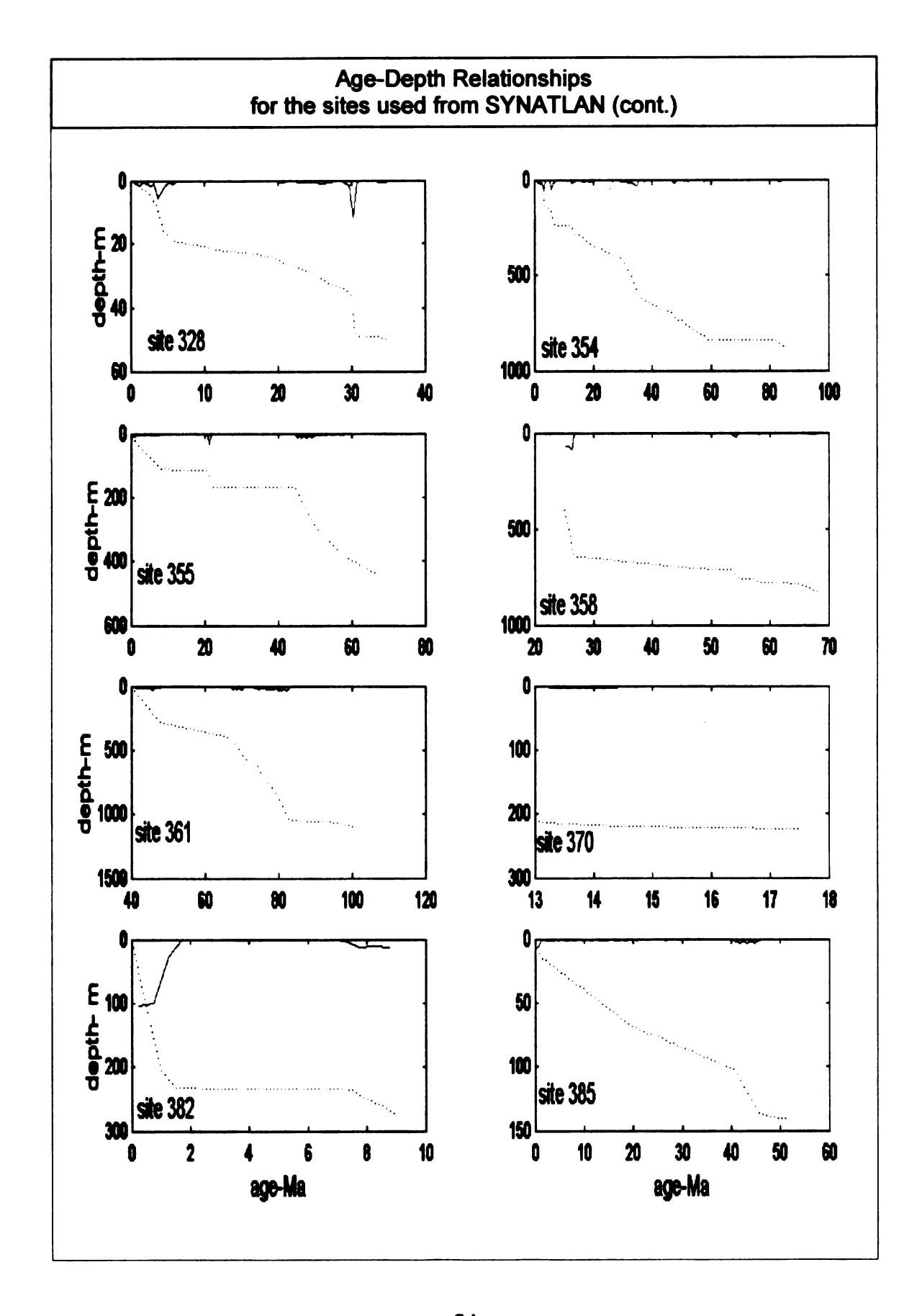
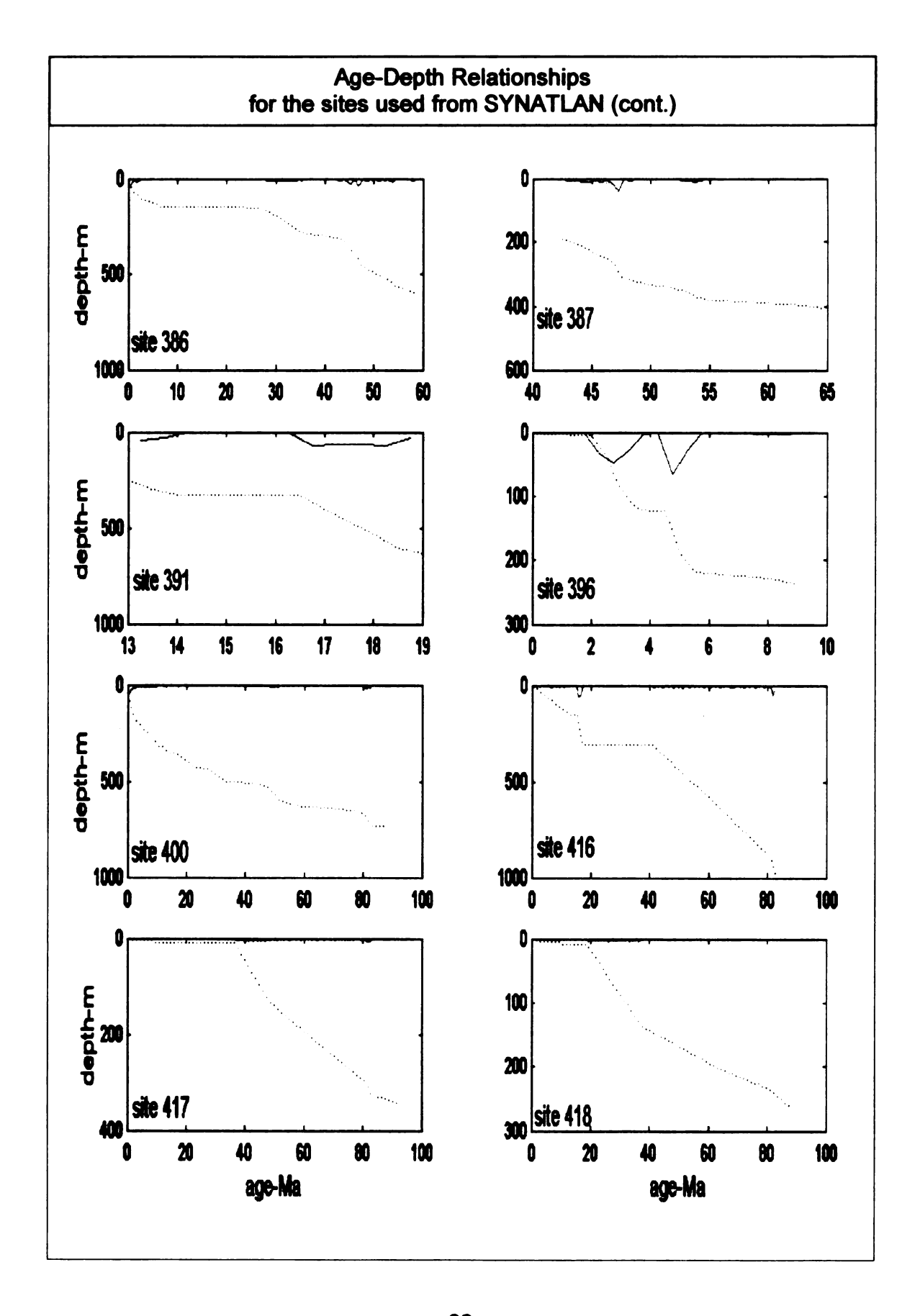
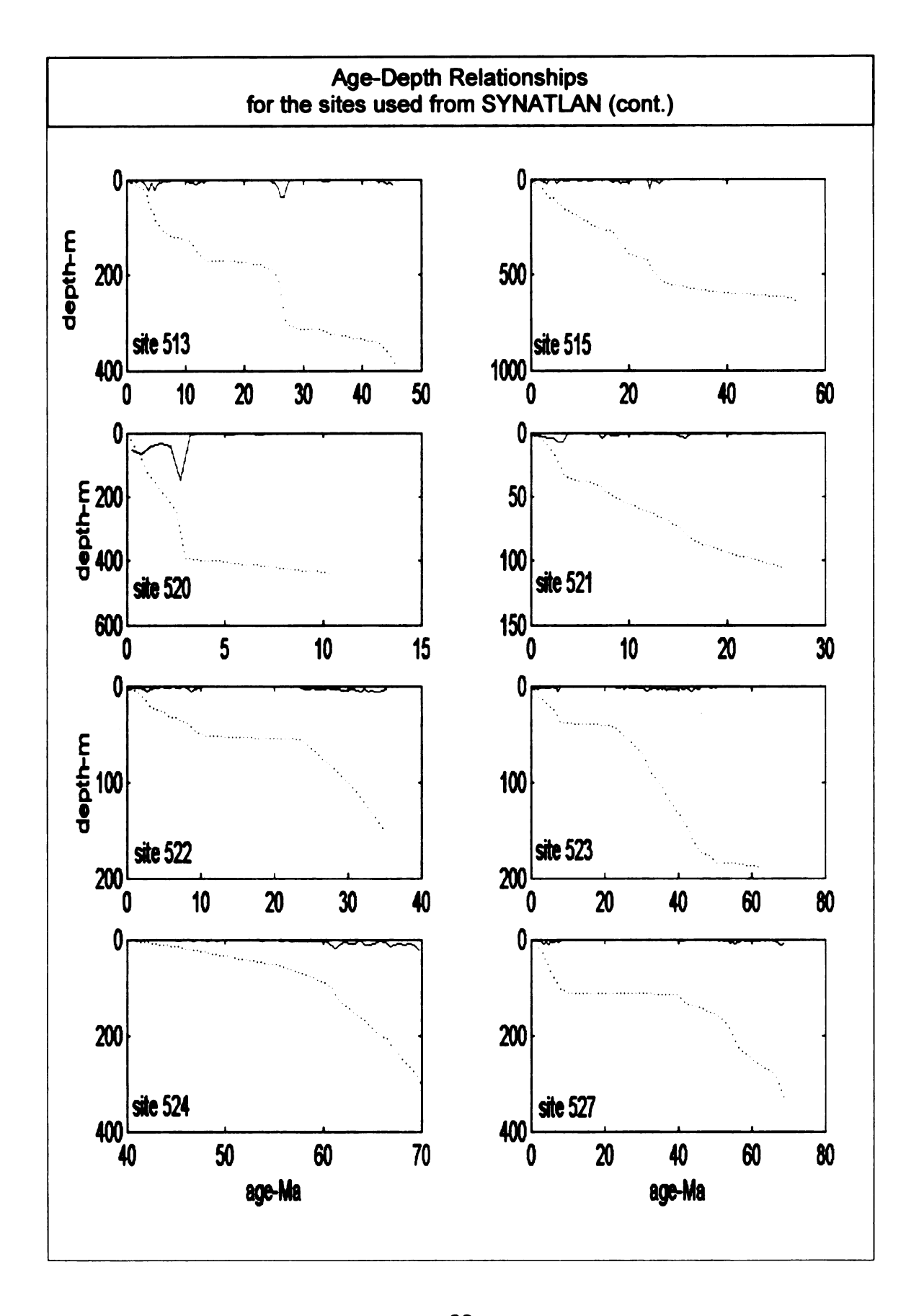
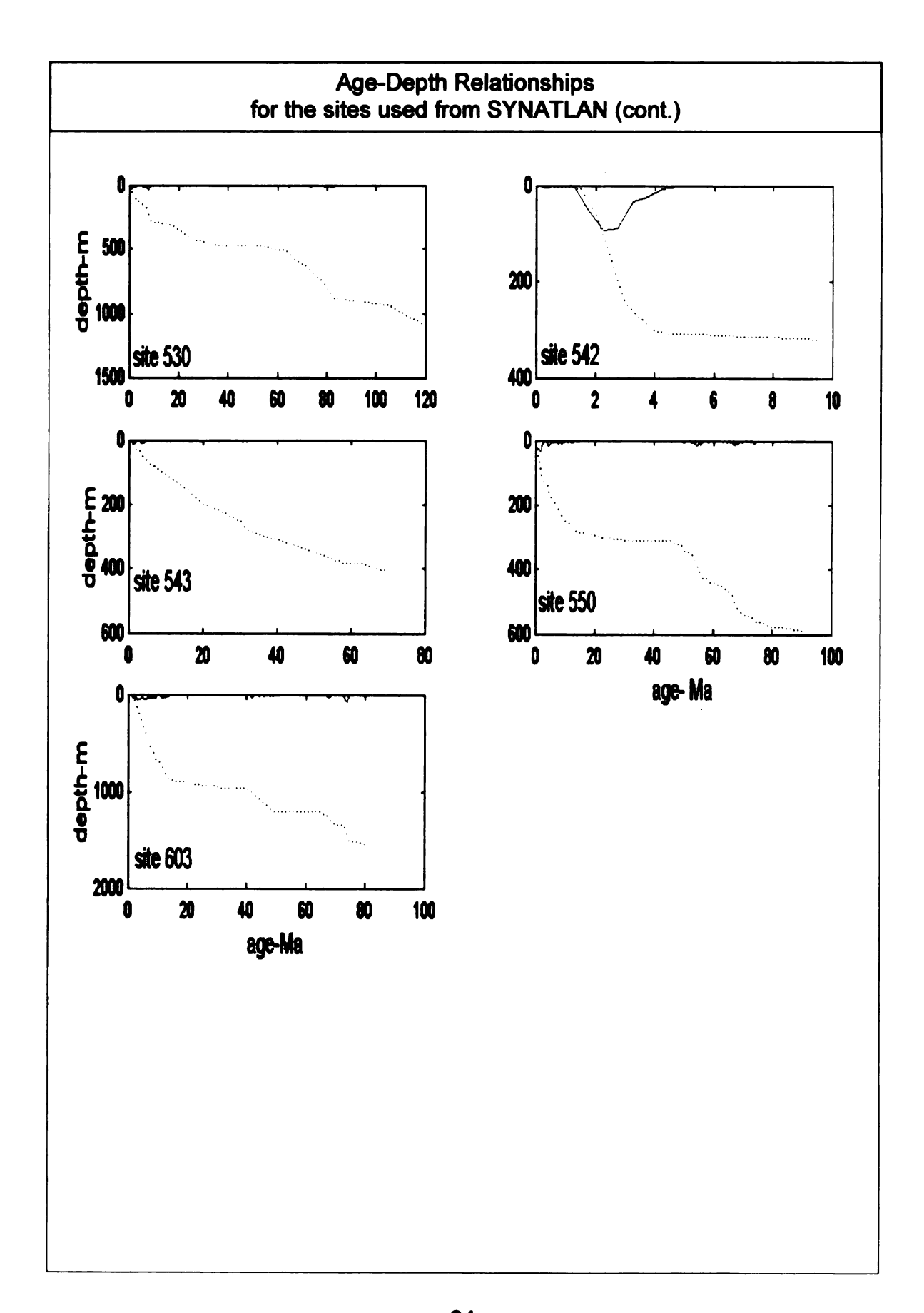


Figure i.2 Depths assigned by SYNATLAN for age at 0.5Ma increments (dotted) and the corresponding accumulation rate (dashed) calculated in m/0.5Ma. Site information given on previous page.









Appendix II Calcium Concentration Data

Since mixing of solutions is not linear with respect to saturation, using data from several sites is not appropriate, so a single site was chosen. Of the deep Atlantic sites that are on in the pelagic basin, 29 have pore water Ca²⁺ measurements, see appendix I, and site 603 has markedly more measurements than any other site. The data came from three holes at the site and were used to fit the function for Ca²⁺ concentration with depth. Minimization of the sum of squared residuals was used to find the constants for the function (figure 5.1):

2.3
$$C(x) = C_{max} - (C_{range} \cdot e^{-k_c \cdot x})$$
 $C_{mex} = 24.2 \text{ mol/m}^3$ $C_{min} = 1.78 \text{ mol/m}^3$ $C_{min} = 2.75*10^3 \text{ m}^{-1}$

Then the derivative is:

2.4
$$\frac{\partial C}{\partial x} = k_c \cdot C_{range} \cdot e^{-k_c \cdot x}$$

4.2
$$\frac{\partial C}{\partial x} = 0.00275 m^{-1} \cdot 22.4 \frac{mol}{m^3} \cdot e^{-0.00275 m^{-1} \cdot x}$$

Interstitial Pore Water Ca²⁺ Concentration for DSDP Site 603

Hole	Depth to	Ca	Fitted	Residual Squared	
	Sample- m	mm/L	Value		
603C	36.75	3.38	3.94	0.32	
603C	65.35	6.01	5.48	0.28	
603C	90.69	6.58	6.74	0.03	
603C	123.85	8.59	8.27	0.10	
603C	171.85	9.31	10.24	0.87	
603	213.05	12.48	11.74	0.54	
603C	219.85	11.21	11.97	0.58	
603C	261.85	13.79	13.31	0.23	
603	269.15	13.58	13.53	0.00	
603	318.65	16.17	14.89	1.63	
603C	322.45	15.38	14.99	0.15	
603C	354.25	14.85	15.76	0.84	
603	368.15	15.69	16.08		
603	454.55	18.22	17.81	0.17	
603	594.05	21.12	19.85	1.60	
603	645.05	18.87	20.43	2.43	
603	670.85	20.31	20.69	0.14	
603	721.87	25.11	21.15	15.67	
603	800.16	20.51	21.75	1.53	
603B	902.65	19.45	22.36	8.46	
603B	938.05	26	22.53	12.03	
603B	989.05	20.7	22.75	4.22	
603B	1031.05	16.1	22.92	46.45	
603B	1076.15	22.12	23.07	0.90	
603B	1178.45	24.62	23.35	1.60	
603B	1268.35	25.4	23.55	3.44	
603B	1298.65	27.22	23.60	13.10	

Table ii.1 Interstitial pore water measurements from DSDP for site 603. Predicted Ca²⁺ concentration from equation 4.2 in which the constants were fitted from minimizing the sum of the residual squared values.

Appendix III Porosity Data

Porosity measurements from several DSDP sites were used. The sites were selected to be carbonate sediment in the deep Atlantic basin. Deep Atlantic

the water depth, crust type, and physiographic feature.

Carbonate content was checked by looking at the percent CaCO₃, which needed to be at least 50% carbonate.

The average was 85.0%, and the distribution is shown in figure iii.1.

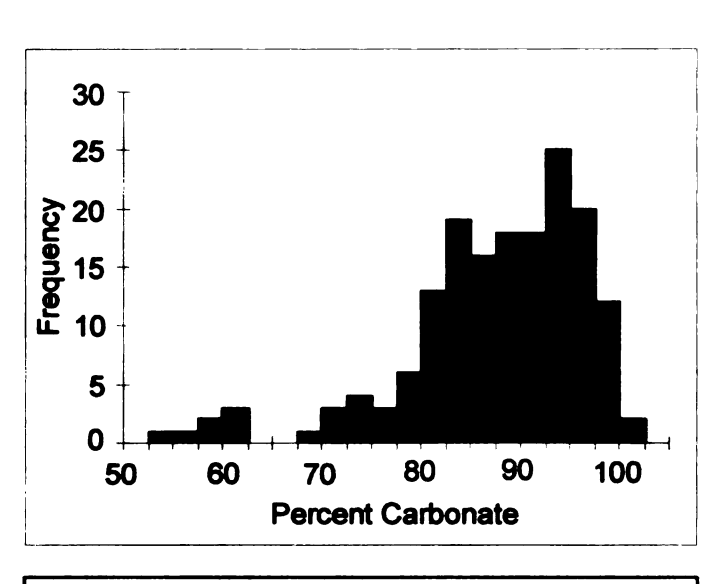


Figure iii.1 Frequency of porosity values for deep Atlantic carbonate sediment.

The data from all appropriate sites were compiled, and the constants for the porosity with depth relationship:

2.8
$$p(x) = p_{\min} + p_{range} \cdot e^{\frac{-x}{k_p}}$$

$$p_{\max} = 75.0$$

$$p_{\min} = 58.5$$

$$p_{range} = 16.5$$

$$k_p = 38.4$$
4.4
$$p(x) = 58.5 + 16.5 \cdot e^{\frac{-x}{36.4m}}$$

were found by minimization of the sum of squared residuals (figure 5.2).

Table iii.1. Porosity Measurements of Deep Atlantic Carbonate Sediment from DSDP

Site	Depth- m	Porosity	Site	Depth- m	Porosity	Site	Depth- m	Porosity
515a	76.05	60.88		115.56	49.5	116		54
116	76.16	57.6			62.37	116		50.8
515a	78.9	61.34			80.03	515b		66.9
12c	79.65	66.2	17b		54	335		55.83
116a	82.66	58.6			50.5	515b		67.06
17b	86.66	52.25			53.25	515b		73.3
515a	87	63.21	335	130.95	52.67	515b		69.5
17b	88.16	52.86		137.25	58	515b		69.78
515a	88.3	64.39			58	515b	356.84	68.51
12c	88.65	48.25			72.16	116		56.6
116a	88.66	54.4	328		72.73	116		50
515a	90.18	63.89		·	56.29	515b		68.35
116a	90.44	64.8			77.05	515b		68.46
17b	91.16	55.43			73.33	515b		67.49
335	91.45	61.17			72.92	515b		65.42
515a	91.92	62.24			60.33	515b		65.81
17b		52	18		64	116		61
515a	93.1	60.28			45.88	515b		65.13
116a	93.44	57.6			72.25	515b		62.87
515a	94.19	65.87			56.2			70.78
17b	94.56	50.4			55.6	515b		66.33
328	94.77	79.48			54.2	515b		64.86
116a	94.94	54.6						66.38
17b	95.76	54			60.4	116		54.2
515a	95.91	62.59			58.67	116		51
328	96.37	77.8			62	515b		66.18
515a	97.1	60.1	334	184.8	63	515b		66.78
17b	97.26	52.29			70.65	515b		65.19
12c	97.4	69	328	193.85	68.45	515b		65.14
515a	98.4	60.85	328	193.88	70.28	515b	507.76	66.63
17b	98.76	51.33	515b	196.7	73.27	515b	516.8	55.77
515b	99.22	60.83	334	200.45	64.29	515b	528.52	52.89
515a	100	60.05	515b	201.78	72.52	515b	537.5	52.75
515b	100.1	60.33	515b	203.36	69.19	515b	541.71	51.69
515a	101.1	58.13	515b	203.36			555.92	
17b	103.26	54.29	116	210.91	52.2	515b	564.21	50.25
515a	104.58	59.71	116	212.21			574.44	49.79
17b	104.96	50.67	116	215.15	56.8	515b	579.52	50.11
515a	106.08		334	219.45	60.83	515b	597.71	49.97
515a	106.08	58.24	335	221.45	56.17	515b	599.61	49.52
17b	106.46	53.75	334			515b	612.57	47.92
515a								41.04
17b								41.27
116								58.2
17b								44.8
12b	110.16							
17b							714.95	50.4
17b	112.71	54.4	515b	283.26	70.87			

Site	Depth- m	Porosity	Site	Depth- m	Porosity	Site	Depth- m	Porosity
515a	0.7	76.49	328b	21.43	75.03	515a	46.1	66.54
328	1.11	73.9	328	21.77	74.67	328b	46.4	80.87
334	1.39	67.83	328	22.25	78.64	116a	46.66	62.2
515a	1.43	75.72	328b		80.3	328b	46.8	76.67
328	2	78.57	515a	22.92	73.41	328b	46.96	79
331	2.05	73.03	328	23.27	72.24	328b	47.21	74.8
328	2.94	74.63	515a	24.04	70.66	515a	47.6	67.75
12c	2.98	62.75	116a	24.15	61.2	328	47.78	78.62
331	3.5	63.77	328b	24.18	72.37	328b	48.16	77.73
515a	3.8	74.28	328	24.42	88.07	328	48.26	77.33
328	4.1	78.43	328	24.5	71.6	328	49.3	75.37
12c	4.48	65.75	328	24.93	71.4	328b	49.3	82.77
515a	4.97	79.08	328b	25.26	71.38	515a	49.3	63.88
331	5.18	62.83	515a	25.58	71.76	328b	50.07	79.8
328	5.25	77.03	328	25.66	74.93	328	50.18	78.2
12c	5.98	66	328b	25.95	76.37	515a	50.48	64.03
515a	6.43	76.18	515a	27.32	71.79	328b	50.75	80.68
515a	6.49	65.71	328b	28.13	80.17	12c	51.96	56.5
331	6.6	70.37	515a	28.49	75.21	515a	51.98	64.29
328	7.2	77.63	116a	28.66	50.2	328b	52.27	78.43
515a	7.93	72.54	328b	29.18	80.8	328b	53.07	79.13
331	8.06	71.43	515a	29.94	70.75	515a	53.39	62.22
331	9	55.37	328b	30.75	76.23	328b	53.84	79.27
515a	9.6	74.7	515a	31.74	67.61	515a	54.88	64.38
328b	9.68	74.7	328b	32.16	78.83	116a	55.66	64.4
116a	10.66	71.2	515a	32.97	67.32	328b	55.81	75.27
515a	10.83	76.73	12c		60.98	515a	56.38	65.7
328b	11.79	75.53	328b		81.16	328b	57.28	63.13
515a	12.33	69.02	12c		56	515a	58.08	61.68
328b	12.94	75.5	515a		68.02	116a	58.66	59
328	13.24	75.23	328b		74.83	328b	58.68	75.47
515a	14.13	74.11	328b		73.56	515a	59.3	65.74
328b	14.22	75.87	515a	36.09	66.3	12c	60.27	50.75
515a	15.22	73.4	328b		74.23	328b	60.28	78.57
328b	15.6	76.53			74.13			61.6
328b		75.53			74.8			58.4
515a		72.45			67.15			79.72
12c	17.28	65			56.6	328b		66.67
328		62.49	515a		65.91	116a	64.65	59.2
328b	17.68	77.5			76.53	515a	66.58	61.86
328	18.07	74.5			65.2	515a		61.93
515a	18.48	72.81	515a		68.68	116		59.6
12c		67	515a		67.89	12c		57.44
328b	19.52	78.63			76.23	515a		64.12
328	19.76	85.28			76.53	116		55.6
515a	20.03	72.54			61.14	515a	72.1	62.2
12c	20.28	57.27	515a		65.41	116a		51.8
328	20.33	77.52			59.67	515a		63.11
328	20.95	77.23			64.5	515a		62.68
515a	21.2	72.14			56.5	515a	75.72	63.3
17b	114.31	53.33	515b	294.93	67.95			

Appendix IV MATLAB Codes

The peripheral model codes not in the text are listed here.

```
original=b;
n=length (original);
%m will refer to the last column of depths
m=size(final,2);
for iy=1:m
    for il=1:n-1
        thick(il,iy)=final(il+1,iy)-final(il,iy);
        end
end
for iy=1:m-1
        chthick(:,iy)=thick(:,iy+1)-thick(:,iy);
end
```

dthick was used to calculate the change in thickness for each layer at every time step.

```
carbpercent=0.85;
n=length(b);
for ib=1:n-1
minthick(ib,1)=(b(ib+1)-b(ib))*(1-0.85);
%min thickness=original thickness*percent noncarbonate
end
```

cpercent calculated the minimum thickness of a layer based on its original thickness and clay content. It appears in line 5 and 41 of the original model.

```
16 sigma=0.05*Do;

27a Ds=Do/(1-log((Pmin+(Prange)*exp(-x/kp))^2));

27b Dsrand=randn*sigma+Ds;

28 flux(ia)=Dsrand*(kc*Crange*exp(-kc*x));
```

carbrand was the original model modified to include a random variation in D_s for each layer of sediment.

```
%This will run the model with random distribution of Ds N times
N=500:
for i=1:N
  carbrand:
  Ma10th(:,i)=final(:,11);
  Ma(:,i)=final(:,101);
  Ma10(:,i)=final(:,1001);
  Ma100(:,i)=final(:,10001);
end
for j=1:51
  avMa10th(j)=mean(Ma10th(j,1:N));
  stMa10th(j)=std(Ma10th(j,1:N));
  avMa(j)=mean(Ma(j,1:N));
  stMa(j)=std(Ma(j,1:N));
  avMa10(j)=mean(Ma10(j,1:N));
  stMa10(j)=std(Ma10(j,1:N));
  avMa100(j)=mean(Ma100(j,1:N));
  stMa100(j)=std(Ma100(j,1:N));
end
```

runs executed the carbrand model multiple times and saved results for 0.1Ma, 1Ma, 10Ma and 100Ma. This code also evaluated the mean and standard deviation of the saved results.

References

- Adler, M., Hensen, C., Schulz, H.D., 2000. CoTReM— Column Transport and Reaction Model, Version 2.3, User Guide. http://www.geochemie.uni-bremen.de/projects/cotrem.html
- Adler, M., Hensen, C., Wenzhofer, F., Pfeifer, Schulz, H.D., 2001. Modeling of calcite dissolution by oxic respiration in supralysoclinal sediments. Marine Geology, 177, p. 167-189
- Archer, D.E., 1996. A data-driven model of the global calcite lysocline. Global Biochemical Cycles, 10, p. 511-526.
- Archer, D.E., 1996. An atlas of the distribution of calcium carbonate in sediments of the deep sea. Global Biochemical Cycles, 10, p. 159-174.
- Archer, D.E., 1991. Modeling the calcite lysocline. Journal of Geophysical Research, 96, p.17037-17050.
- Archer, D., Emerson, S., and Reimers, C., 1989. Dissolution of calcite in deep-sea sediments: pH and O₂ microelectrode results. Geochimica et Cosmochimica Acta, 53, p. 2831-2845.
- Archer, D., and Winguth, A., 2000. What caused the glacial/interglacial atmospheric pCO₂ cycles?. Reviews of Geophysics, 38, p. 159-189
- Berelson, W.M., Hammond, D.E., and Cutter, G.A., 1990. In situ measurements of calcium carbonate dissolution rates in deep-sea sediments. Geochemica et Cosmica Acta, 54, p. 3013-3020.
- Berelson, W.M., Hammond, D.E., McManus, J., and Kilgore, T.E., 1994. Dissolution Kinetics of calcium carbonate in equatorial Pacific sediments. Global Biochemical Cycles, 8, p. 219-235.
- Berger, W.H., Vincent, E., Thierstein, H.R., 1981. The deep-sea record: Major steps in Cenozoic ocean evolution. in The Deep Sea Drilling Project: a decade of progress, SEPM Special Publication 32, p. 335-394
- Berggren, W.A., Hollister, C.D., 1974. Paleogeography, paleobiogeography, and the history of circulation in the Atlantic Ocean. in Studies in Paleo-oceanography, SEPM Special Publication 20, Hay, W.W., ed., p. 126-186
- Berner, R.A., 1971. Principles of Chemical Sedimentology. McGraw-Hill Inc.
- Berry, J.P., Wilkinson, B.H., 1994. Paleoclimatic and tectonic control on the accumulation of North American cratonic sediment. GSA Bulletin, 106, p. 855-65
- Blatt, H., Middleton, G., and Murray, R., 1979. Origin of Sedimentary Rocks. Prentice-Hall.
- Boudreau, B.P., 1996. Diagenetic Models and Their Implementation— Modeling
 Transport and Reactions in Aquatic Sediments. Springer Heidelberg, Berlin, New
 York

- Broeker, W.S., Klas, M., Clark, E., Bonani, G., Ivy, S., Wolf, W., 1991. The influence of a CaCO₃ dissolution on core top radiocarbon ages for deep-sea sediments. Paleoceanography, 6, p. 593-608
- Chapra, S.C., 1997. Surface Water-Quality Modeling. McGraw-Hill, Boston
- Crowley, T.J., 1983. Calcium-carbonate preservation patterns in the central north Atlantic during the last 150,000 years. Marine Geology, 51, p.1-14
- Davies, T.A., Worsley, T.R., 1981. Paleoenvironmental implications of oceanic carbonate sedimentation rates. in The Deep Sea Drilling Project: a decade of progress, SEPM Special Publication 32, p. 335-394
- Drever, J.I., 1982. The Geochemistry of Natural Waters. Prentice-Hall, New Jersey
- Ehrmann, W.U., Thiede, J.,1985. History of Mesozoic and Cenozoic Sediment Fluxes to the North Atlantic Ocean: Contributions to Sedimentology, 15, Germany, E. Schweizerbart'sche Verlagsbuchhandlung Stuttgart
- Farrell, J.W., Prell, W.L., 1989. Climatic changes and CaCO₃ preservation: an 800,000 year bathymetric reconstruction from the central equatorial Pacific Ocean. Paleoceanography, 4, p. 447-466
- Fetter, C.W., 1994. Applied Hydrogeology, 3rd edition. Prentice Hall
- Garrels, R.M., 1988. Sediment cycling during Earth history. in Physical and Chemical Weathering in Geochemical Cycles, Lerman, A., and Meybeck, M., eds., Kluwer Academic Publishers, p. 341-355
- Garrels, R.M., Mackenzie, F.T., 1971. Evolution of Sedimentary Rocks. New York, W.W. Norton & Company, p. 253-276
- Garrison, R.E., 1981. Diagenesis of ocean carbonate sediments: a review of the DSDP perspective. in The Deep Sea Drilling Project: a Decade of Progress, SEPM Special Publication 32, p. 181-208
- Gawenda, P., Winkler, W., Schmitz, B., Adatte, T., 1999. Climate and bioproductivity control on carbonate turbidite sedimentation (Paleocene to earliest Eocene, Gulf of Biscay, Zumaia, Spain). Journal of Sedimentary Research, 69, p. 1253-1261
- Gregor, C.B., 1985. The mass-age distribution of Phanerozoic sediments. in The Chronology of the Geologic Record, Snelling, N.J., ed., Oxford, Blackwell, p. 284-89
- Hales, B., and Emerson, S., 1997. Evidence is support of first-order dissolution kinetics of calcite in seawater. Earth and Planetary Science Letters, 148, p. 317-327
- Hamilton, E.L., 1976. Variations of density and porosity with depth in deep-sea sediments. Journal of Sedimentary Petrology, 46, p. 280-300
- Haq, B.U., Hardenbol, J., Vail, P.R., 1988. Mesozoic and Cenozoic chronostratigraphy and cycles of sea-level change. in Sea-Level Changes- An Integrated Approach, SEPM Special Publication No. 42

- Hay, W.H., Sloan II, J.L., Wold, C.N., 1988. Mass/age distribution and composition of sediments on the ocean floor and the global rate of sediment subduction. Journal of Geophysical Research, 93, p. 14933-40
- Heath, G.R., 1974. Dissolved silica and deep-sea sediments. in Studies in Paleooceanography, SEPM Special Publication 20, Hay, W.W., ed., p. 77-93
- Hebbeln, D., Wefer, G., Berger, W.H., 1990. Pleistocene dissolution fluctuations from apparent depth of deposition in core ERDC-127P, West-equatorial Pacific.

 Marine Geology, 92, p. 162-176
- Hensen, C., Landenberger, H., Zabel, M., Gunderson, J.K., Glud, R.N., 1997. Simulation of early diagenetic processes in continental slope sediment off southwest Africa: the computer model CoTAM tested. Marine Geology, 144, p. 191-210
- Honjo, S., Manganini, S.J., and Cole, J.J., 1982. Sedimentation of biogenic matter in the deep ocean. Deep Sea Research 29, 609-625
- Ingebritsen, S.E., Sanford, W.E., 1998. Groundwater in geologic processes. Cambridge University Press, New York, NY, p.35-79.
- Jahnke, R.A., 1996. The global ocean flux of particulate organic carbon: Areal distribution and magnitude. Global Biogeochemical Cycles, 10, p. 71-88
- Keir, R. S., 1980. The dissolution kinetics of biogenic calcium carbonates in seawater. Geochemica et Cosmica Acta, 44, p. 241-252
- Kier, R.S., 1980. Recent increase in Pacific CaCO₃ dissolution: a mechanism for generation of old ¹⁴C ages. Marine Geology, 61, p. 3-74
- Knebel, H.J., 1984. Sedimentary processes on the Atlantic continental slope of the United States. Marine Geology, 61, p. 3-74
- Langmuir, D., 1997. Aqueous Environmental Geochemistry, Prentice-Hall, Inc., p.600
- Lisitzin, A.P., 1972. Sedimentation in the World Ocean, SEPM Special Publication No. 17
- Lisitzin, A.P., 1991. Characteristics of global-sediment formation in regions of high- and superhigh-accumulation rates. in From Shoreline to Abyss: Contribution in Marine Geology in Honor of Francis Parker Shepard, SEPM Special Publication No. 46, p. 79-98
- Miall A.D., 2000. Principles of Sedimentary Basin Analysis, 3rd edition. Springer, p. 453
- Milliman, J.D., 1993. Production and accumulation of calcium carbonate in the ocean: budget of a nonsteady state. Global Biochemical Cycles, 7, p. 927-957
- Milliman, J.D., Droxler, A. W., 1996. Neritic and pelagic carbonate sedimentation in the marine environment: ignorance is not a bliss. Geologische Rundschau, 85, p. 496-504
- Moore, T.C., VanAndel, T.H., Sancetta, C., Pisias, N., 1978. Cenozoic hiatuses in pelagic sediments. Micropaleontology, 24, p. 113-138
- Moore, T.C., Heath, G.R., 1977. Survival of deep-sea sedimentary sections. Earth and Planetary Science Letters, 37, p. 71-80

- Morse, J.W., 1978. Dissolution kinetics of calcium carbonate in seawater: VI, The near-equilibrium dissolution kinetics of calcium carbonate-rich deep-sea sediments. American Journal of Science, 278, p. 344-353
- Morse, J.W., and Mackenzie, F.T., 1990. Geochemistry of Sedimentary Carbonates: Developments in Sedimentology 48. Elsevier.
- Normark, W.R., Piper, D.J., 1991. Initiation processes and flow evolution of turbidity currents: implications for the depositional record. in From Shoreline to Abyss: Contribution in Marine Geology in Honor of Francis Parker Shepard, SEPM Special Publication No. 46, p.207-31
- Rabouille, C., Gaillard, J.F., 1991. Towards the EDGE: early diagenetic global explanation. A model depicting the early diagenesis of organic matter, O₂, NO₃, Mn, and PO₄. Geochemica et Cosmochimica Acta, 55, p. 2511-2525
- Ramsay, A.T.S., 1974. The distribution of calcium carbonate in deep sea sediments. in Studies in Paleo-oceanography, SEPM Special Publication 20, p. 58-76
- Ronov, A.B., Khain, V.E., Balukhovsky, A.N., Seslavinsky, K.B., 1980. Quanitative analysis of Phanerozoic Sedimentation. Sedimentary Geology, 25, p. 311-25
- Sadler, P.M., 1999. The influence of hiatuses on sediment accumulation rates. in On the Determination of Sediment Accumulation Rates, Bruns, P. and Hass, H.C., eds., Trans Tech Publications, p. 15-40
- Sadler, P.M., 1981. Sediment accumulation rates and the completeness of stratigraphic sections. Journal of Geology, 89, p. 569-84
- Sadler, P.M., Strauss, D.J., 1990. Estimation of completeness of stratigraphical sections using empirical data and theoretical models. Journal of the Geological Society, London, 147, p. 471-85
- Sclater, J.G., Hellinger, S., and Tapscott, C., 1977. The paleobathymetry of the Atlantic Ocean from the Jurassic to the Present. The Journal of Geology, 85, p. 509-552
- Schneider, R.R., Schulz, H.D., Hensen, C., 2000. Marine carbonates; their formation and destruction. in Marine Geochemistry, eds. Schulz, H D, and Mattais, Z., Springer-Verlag, p. 283-307
- Simmons, G.R., 1990. Subsidence history of basement sites and sites along a carbonate dissolution profile. Leg 115, Proc. ODP, 115, p. 123-126
- Smith, D.G., 1990. The nature and analysis of the stratigraphic record. Journal of the Geological Society, London, 147, p. 469-70
- Southam, J.R., Hay, W.W., 1977. Time scales and dynamic models of deep-sea sedimentation. Journal of Geophysical Research, 82, p. 3825-3421
- Svensson, U., Dreybrodt, W., 1992. Dissolution kinetics of natural calcite minerals in CO₂ –water systems approaching calcite equilibrium. Chemical Geology, 100, p. 129-145
- Sykes, T.J.S., Ramsay, A.T.S., 1995. Calculation of mass accumulation rates in the absence of density or porosity measurements. Marine Geology, 122, p. 173-179

- Takahashi, T., Broecker, W. S., 1977. Mechanisms of calcite dissolution in the sea floor. in The Fate of fossil fuel CO-b2-s in the oceans, eds. Andersen, N R, Malahoff, A., New York., p. 455-477
- Thiede, J., Strand, S., Agdestein, T., 1981. The distribution of Major Pelagic sediment components in the Mesozoic and Cenozoic north Atlantic Ocean. in The Deep Sea Drilling Project: a decade of progress, SEPM Special Publication 32, p. 67-90
- Thierstein, H.R., 1981. Late Cretaceous nannoplankton and the change at the Cretaceous-Tertiary boundary. in The Deep Sea Drilling Project: a decade of progress, SEPM Special Publication 32, p. 335-394
- Thunell, R.C., 1982. Carbonate dissolution and abyssal hydrography in the Atlantic Ocean. Marine Geology, 47, p. 165-180
- Thurmann, H.V., 1994. Introductory Oceanography. Macmillan Publishing Company, p. 1-550.
- Tucker, M.E., Wright, V.P., 1990. Carbonate Sedimentology. Blackwell Scientific Publications, p. 1-482.
- VanAndel, T.H., 1975. Mesozoic/Cenozoic compensation depth and the global distribution of calcareous sediments. Earth and Planetary Science Letters, 26, p. 187-194
- VanAndel, T.H., Thiede, J., Sclater, J.G., Hay, W.W., 1977. Depositional history of the South Atlantic Ocean during the last 125 million years. Journal of Geology, 85, p. 651-698
- VanHinte, J.E., 1976. A Cretaceous time scale. AAPG Bulletin, 60, p. 498-516
- Veizer, J., Jansen, S.L., 1985. Basement and sedimentary recycling- time dimension to global tectonics. The Journal of Geology, 93, p. 625-43
- Wenzhofer, F., Adler, M., Kohls, O., Hensen, C., Strotmann, B., Boehme, S., Schultz, H.D., 2001. Calcite dissolution driven by benthic mineralization in the deep-sea: in situ measurements of Ca²⁺, pH, pCO₂, and O₂. Geochimica et Cosmochimica Acta, 65, p. 2677-2690.
- Wold, C.N., Hay, W.W., 1990. Estimating ancient sediment fluxes. American Journal of Science, 290, p.1069-1089
- Wolf-Welling, T.C.W., Mienert, J., Brenner, W., Thiede, J., 1999. A stratigraphic database for the Atlantic Ocean sediment Record. in On the Determination of Sediment Accumulation Rates, Bruns, P. and Hass, H.C., eds., Trans Tech Publications, p. 169-184
- Wolf-Welling, T.C.W., Mienert, J., Thiede, J., 1997. SYNATLAN database: http://www.geomar.de/~twolf/SYNATLAN-home.html
- World Data Center for Marine Geology & Geophysics, 2000. Core data from the Deep Sea Drilling Project Legs 1-96. Boulder CDROM Seafloor Series 1.

